CHAOS, STRANGE ATTRACTORS AND BIFURCATIONS IN DISSIPATIVE DYNAMICAL SYSTEMS

with 70 Figures

A thesis

submitted in fulfilment of the

requirements for the Degree

of

Master of Science in Mathematics

in the

University of Canterbury

by

L.C. Beale

University of Canterbury

1988

CONTENTS

Abstract

In this dissertation a study is made of chaotic behaviour, the bifurcation sequences leading to chaos and the manifestation of chaos in the form of a strange attractor in dissipative dynamical systems.

In chapter 1 we provide an overview of the material covered in this review and introduce several concepts from the basic theory of dynamical systems, such as Poincaré return maps and simple bifurcations.

After introducing the concept of chaos and strange attractors in dissipative dynamical systems, we divide higher dimensional systems into three categories in chapter 2. Each is illustrated with examples. Central to the discussion is the well studied Lorenz system. Other important mathematical models are looked at, in particular the Rössler model and the two-dimensional Hénon map.

The various measures of dimension, in the fractal context, and the numerical methods currently in use for determining these quantities are presented in chapter 3.

In view of their relative computational simplicity and direct relevance to chaos, one-dimensional mappings are looked at in chapter 4.

In chapter 5, the idea of the transition to turbulence being a chaotic regime is introduced and the various routes to turbulence are examined in turn.

In chapter 6, we present a Fourier series method for approximating the phase-space trajectories of a dynamical system. We illustrate the technique by carrying out the calculations required on the equations describing the evolution of the spherical pendulum model of Miles (1984b).

No attempt is made to cover the whole field of research chaos. The use of symbolic dynamics is avoided wherever possible for simplicity and brevity in this review.

CHAPTER 1

INTRODUCTION AND OVERVIEW

1.1 GENERAL INTRODUCTION

Recently, chaotic motions that arise due to nonlinearities of dissipative dynamical systems have received a great deal of interest in physical and nonphysical fields. In dissipative dynamical systems, the phase space volume is not constant but rather contracts as the system evolves. The study of regular motion in these systems dates back to Newton and the subsequent development of the theory of ordinary differential equations. It was recognized in these early studies that the motion can contract onto simple attractors such as points, closed orbits (limit cycles), or tori, representing a steady state i.e., respectively stationary, periodic, or quasi-periodic.

In contrast, the recognition that intrinsically chaotic motion occurs in dissipative dynamical systems is quite recent dating from Poincaré's studies of the three-body problem. The Pioneering work in this field however was done by Lorenz, who in 1963, via numerical computation, found an attractor embedded in the motion described by a system of nonlinear ordinary differential equations. The term *strange attractor* used to describe these attractors on which the motion appeared chaotic, was coined by Ruelle and Takens, who independently proposed strange attractor behaviour as a model of fluid turbulence.

The topology of strange attractors is quite remarkable, showing a geometric invariance, in which the structure of the attractor repeats itself on ever finer spatial scales. Such structures are called fractals and have the property of fractional dimensionality. To be more specific, we say that the strange attractor has a cantor set structure. Furthermore, trajectories on the strange attractor which are initially infinitesimally close together, depart exponentially with time evolution

of the system. The consequence of this is that the system is highly sensitive to initial data.

As the geometric structure of strange attractors has become more clear, a qualitative picture has emerged in which an important feature is the close correspondence between motion on a strange attractor and motion described by noninvertible one-dimensional maps. These maps do not arise directly from dissipative flows, but are important examples of simple systems exhibiting chaotic behaviour. These mappings have found application in such diverse fields as economics and ecology. Noninvertible one-dimensional maps undergo a sequence of bifurcations as a parameter is varied such that the period of an attracting periodic orbit repeatedly doubles, accumulating at a critical parameter value, beyond which the behaviour is chaotic. This process has been shown to have a universal nature by Feigenbaum (1978). The theory of one-dimensional maps is relatively complete. It is in two-dimensional invertible maps (and their related three-dimensional flows) however, that strange attractors first appear. The period doubling bifurcation sequence is also present for these systems.

The appearance of strange attractors in three-dimensional flows, such as the Lorenz system suggest various routes to turbulence in fluids which improve markedly on the now outdated model of Landau. The main three accepted models are those by Ruelle-Takens-Newhouse, Feigenbaum and Pomeau-Manneville. These models have all been observed in practice; sometimes there being evidence of two possible routes in the same experiment.

1.2 CONTENTS OF THIS DISSERTATION

It is the aim of this review to provide the reader with a comprehensive (yet nonrigorous) overview of chaos, strange attractors and the bifurcation sequences leading to chaos in dissipative dynamical systems. It is assumed that the reader has an intermediate knowledge

of the theory of dynamical systems and bifurcations, covering both ordinary differential equations (flows) and discrete mappings (usually diffeomorphisms). Basic concepts are introduced where possible during the discussion of a particular topic, but for a sound background of elementary dynamical systems theory the reader is referred to Guckenheimer and Holmes (1983), Hirsch and Smale (1974) and Guckenheimer (1979). Specific examples are employed where possible to illustrate the point under discussion and we have included as many figures as possible to further illuminate the reader.

In chapter 2 we discuss chaos in higher dimensional systems. These systems are divided conveniently (following Hao (1984)) into three different groups, those being: discrete mappings of two or more dimensions (difference equations of second order or higher), ordinary differential equations (autonomous, nonautonomous and time-delayed) and partial differential equations. After the reader is introduced to the notion of a strange attractor in dissipative dynamical systems, two very important concepts associated with the geometry of the attractor are introduced. These are the structure of a Cantor set and the importance of sensitivity to initial conditions.

As well as these two factors which distinguish strange attractors from simple attractors there is a third, that being the presence of broadband noise in the power spectrum. The Rössler system (an autonomous system of ordinary differential equations), which is relatively simple and of historical importance is used to illustrate this, and more. The Lorenz system is covered in detail because of its historical significance and because information is very accessible on this system (there is a substantial volume of literature on the Lorenz system). That system is derived as a model for Rayleigh-Bénard convection (using the Gälerkin approximation) and the validity of the model is discussed. The system of Howard, Malkus and Welander is presented as an example of a system

whose behaviour is governed more precisely by the Lorenz equations. Properties of the Lorenz attractor are examined in turn followed by a summary of the evolution of the system as the parameter r (Rayleigh number) is varied.

The Van der Pol equation is introduced as a simple example of a nonautonomous system which also serves to illustrate the concept of phase locking (which is involved in chapter 5). Other important systems are mentioned. Time-delayed equations are merely touched upon. Also partial differential equations are briefly discussed since these systems have been the subject of very little experimental work.

The key example in the section on two and higher dimensional mappings is the Hénon mapping, which is studied in detail. More theoretical is the material on transverse homoclinic orbits and Smale's horseshoe. We consider these two concepts as fairly important since they are found in most of the current literature concerning experimental work on chaos, particularly the presence of horseshoes in Poincaré return maps.

Finally we look at methods for studying chaotic behaviour in dissipative dynamical systems, by dividing the methods into analytical and numerical. The analytical methods discussed are those due to Melnikov and Silnikov. The subsection on numerical methods is a brief overview, which is concluded by a table summarizing the experimental findings for a variety of systems; by various methods, taken from Hao (1984).

Chapter 3 is concerned with characterizing and classifying the attractors. After discussing why it is important to have a classification scheme for strange attractors, the various notions of dimension are introduced, i.e., Hausdorff dimension, Kolmogorov capacity and information dimension. Furthermore, a mention of box-counting algorithms is included. The correlation integral idea is looked at, as are methods

to calculate the approximate fractal dimension. A derivation of Lyapunov characteristic exponents (LCE's) is provided followed by a discussion of properties. We also look at the conjectures concerning a relationship between fractal dimension and the spectrum of LCE's. The use of LCE's in the form of signatures, as a possible classification scheme is covered. Finally we discuss LCE's for one-dimensional maps and attempts to reconstruct strange attractors numerically.

In chapter 4, we first discuss the relevance of one-dimensional maps to a study of chaos followed by examples; in particular the logistic map. Some discussion is on the definitions and terminology used in studying the maps. Mirror symmetry and periodic behaviour are covered as properties of one-dimensional mappings. Period-doubling bifurcations are discussed; and two approaches to renormalization theory are presented, that of Feigenbaum and an algebraic approach. The birth of new cycles by tangent bifurcation is examined. Chaotic behaviour, and reverse bifurcations of chaotic bands then follows. We look at counting and ordering the orbits, during which the Šarkovskii theorem and concept of U-sequences are introduced. Discussion on intermittency follows, and we finally discuss invariant distributions.

In chapter 5 we examine the various routes to turbulence. Routes suggested by Landau, Ruelle and Takens, Feigenbaum and Pomeau and Manneville are discussed.

Finally, in chapter 6, a Fourier series method is explained. This method approximates the phase-space trajectories by a Fourier series expansion and refines Fourier coefficients by iteration (Newton's method). The initial values of the coefficients are obtained from time-stepping. Using this method one can scrutinize important regions of evolution of the dynamical system more closely, i.e., nearing period-doubling bifurcations. The various calculations required are demonstrated on the spherical pendulum model of Miles (1984).

Before beginning chapter 2, we first briefly introduce the ideas of a Poincaré return map and some bifurcation theory; in particular the Hopf bifurcation.

1.3 THE POINCARÉ MAP

The systems of differential equations we shall be working with are mostly of the form:

$$\frac{d\underset{\sim}{x}}{dt} = \underset{\sim}{F}(\underset{\sim}{x}) \quad . \tag{1.1}$$

this is a system of N first order *autonomous* ordinary differential equations. The quantities $\underset{\sim}{x}$ and $\underset{\sim}{F}$ are N-vectors and $\underset{\sim}{F}$ is explicitly independent of time. The *phase space* for this system is N-dimensional, having coordinates x_i ; i = 1, N. If $\underset{\sim}{F}$ is smooth, then a *solution flow* $\underset{\sim}{x}(\underset{\sim}{x}_0, t)$ exists for all t. A point in phase space specifies a unique state of the system (1.1). In classical texts on differential equations the stability of periodic solutions is discussed in terms of *characteristic* or *Floquet multipliers*. We take a geometrical approach: the *Poincaré map*, also known as the *return map* or *Poincaré surface of section*.

Figure 1.1 shows a surface of section Σ_R in the phase space of the coordinates. The Poincaré map is found by choosing a point $\underset{\sim}{x}_n$ on Σ_R and integrating (1.1) to find the next intersection, $\underset{\sim}{x}_{n+1}$, of the trajectory with Σ_R. In this way, the map

$$\underset{\sim}{x}_{n+1} = \underset{\sim}{G}(\underset{\sim}{x}_n) \tag{1.2}$$

is constructed. $\underset{\sim}{G}$ and $\underset{\sim}{x}$ are vectors of dimension N - 1. By carrying out this procedure we are essentially replacing the integration of N-dimensional flow equations by the iteration of (N-1)-dimensional mappings. As a result, the motion of a point in phase space could be followed over extremely large numbers of oscillation periods.

If $\underset{\sim}{F}$ is smooth and Σ_R is everywhere transverse to $\underset{\sim}{F}$, then it

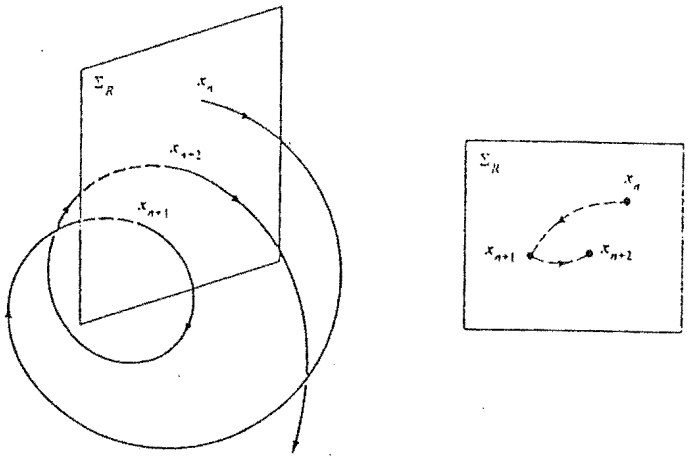

Fig 1.1. Intersections of a trajectory with the surface of section (after Lichtenberg and Lieberman, 1982).

can be shown that the Poincaré map $\underset{\sim}{G}$ is also smooth. Since the solution flow $\underset{\sim}{x}(\underset{\sim}{x}_0,t)$ exists for all times, it follows that $\underset{\sim}{G}$ is invertible i.e., one can solve (1.2) to obtain:

$$\underset{\sim}{x}_n = \underset{\sim}{G}^{-1}(\underset{\sim}{x}_{n+1}) . \tag{1.3}$$

This corresponds to generating $\underset{\sim}{G}^{-1}$ by reversing the direction at time and integrating (1.1) from $\underset{\sim}{x}_{n+1}$ to $\underset{\sim}{x}_n$, in Figure 1.1. For further information and examples, see Guckenheimer and Holmes (1983).

The definition of the Poincaré map relies on knowledge of the flow of the differential equation. Hence Poincaré maps cannot be computed unless general solutions of these equations are known.

1.4 LOCAL BIFURCATIONS

In this section, we discuss the *local* bifurcations of vector fields. An analogous theory exists for maps. Key references on bifurcation theory are Marsden and McCracken (1976), and Guckenheimer and Holmes (1983). Generally speaking, *bifurcation theory* is the study of *equilibrium solutions* of nonlinear evolution equations, and how they change with changes in the parameters of the problem. The term "bifurcation" was first coined by Poincaré to describe the splitting of equilibrium solutions in a family of differential equations. In dynamical situations

we are usually interested in equilibrium solutions of evolution equations of the form:

$$\dot{\underset{\sim}{x}} = G(\underset{\sim}{x},\lambda) = G_\lambda(x) \; ; x \in R^n, \lambda \in R^k, \tag{1.4}$$

where $\dot{\underset{\sim}{x}}$ is the velocity vector and λ is a k-dimensional parameter. An equilibrium solution is taken to mean the solution of (1.4) as x(t) evolves, after the transient effects associated with the initial values have died away. The equilibrium solutions of (1.4) are given by the solutions of the equation $G_\lambda(\underset{\sim}{x}) = 0$. Equilibrium solutions may be time invariant, time-periodic, quasi-periodic, or chaotic depending on conditions.

As the k-dimensional parameter λ is varied, the implicit function theorem implies that these equilibria are described by smooth functions of λ away from those points at which the Jacobian derivative of $G_\lambda(\underset{\sim}{x})$ with respect to $\underset{\sim}{x}$, $D_x G_\lambda$ has a zero eigenvalue. The graph of each of these functions is a branch of equilibria of (1.4). At an equilibrium $(\underset{\sim}{x}_0,\lambda_0)$, where $D_x G_\lambda$ has a zero eigenvalue, several branches of equilibria may come together, and one says that $(\underset{\sim}{x}_0,\lambda_0)$ is a *bifurcation point*.

The bifurcations we examine are termed *"local"* since the analysis of such bifurcations is generally performed by studying the vector field near the degenerate (bifurcating) equilibrium point or closed orbit. For further information on *global* bifurcation theory see Guckenheimer and Holmes (1983).

Figure 1.2 shows the only bifurcations that are present generically in one- and two-dimensional flows. These are the simplest bifurcations of equilibria. One can reduce the study of (1.4) to one of the following four differential equations which depend on a single parameter λ :

(i)	$\dot{x} = \lambda - x^2$	saddle-node (tangent)
(ii)	$\dot{x} = \lambda x - x^2$	transcritical (exchange of stability)
(iii)	$\dot{x} = \lambda x - x^3$	pitchfork

$$\text{(iv)}\quad \left.\begin{aligned} \dot{x} &= -y + x(\lambda - (x^2+y^2)) \\ \dot{y} &= x + y(\lambda - (x^2+y^2)) \end{aligned}\right\} \quad \text{Hopf} \tag{1.5}$$

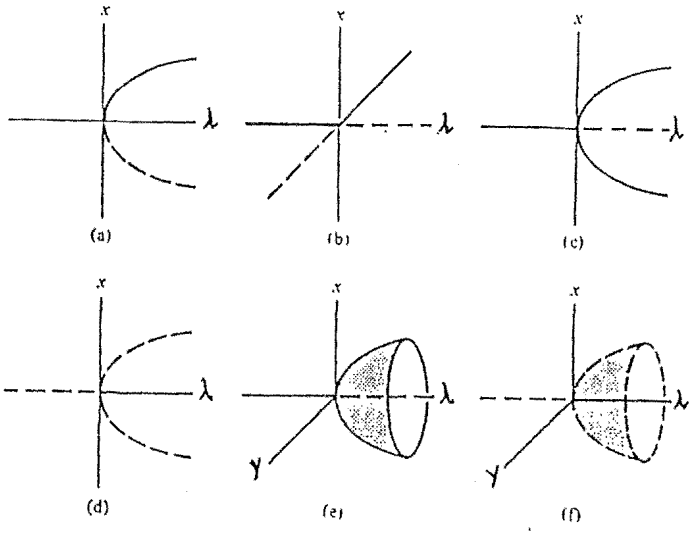

Figure 1.2 Bifurcations in one- and two-dimensional flows. (a) Tangent or saddle node: (b) Exchange of stability or transcritical; (c) pitchfork; (d) anti-pitchfork; (e) Hopf; (f) inverted Hopf. Cases (a)-(d) are generic for one-dimensional flows; cases (a)-(f) are generic for two-dimensional flows. A solid (dashed) line denotes a stable (unstable) solution. (after Lichtenberg and Lieberman, 1982).

Equation (1.4)(i) has fixed points at $x = 0$, which occur at $x = \pm \sqrt{\lambda}$. If we graph x versus λ for a fixed x and $\lambda > 0$, we see that there is a stable root $x = +\sqrt{\lambda}$ and an unstable fixed point at $x = -\sqrt{\lambda}$. For $\lambda > 0$, there are no fixed points for real x. The creation of these two fixed points as λ passes through zero, as shown in Figure 1.2 (a), is called a *saddle-node* or *tangent bifurcation*.

The *bifurcation diagram* of (1.4) is shown in Figure 1.2 (b) where there is an *exchange of stability* or a *transcritical* bifurcation. The sink (solid line) passes from the fixed point at $x = 0$ to the fixed point at $x = \lambda$ as λ passes through zero from left to right.

Equation (1.4) (iii) is shown in Figure 1.2 (c) and represents a *pitchfork bifurcation*. The sink $x = 0$ is destroyed and two new sinks at $x = \pm\sqrt{\lambda}$ are created. There can also be a reverse pitchfork bifurcation as shown in Figure 1.2 (d). Except for the nongeneric cases,

these are the only bifurcations present on one-dimensional flows.

For a two-dimensional flow within a finite section of the plane, the *Poincaré-Bendixson theorem* states that there are only two types of attractors: fixed points (sinks) and periodic solutions (limit cycles). The change from sink to limit cycle as λ passes through zero is called a *Hopf bifurcation*, and is shown in Figure 1.2 (e). The inverted Hopf bifurcation, as shown in Figure 1.2 (f) is also possible.

Figure 1.2 (a)-(f) show the only bifurcations that are present generically in two-dimensional flows. The Hopf bifurcation idea is of paramount importance in a study of chaos, particularly with respect to the models of turbulence, so we expand on the idea in the following section.

1.2 THE HOPF BIFURCATION

As we have seen, the process of generating a limit cycle from a fixed point is called a Hopf bifurcation. We now look at several physical examples to clarify the notion. The first example is by Hao (1984) and is from the realm of fluid mechanics. See Figure 1.3 (a)-(c).

When the Reynolds number R remains small enough, the fluid motion which it represents is laminar and stationary. This corresponds to a stable fixed point in phase space. A stable fixed point acts as an attractor. As the Reynolds number is increased infinitesimally larger than the first critical value R_c, the fixed point loses stability and begins to repel all trajectories. The common sense argument presented in Hao (1984) is as follows. Such a small change in R cannot cause such a drastic consequence as inverting the direction of all flows on the whole phase space. Hence the neighbourhood of the fixed point may become repelling; but it must remain attracting with respect to regions located far away. Local repulsion and global attraction of the flow requires the formation of a limit cycle around the new unstable fixed point and this curve attracts all nearby flows. The limit cycle

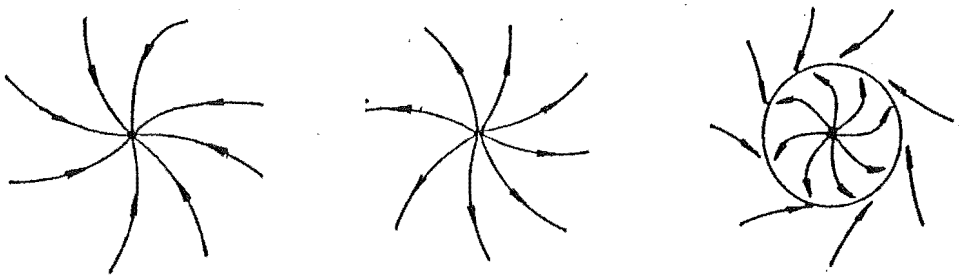

(a) (b) (c)

Figure 1.3 (a) A stable fixed point; (b) An unstable fixed point; (c) A compromise appearance of a limit cycle (after Hao,(1984)).

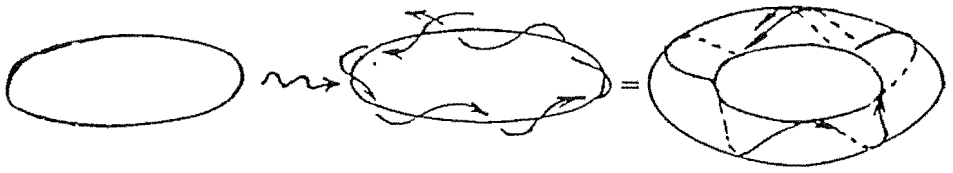

Figure 1.4 Creation of a 2-torus. (after Chapman and Tobak,(1985)).

corresponds to periodic motion of the system. This in turn can become unstable, with the limit cycle being expelled and the creation of a 2-torus as Figure 1.4.

An illuminating example is from mechanics and is presented in Marsden and McCracken (1976). The example concerns a rigid hollow sphere with a small ball inside it. The sphere hangs from the ceiling and rotates with frequency ω about a vertical axis through its center. For small ω_0, the bottom of the sphere is a stable point, but for $\omega > \omega_0$ the ball moves up the side of the sphere to a new fixed point. For each $\omega > \omega_0$ there is a stable invariant circle of fixed points. We get a circle of fixed points rather than an isolated one because of the symmetries of the problem. See Figure 1.5 (a)-(b). For further elaboration on this example, see Marsden and McCracken (1976) for references.[+]

It is possible to have *subcritical* and *supercritical* Hopf

[+]This example is due to F. Calabi

bifurcations. The bifurcation is termed subcritical if it occurs before the bifurcation value and supercritical if it occurs after the bifurcation value. See Figure 1.6 (a)-(b)

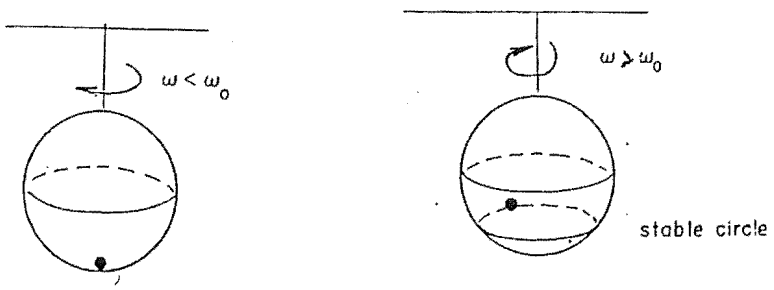

Figure 1.5 Creation of a limit cycle (after Marsden and McCracken (1976)

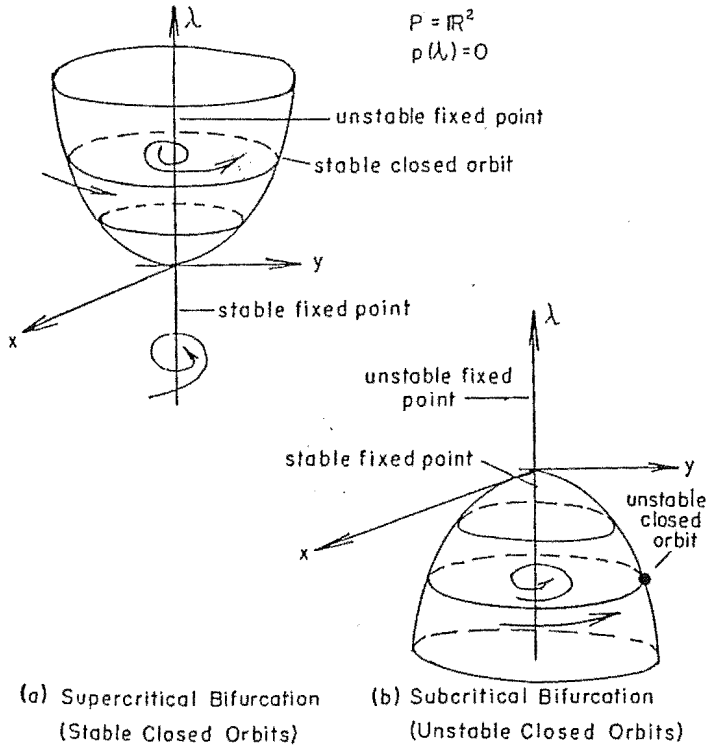

Figure 1.6 The general nature of the Hopf bifurcation (after Marsden and McCracken, 1976).

For a rigorous definition and proof of the Hopf bifurcation theorem for flows and diffeomorphisms, see Marsden and McCracken (1976). This concludes our discussion on bifurcation theory. Bifurcation theory is now highly developed and is a complex study in itself.

CHAPTER 2

CHAOS AND STRANGE ATTRACTORS IN HIGHER-DIMENSIONAL SYSTEMS

The vast majority of physical processes are described by ordinary or partial differential equations. Hence we are primarily concerned with chaotic behaviour in these higher-dimensional systems. Important to this study are one-dimensional mappings as they often provide the necessary clues for an understanding of chaotic transitions in higher-dimensional systems.

Higher-dimensional systems may be divided into three main categories: discrete mappings of two or more dimensions (difference equations of second order or higher); ordinary differential equations (ODE's, autonomous, nonautonomous, and time-delayed), and partial differential equations (PDE's).

In this chapter we first establish some background on chaos and strange attractors in dissipative systems. The theory of dynamical systems has been developed in terms of autonomous differential equations. Consequently most of our discussion is concerned with these systems. In particular, the Lorenz system, which is now generally well understood, is covered in detail. All the mathematical models presented in this chapter are encountered frequently in the current literature.

Finally, we briefly look at analytical and numerical methods used to study those systems with more emphasis on the latter.

2.1 DISSIPATIVE SYSTEMS AND CHAOS

By *Liouvilles theorem*, the motion for a Hamiltonian system conserves the volume in phase space. No such theorem exists for dissipative systems. Those systems are characterized by continued contraction of the phase-space volume with increasing time. (For bounded motions, phase-space volumes cannot, on the average expand).

For details on how to calculate this rate of volume contraction, see Lichtenberg and Lieberman (1982) or Appendix A. This leads to a contraction onto a surface of lower dimensionality than the original phase-space. The motion is generally described by a set of differential equations of the form

$$\frac{d\underset{\sim}{x}}{dt} = \underset{\sim}{G}(\underset{\sim}{x}) \tag{2.1}$$

where if $\underset{\sim}{x}$ and $\underset{\sim}{G}$ have N components, then the phase space is N-dimensional. As already mentioned, the trajectory $\underset{\sim}{x}$ is then called an N-dimensional flow.

Roughly speaking, this lower dimensional surface is called an attractor. There appears to be no universally accepted definition of an attractor. We present a definition following Lanford (1981). We call a subset X of the phase space an *attractor* if:

(i) X is invariant under the flow.

(ii) There is an open neighbourhood around X that shrinks down to X under the flow.

(iii) No part of X is transient.

(iv) X cannot be decomposed into two nonoverlapping pieces.

The set of states in phase space that approach X at $t \to \infty$, is called the *basin of attraction* of X. Frequently there are a finite number of attractors $X_1, \ldots, X_m$ for an N-dimensional flow. Cases are known however, that have infinitely many attractors. All initial states lie in the basin of one of the M attractors, except for a set of measure zero.

For regular motion the attractor of the flow represents a simple motion. For example as a fixed point *(sink)* or a singly periodic orbit *(limit cycle)*. For one-dimensional flows, the only possible attractors are stable fixed points; and for a two-dimensional flow within a finite section of the plane, the *Poincaré-Bendixson* theorem states that there

are only two kinds of attractors, those being fixed points (sinks) and periodic solutions (limit cycles).

For three-dimensional flows, as well as sinks and limit cycles, doubly periodic orbits are possible. It is, however, incorrect to reason by analogy that these are the only possible attractors in a volume contracting three-dimensional flow. It has been shown that attractors exist for dissipative flows in three or more dimensions that have very complicated geometric structures. These solutions are distinguished from regular solutions by at least three features. (Taken from Miles (1984(a))):

(i) they are exponentially sensitive to small changes in initial conditions (nearby orbits, though bounded, diverge exponentially)

(ii) their power spectra are irregular and comprise broadband components

(iii) the surfaces on which they lie in the space of the dependent variables are of fractional dimension.

This complicated set, to which nearby solutions are drawn is called a *strange attractor*.

To help visualize the strange attractor we present a thought experiment from Lichtenberg and Lieberman (1982), after Shaw (1981). Imagine a three-dimensional flow which consists of a layer containing infinitely many two-dimensional sheets. This layer expands along its width and folds over on itself, as shown in Figure 2.1 a. The two ends, labelled AB and A'B' in the sketch are smoothly joined together. Now A'B', having two distinct sheets, joins to AB, which has one distinct sheet. Hence there must be infinitely many sheets for the joining to be smooth, otherwise there would be a discontinuity yielding non-invertible flow. This infinitely leaved structure, when smoothly joined and embedded in a three-dimensional phase space is as shown in Figure 2.1 b.

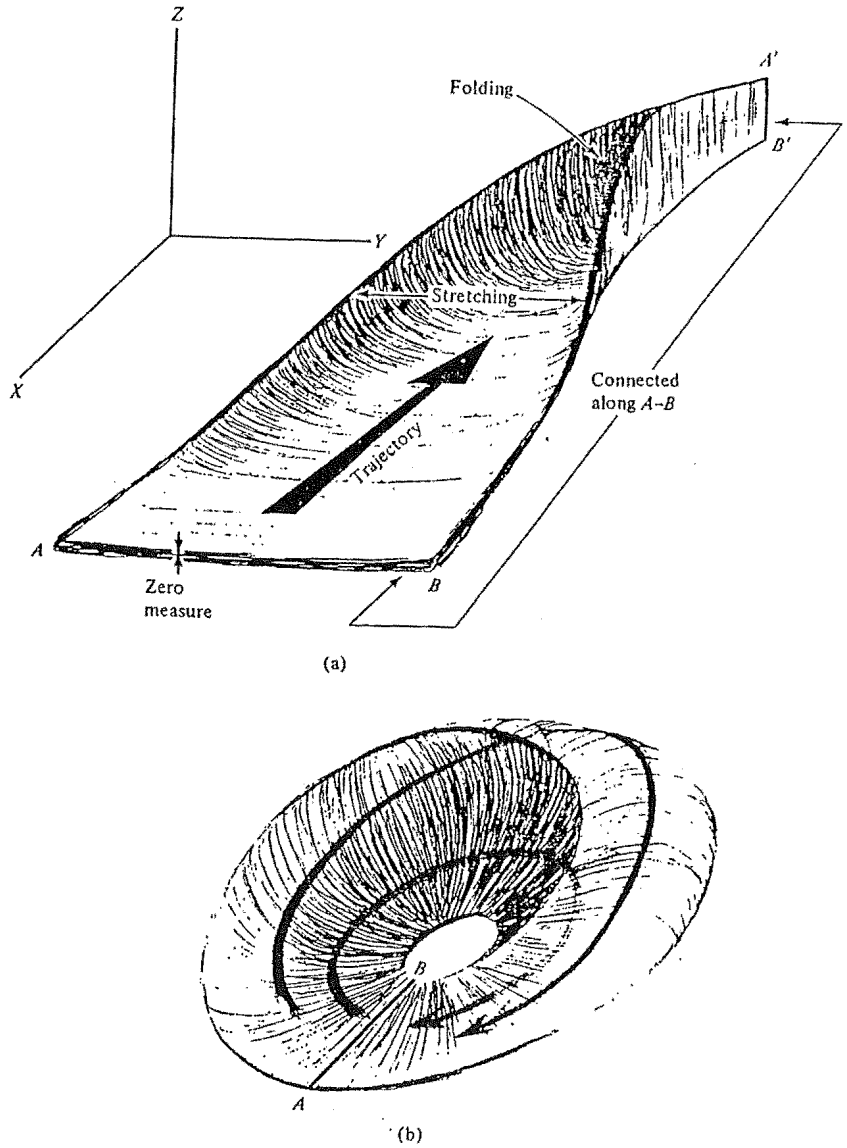

Figure 2.1 Qualitative illustration of a strange attractor.
(a) An infinite layer of ribbons is stretched and folded.
(b) The structure is joined head-to-tail and embedded in three-dimensional space. (after Shaw, 1981).

Note that the structure of the leaves is such that on finer and finer scales, this basic leaf pattern reappears. As pointed out in Lichtenberg and Lieberman (1982), this similarity on finer scales is also characteristic of the island structure of Hamiltonian systems. It serves as one of the tools for analyzing both Hamiltonian and dissipative systems. This typically leaf structure is characterized mathematically as a *Cantor set*.

Inside the attractor, as we have stated, the solutions behave in a complicated fashion which makes it impossible to predict the

location of the solution in the attractor at a large time in the future based on an approximate knowledge of its current value. This feature of these systems we call *chaotic*. This term is commonly used to describe this random motion in dissipative systems. The term *stochastic* is more often used for Hamiltonian systems. These two words are essentially synonymous and they are different by convention, not to distinguish between degrees of randomness.

Equations (2.1) (from which the strange attractor arises), are usually parametrized by some quantity whose variation changes the character of the solutions. When we change this parameter, the system may change from periodic motion to the chaotic motion on a strange attractor. Usually this change proceeds by successive period doublings of the singly periodic motion to a limiting point, after which the attractor changes character and becomes chaotic. Changing the parameter further can lead to an inverse process. Also simple attractor basins with other symmetries can appear. Another important aspect of these systems is that a surface of section can usually be found in which the motion reduces approximately, to a noninvertible mapping of a single variable. i.e., a mapping that becomes multivalued on time reversal. We discuss the importance of and properties of embedded one-dimensional mappings in detail in chapter 4.

These chaotic solutions of dissipative systems (with regular forcing) were first discovered by Lorenz in 1963, who (following Saltzman) presented an analysis on a coupled set of three quadratic ordinary differential equations representing three modes (one in velocity and two in temperature) of the Oberbeck-Boussinesq equations for fluid convection in a two-dimensional layer heated from below (Rayleigh-Bénard convection). This is fairly recent considering that the problem of unpredictability in deterministic systems without random input was posed about one hundred years ago in connection with turbulence, and Birkhoff (1927), predicted in theory at least, the existence of strange

attractors. The term "strange attractor" was coined by Ruelle and Takens (1971), who discovered the phenomenon independently of Lorenz and suggested its relevance to turbulence. As suggested by Mandelbrot (1982), a more appropriate name would be *"fractal attractor"* in view of (iii) above.

It is important to understand that chaos happens more frequently than order in nature, just as there are more irrational numbers than rationals. To quote Hao (1984) "chaos can be thought of as a new regime of nonlinear oscillations, as a compromise between competing periodicities. As an accumulation of many instabilities, as the prelude to turbulence".

It is interesting, as Miles (1984(a)) points out in his review, that historical accounts indicate that physicists seem to have tacitly assumed that dissipation eliminates the transition to chaos. Now that we have established some background on chaos and strange attractors, let us now examine the consequences of this sensitivity to initial conditions, and geometric invariance property in which the fine structure of the strange attractor repeats itself on finer and finer spatial scales.

2.2 CANTOR SETS

We now discuss a set T of real numbers, called a *Cantor* or *ternary set*, which has some remarkable properties highly relevant to the structure of the strange attractor.

A Cantor set is a compact metric space that is totally disconnected, uncountable and may have zero measure.[+] In this section we shall construct an example of a Cantor set to illustrate its properties. In the next chapter we shall look at the dimensionality of the Cantor set in depth. It typically has a fractional dimension, $0 < D < 1$ and displays rescaling invariance i.e. a subset of the set, when properly magnified, looks like the original set. Numerical results on the two-dimensional *Hénon mapping*:

[+]An alternative definition is that a Cantor set is a closed and bounded set of reals which contains no interior points or isolated points.

$$x_{n+1} = 1 - ax_n^2 + y_n$$
$$y_{n+1} = bx_n \qquad (2.2)$$

for example, indicate that the many leaved structure of the attractor repeats itself on finer and finer spatial scales. This leaved structure can be put in correspondence with a Cantor set, whose general properties then give considerable insight into the nature of the attractor. In fact this strange attractor appears to be the product of a one-dimensional manifold by a Cantor set.

We now construct an example of a Cantor set known as the "*middle-thirds Cantor set*". Trisect the closed interval $I = [0,1]$ at the points $\frac{1}{3}$ and $\frac{2}{3}$ and then delete the open interval $(\frac{1}{3}, \frac{2}{3})$, called the "middle third". Let T_1 denote the remainder of the points in I. i.e. $T_1 = [0, \frac{1}{3}] \cup [\frac{2}{3}, 1]$. Now trisect each of the two segments in T_1 at $\frac{1}{9}$ and $\frac{2}{9}$ and at $\frac{7}{9}$ and $\frac{8}{9}$ and then delete the middle third from each segment as before i.e. $(\frac{1}{9}, \frac{2}{9})$ and $(\frac{7}{9}, \frac{8}{9})$. Let T_2 denote the remainder of the points in T_1 i.e. $T_2 = [0, \frac{1}{9}] \cup [\frac{2}{9}, \frac{1}{3}] \cup [\frac{2}{3}, \frac{7}{9}] \cup [\frac{8}{9}, 1]$. We continue indefinitely in this way constructing $T_3, T_4, \ldots$ and obtain a descending sequence of sets $T_1 \supset T_2 \supset T_3 \supset \ldots$, where T_n consists of the points in T_{n-1} excluding the middle thirds as shown in Figure 2.2. Note that T_n consists of $M = 2^n$ disjoint closed intervals, each of length $\varepsilon = \frac{1}{3^n}$. By numbering them from left to right, we can speak of the odd or even intervals in T_n. The Cantor set is the intersection of all these sets i.e. $T = \cap \{T_i, i \in \mathbb{N}\}$. (Loosely speaking, the intersection is the "limiting T_i"). We can now look at some of the properties of this Cantor set.

(a) T has "measure zero" since the measure of the complement of T relative to $I = [0,1]$ (the union of all the middle thirds) equals $\frac{1}{3} + \frac{2}{9} + \frac{4}{27} + \ldots + \frac{2^{n-1}}{3^n} + \ldots = 1$, but the measure of $I = [0,1]$ is also 1.

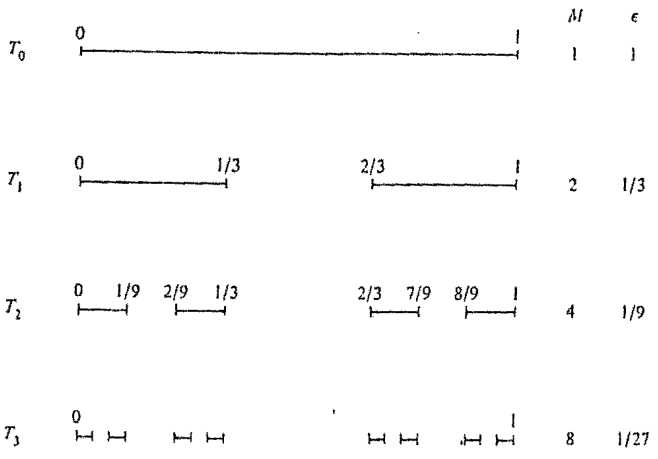

Figure 2.2 The construction of a Cantor set, with some values of the number M of line segments of length ε required to cover the set T_n.

(b) We can show T is uncountable (nondenumerable) as follows:

For any real number x between 0 and 1, there is a "decimal expansion" of x written to the base 3.

i.e. $x = a_1(\frac{1}{3}) + a_2(\frac{1}{9}) + a_3(\frac{1}{27}) + \ldots + a_m(\frac{1}{3^m}) + \ldots$, where a_i is one of the values 0 or 2. If any $a_i = 1$, then by construction x is excluded from T_i* and hence x is not in T_i. Thus all x's in T can be written as a sequence of 0's and 1's; hence they can be put in a one-to-one correspondence with the binary representation of the real numbers between 0 and 1, which has cardinality $2^{N_0} = c$, where N_0 is aleph null and c is the power of the continuum.

(c) the "fractal dimension" of T is $D = \lim_{n\to\infty} \frac{\ln 2^n}{\ln 3^n} = 0.630$.
(This will be clarified in chapter 3).

2.3 THE IMPORTANCE OF SENSITIVITY TO INITIAL CONDITIONS

We shall now discuss the importance and consequences of dynamical systems showing macroscopic sensitivity to initial conditions. To make the discussion more concrete let us follow the example put forward by Yorke and Yorke (1979).

This sensitivity to initial conditions property has consequences

*Sequences such as 0.1222... = 0.2000... are excluded.

on both the experimental and computational levels. As an example of an insensitive system we consider the simple pendulum. Two pendulums are started out with slightly different initial positions and velocities. The trajectories in phase space are followed as time increases i.e. $(x,\dot{x})$ space. It follows that the trajectories will remain close to each other for all time.

On the experimental level, this means that each time the experiment is conducted, a similar description of the detailed behaviour of the system will result. This is provided we have sufficient fine control of the conditions. Small (uncontrollable) errors in the initial conditions and the presence of noise during the experiment will not cause substantial deviations in the measurements. On the other hand in systems which are sensitive to initial conditions, small changes in initial conditions will lead to large and unpredictable changes in the long-term evolution of the system. Two trajectories starting out close together, will depart exponentially from each other, and hence no long-term pattern can be discerned. An experimentalist would find a different pattern during each run.

Computationally, the insensitive system is well-behaved compared to the sensitive system. In the case where numerical calculations must be performed, small errors like roundoff need not increase with time in the insensitive system. We can safely predict that trajectories starting in the same neighbourhood as that of a known trajectory will be similar in the long-term. For a sensitive system, computations of long-term behaviour will be critically affected by small errors.

As we have already mentioned, systems exhibiting sensitivity to initial conditions occur more frequently in nature than nonsensitive systems. In this sense, sensitivity to initial conditions is a generic property of dissipative dynamical systems. The most important natural system with this sensitivity to initial conditions may be the atmosphere. This idea was first put forward by Lorenz in his paper "*Deterministic*

Nonperiodic Flow; a pioneering paper from which all the recent interest in chaos was generated. The consequences of this sensitivity on long-range weather forecasting in meteorology are far reaching. Even if substantial advancements were made in modelling and data collection, it would be doubtful that accurate weather forecasts could be made even a few weeks in advance.

2.4 THE RÖSSLER ATTRACTOR

So far we have seen that the fractional dimensionality of the strange attractor comes about because of its local Cantor set structure and that flows on this attractor are exponentially sensitive to initial conditions. These are two of the features listed in section 2.1 which distinguish strange attractors from simple attractors. The Rössler system serves to illustrate the third feature on that list i.e. the presence of *broadband noise* in the power spectrum. This system shall also be used to follow the evolution of a dissipative system and to view the associated changes in phase-space and power spectra. It also serves to illustrate the importance of embedded one-dimensional mappings.

Due to the behaviour of the Lorenz model being fairly complicated, Rössler attempted to construct a strange attractor which was as simple as possible but still exhibiting chaotic behaviour. The simplest of his models is the following autonomous system which contains only one quadratic nonlinear term:

$$\begin{aligned} \dot{x} &= (y + z) \\ \dot{y} &= x + \alpha y \\ \dot{z} &= \beta + xz - \gamma z \,. \end{aligned} \tag{2.3}$$

For this discussion we fix $\alpha = \frac{1}{5}$, $\beta = \frac{1}{5}$ and vary γ.

For a wide class of dissipative systems the transition to chaos proceeds via a sequence of period-doubling bifurcations that converge at some limiting value of the parameter. Past this particular value, we generally find chaotic behaviour superimposed on a reverse bifurcation

sequence with period-halving on successive bifurcations. Figure 2.3 illustrates these bifurcations for the Rössler attractor. In Figure 2.3 (a), we start with $\gamma = 2.6$. Here the attractor is a simple limit cycle. In Figure 2.3 (b),(c) show the period-doubling bifurcations. Observe that the power spectra are sharply peaked. This is a characteristic feature of regular motion. The transition to chaos occurs near $\gamma_\infty = 4.20$. Figure 2.3 (d),(e) and (f) show the strange attractors for $\gamma > \gamma_\infty$, which appear as chaotic bands that lie between the regular trajectories shown previously. The power spectra consist of an overlap of broadland noise due to the chaotic component and sharp peaks due to the periodic component of the motion. One can also see the reverse bifurcations and their period-halvings.

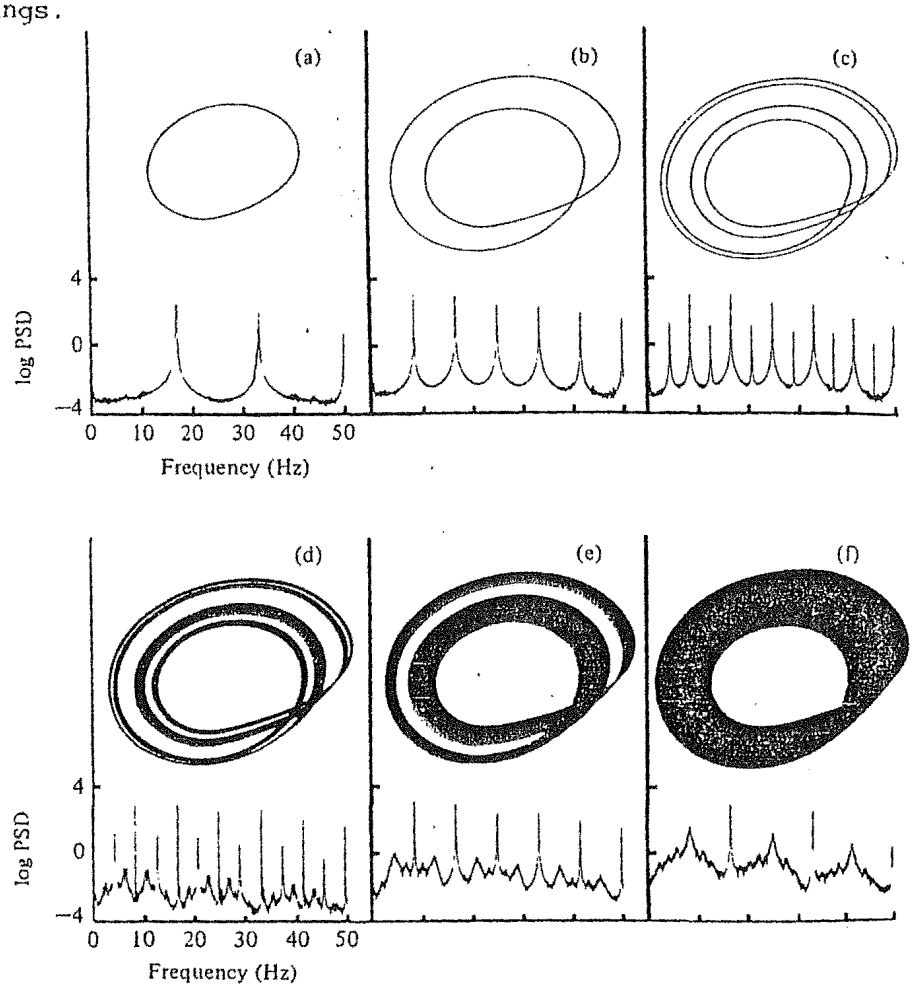

Figure 2.3 Period-doubling bifurcations of the Rössler attractor projected onto the x-y plane, along with the corresponding power spectral density of z(t).
(a) $\gamma = 2.6$ (b) $\gamma = 3.5$ (c) $\gamma = 4.1$ (d) $\gamma = 4.23$
(e) $\gamma = 4.30$ (f) $\gamma = 5.60$
(after Crutchfield et al., 1980)

Figure 2.4 (a) shows an analog computer situation of (2.3) for $\gamma = 5.7$. Projecting the attractor onto the X-Y plane yields a structure closely resembling Figure 2.4 (b), when viewed from above. Take a section across the attractor as shown in Figure 2.4 (a). If we now plot x at the $(n+1)$st crossing as a function of x at the nth crossing, we obtain approximately the one-dimensional noninvertible map shown in Figure 2.4 (b). Chaotic motion on the attractor is described (approximately) by the dynamics of the map for x. This reduction from three-dimensional to one-dimension is only approximate. The volume contraction rate for this attractor (and many others) is so large, that all the leaves appear merged into one in any simulation. The line in Figure 2.4 (b) should be thickened since the layer sectioned at $y = 0$ actually contains infinitely many leaves. The one-dimensional map preserves most of the behaviour of the original flow. One-dimensional mappings are much simpler analytically, and less expensive computationally to deal with. Hence we can learn much about a higher order system by considering the associated one-dimensional mapping.

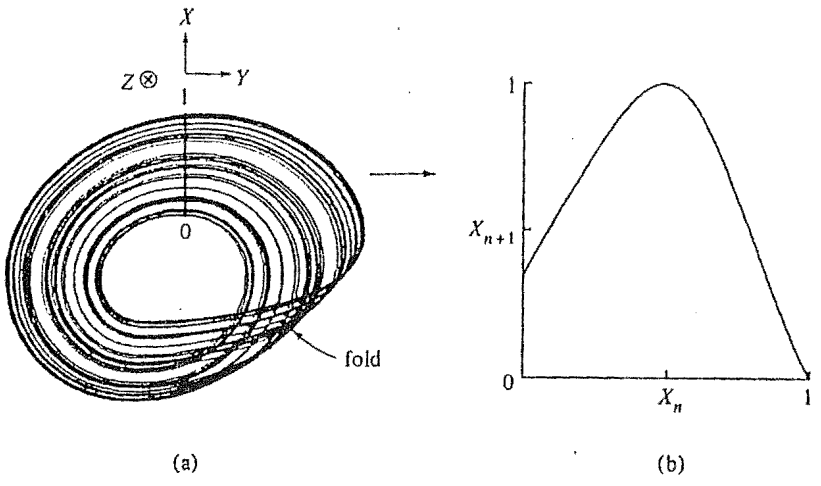

Figure 2.4 The Rössler attractor
(a) Projection of the motion onto the X-Y plane;
(b) one-dimensional map, generated by successive intersections of the projected flow with surface of section Y = 0 (after Shaw, 1981)

The chaotic bands discussed earlier form a hierarchy. The interested reader is referred to Hao and Zhang (1982), who found that

embedded in the chaotic bands of the primary bifurcation sequence there are many secondary sequences within which tertiary sequences of similar structure exist. The model used was a forced limit cycle oscillator (the *Brusselator*).

Also the scaling of the bifurcation sequence as a parameter is varied, and the shape of the power spectrum, are universal near the transition point γ_∞. Having now looked at each of the three distinguishing features of strange attractors in chaotic systems, we are now ready to look at one system in detail: the Lorenz system.

2.5 AUTONOMOUS SYSTEMS

As mentioned earlier, we can divide systems of ODE's exhibiting chaotic behaviour into three groups, one of which is autonomous systems with three or more variables. Recall that a system of ODE's is called *autonomous* when there is no explicit time dependence on the right hand side of the standard form:

$$\frac{dx_i}{dt} = G_i(x_1, \ldots, x_N) \qquad i = 1,2,\ldots, N. \tag{2.4}$$

To make clear why at least three variables are required to allow chaotic behaviour. We present an argument put forward by Hao (1984). Taking period-doubling as the first step leading to chaos, there is no reason for a trajectory to radically change at an infinitesimal increase of the parameter value. Still, the period T doubles to 2T. The only concievable possibility is an almost imperceptible splitting of the original orbit. Now if this takes place in the plane, then there must be at least one point where the orbit intersects with itself and thus violates the uniqueness of the solution. The systems of ODE's under consideration are usually good enough to ensure the validity of the uniqueness theorem. Therefore, the splitting of a trajectory without self-intersection is only possible in three- and higher-dimensional space. The bifurcations and development of chaotic orbits thereafter follow the same rule.

2.6 THE CONVECTION MODEL OF LORENZ

In 1963, E.N. Lorenz (1963), a meteorologist working on the basis of earlier results due to B. Saltzman (1962) wrote a remarkable paper which was in many ways ahead of its time. Lorenz was searching for a three-dimensional set of ODE's which would model some of the unpredictable behaviour associated with the weather. This search is described in Lorenz (1979). The equations he eventually obtained were derived from a mathematical model of fluid convection. We shall derive these equations from first principles. We follow the derivation presented in Lichtenberg and Lieberman (1982). The equations are as follows:

$$\begin{aligned} \frac{dx}{dt} &= \sigma(y - x) \\ \frac{dy}{dt} &= rx - y - xz \\ \frac{dz}{dt} &= xy - bz \,. \end{aligned} \tag{2.5}$$

The meanings of the quantities x,y, and z, and the parameters σ,r and b will be made clear in the derivation we present later. Notice that the Lorenz equations are *deterministic*. They contain no random, noisy or stochastic terms and they determine a unique flow which is valid for all time. These equations have been studied by many authors since 1963, with well over 50 articles in print. A solution of the Lorenz system is presented in Figure 2.5 (a), along with the associated power spectrum, which is shown in Figure 2.5 (b). Before deriving the equations from a model of Rayleigh-Bénard convection, we discuss the truncation procedure which will be employed in that derivation.

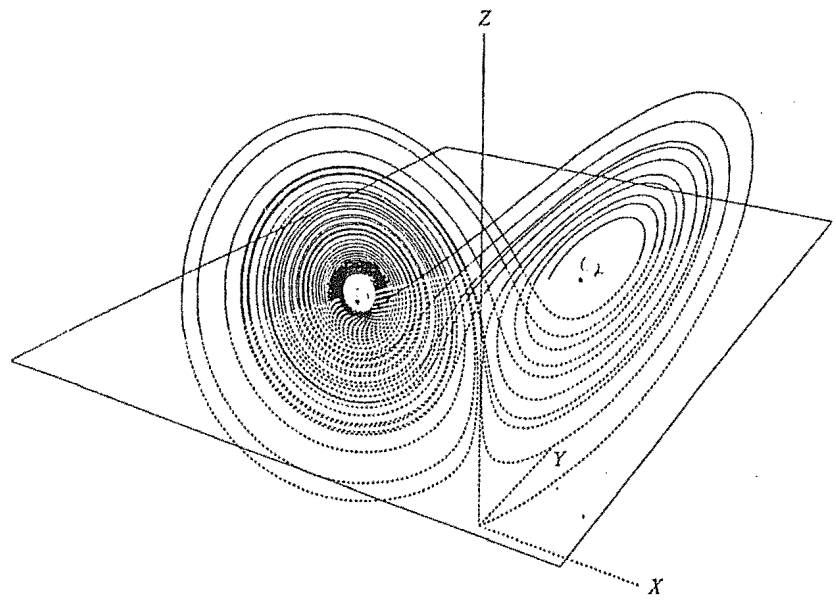

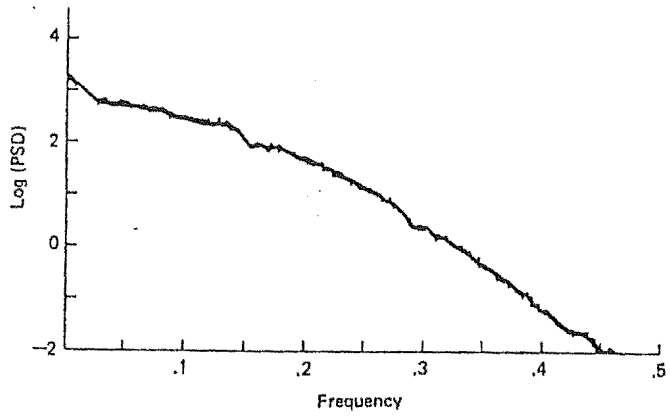

Figure 2.5
(a) A chaotic trajectory for the Lorenz attractor at r = 28; the horizontal plane is at z = 27 (after Lanford, 1977)
(b) Power spectrum of X(t) in the Lorenz attractor at r = 28. Here the lowest frequencies have the highest power. Such a "continuous" spectrum reflects the nonperiodic chaotic behaviour on the attractor (after Crutchfield et al., 1980)

2.6a THE GÄLERKIN APPROXIMATION

The following background theory is taken from Lichtenberg and Lieberman (1982). Let us consider motion in fluid systems or other infinite dimensional systems described by PDE's of the following form:

$$\frac{\partial \zeta(x,t)}{\partial t} = \eta(x)\zeta(x,t) \qquad (2.6)$$

where ζ = k-dimensional vector which specifies the state of the fluid systems for example, pressure $P(x,t)$, fluid velocity $v(x,t)$, mass density $p(x,t)$.

$x(t)$ = configuration space, with components x,y and z in three dimensions.

$\eta(x)$ = nonlinear differential operator which is independent of time.

When studying the behaviour of (2.6), it is a common technique to Fourier analyze ζ into mode amplitudes:

$$\zeta(x,t) = \sum_j \ell_j(t) e^{ij\cdot x} \tag{2.7}$$

where

$$\ell_j(t) = \frac{1}{(2\pi)^3} \int d^3x \cdot \zeta(x,t) \cdot e^{ij\cdot x} . \tag{2.8}$$

Substituting (2.7) into (2.6) and using the orthogonality of the exponential functions $e^{ij\cdot x}$, for each mode ℓ_j, we obtain an equation of form:

$$\dot{\ell}_j = Z_j(\ell_1, \ldots, \ell_j) \tag{2.9}$$

where $\dot{} = \frac{\partial}{\partial t}$.

Now if only the M "most important modes" in the summation (2.7) are retained, then (2.9) is a set of $M \cdot k$ first order ODE's describing the evolution in time of the mode amplitude components.

This technique of Fourier analysis followed by truncation is usually called the *Gälerkin approximation*. Applying this procedure to Rayleigh-Bénard convection, and deriving an extreme truncation which keeps only the three "most important modes" leads to the Lorenz equations.

2.6b RAYLEIGH-BÉNARD CONVECTION

The problem is depicted in Figure 2.6 (a). Rayleigh (1916) studied a model in which a fluid slab is heated from below. A temperature difference ΔT is maintained between the hot lower surface and the cold top surface. The separation of the boundaries is denoted by h, and gravity

acts downward. We assume only two-dimensional motion $\left(\frac{\partial}{\partial z} \equiv 0\right)$. The original problem is governed by the following four PDE's: two components of the Navier-Stokes equation in the Boussinesq approximation, with the buoyancy force included in the vertical component, the equation of continuity, and the heat conduction equation. Define a stream function $\psi(x,y,t)$ for the motion, such that the fluid velocity $\underset{\sim}{u}(x,y,t)$ is:

$$\underset{\sim}{u} = \nabla X(z\psi) \ . \tag{2.10}$$

Define θ to be the departure of temperature from that occurring in the state of no convection, which decreases linearly with the height y, i.e.;

$$\theta = T - \frac{\Delta T y}{h} \ . \tag{2.11}$$

(So $\theta = 0$ if the fluid has no convection)

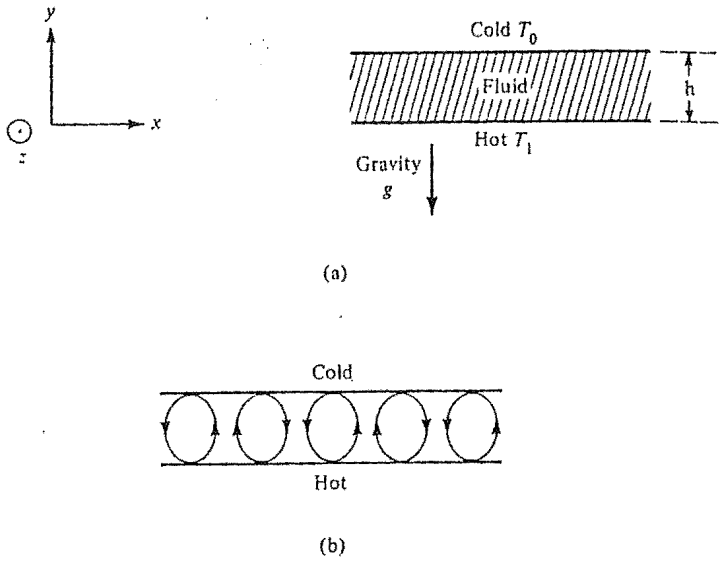

Figure 2.6 The Rayleigh-Bénard convection problem from which the Lorenz system is derived.
(a) Fluid system with $\Delta T = T_1 - T_0 > 0$
(b) Steady convection for $\Delta T \gtrsim \Delta T_0$.
(after Lichtenberg and Lieberman, 1982).

The four PDE's are reduced to the following two PDE's through the introduction of these quantities:

$$\frac{\partial}{\partial t}(\nabla^2\psi) = \frac{\partial(\psi,\nabla^2\psi)}{\partial(x,y)} + \gamma\nabla^4\psi + g\alpha\frac{\partial\theta}{\partial y} \tag{2.11a}$$

$$\frac{\partial}{\partial t}(\theta) = \frac{\partial(\psi,\theta)}{\partial(x,y)} + \frac{\Delta T}{h}\frac{\partial \psi}{\partial y} + \kappa\nabla^2\theta \qquad (2.11b)$$

where γ = kinematic viscosity, g = acceleration due to gravity, α = thermal expansion coefficient and κ = thermal conductivity. Take both the upper and lower boundaries to be free so that $\psi = 0$ and $\nabla^2\psi = 0$ at both surfaces.

When ΔT is small, the system possesses the steady state solution $\psi = 0$, $\theta = 0$. i.e., the fluid is stationary with heat being transported from the bottom to the top surface by thermal conduction. Linear stability analysis shows that above a critical value ΔT_c, the solution is unstable, and a new equilibrium is established. This is characterized by stable circulating flow. See Figure 2.6 (b).

Rayleigh found that fields of motion of the form:

$$\psi = \psi_0 \sin\left(\frac{\pi a x}{h}\right) \sin\left(\frac{\pi y}{h}\right) \qquad (2.12a)$$

$$\theta = \theta_0 \cos\left(\frac{\pi a x}{h}\right) \sin\left(\frac{\pi y}{h}\right) \qquad (2.12b)$$

would develop if the Rayleigh number (what is now known as the Rayleigh number) exceeded a certain critical value. The Rayleigh number is defined to be the quantity:

$$R_a = \frac{g\alpha h^3 \Delta T}{\gamma\kappa} \qquad (2.13)$$

which is a dimensionless measure of the temperature difference. The parameter a characterizes the wavelength along x and is called the *aspect ratio*. ΔT_c has a minimum value at $a = \frac{1}{\sqrt{2}}$. The critical Rayleigh number is defined as:

$$R_c = \frac{\pi^4 (1 + a^2)^3}{a^2} \qquad (2.14)$$

and it takes a minimum value of $\frac{27\pi^4}{4}$ at $a = \frac{1}{\sqrt{2}}$.

Increasing R_a further above R_c, one finds that the steady convection equilibrium becomes linearly unstable. Experimentally, for this value

of R_a, one finds that the convection takes place in an irregular, unsteady or chaotic manner.

Saltzman (1962) expanded ψ and θ in *double Fourier series* in x and y, with functions of t alone for coefficients, and substituted these series in (2.11a,b). He rearranged these equations and equated coefficients of similar functions in x and y. He then truncated the series to a finite number of terms, thus obtaining the motion in the finite dimensional phase-space of Fourier coefficients. Saltzman's truncation was initially at 52, then finally at 7 terms. He found solutions with chaotic behaviour numerically. Lorenz decided that these same solutions would have been obtained if the series had been truncated at the start to only three terms. Lorenz took the following simplified system in which only three Fourier coefficients were kept:

$$a(1+a^2)^{-1}\kappa^{-1}\psi = \sqrt{2}\, X(t) \sin\left(\frac{\pi a x}{h}\right) \sin\left(\frac{\pi y}{h}\right) \tag{2.15a}$$

$$\pi R_c^{-1} R_a (\Delta T)^{-1}\theta = \sqrt{2}\, Y(t) \cos\left(\frac{\pi a x}{h}\right) \sin\left(\frac{\pi y}{h}\right) - z(t)\left(\frac{2\pi y}{h}\right) \tag{2.15b}$$

where X,Y,Z are dimensionless Fourier amplitudes with:

X = rate of convective overturning

Y = temperature difference between ascending and descending currents.

i.e., similar signs on x and y mean that cold water is descending and warm water rising

Z = distortion of the vertical temperature profile from linearity.

Substituting these forms into the vorticity and heat conduction equations (2.11a,b) yields the following three, first-order nonlinear ODE's:

$$\begin{aligned} \dot{X} &= -\sigma X + \sigma Y \\ \dot{Y} &= -YZ + rX - Y \\ \dot{Z} &= XY - bZ \end{aligned} \tag{2.16}$$

where the dot represents differentiation with respect to the normalized time:

$$\tau = \pi^2 h^{-2}(1+a^2)\kappa t \qquad (2.17)$$

these are the Lorenz equations. Usually σ and b are fixed and the system is studied as r is varied. Usually $\sigma = 10$ and $b = \frac{8}{3}$. The meanings of the parameters are as follows:

$\sigma = \frac{\gamma}{\kappa}$ is the Prandtl number

$b = \frac{4}{(1+a^2)}$ is a geometry factor and

$r = \frac{Ra}{R_c}$ is the normalized Rayleigh number.

2.6c CORRECTNESS OF THE MODEL

These results by Lorenz suggest that complicated chaotic (or turbulent) behaviour in systems with an infinite number of degrees of freedom (like the atmosphere) may be modelled by simple deterministic finite-dimensional systems. This is perhaps why the Lorenz equations have generated so much interest. The existence of a relationship between chaotic behaviour in the real world and turbulent behaviour in finite dimensional systems has yet to be established. Whether or not the Lorenz equations are a valid model of fluid convection is irrelevant to this debate.

We now require to see in what sense the exact solution to the Rayleigh-Bénard convection problem behaves like the Lorenz system i.e., for the same initial flow, do both systems tend to the same final state as $t \to \infty$. In fact, the three-mode truncation only accurately reflects the dominant convective properties of the fluid near Rayleigh number $r = 1$. Realistic results may also be obtained when the Rayleigh number is slightly supercritical, but the results are inaccurate when strong convection occurs. As the Rayleigh number increases, higher-order modes become important and predictions made on the basis of the three mode truncation are of doubtful physical relevance. Lorenz (1979) himself admits that the equations are not a realistic model if the Rayleigh number r is far from unity. Truncated equations with 4,5,6,7 or more modes retained have been suggested, among which are the following

two-parameter family of seven-mode equations:

$$\begin{aligned}
\dot{x}_1 &= -\ 2x_1 + 4\sqrt{5}\ x_2x_3 + 4\sqrt{5}\ x_4x_5 \\
\dot{x}_2 &= -\ 9x_2 + 3\sqrt{5}\ x_1x_3 \\
\dot{x}_3 &= -\ 5x_3 - 7\sqrt{5}\ x_1x_2 + 9\ \epsilon\ x_1x_2 + R \\
\dot{x}_4 &= -\ 5x\ \ - \sqrt{5}\ x_1x_5 \\
\dot{x}_5 &= -\ x_5 - 3\sqrt{5}\ x_1x_4 + \ 5\ \epsilon\ x_1x_6 \\
\dot{x}_6 &= -\ x_6 - 5\ \epsilon\ x_1x_5 \\
\dot{x}_7 &= -\ 5x_7 - 9\ \epsilon\ x_1x_3 \ .
\end{aligned} \qquad (2.17(a))$$

these permit a continuous transition from five-mode (t = 0) to a seven-mode (t = 1) model. Both these systems are well studied in the literature.

Systematic extensions of the Lorenz equations to these higher-mode truncation exhibit behaviour with some features similar to that of the Lorenz system, in particular the presence of strange attractors. Calculations by McLaughlin and Martin (1975) and Curry (1978) have shown that higher-order truncations of, or changes of the Prandtl number in the Rayleigh-Bénard problem, alter the bifurcation sequence that leads to chaos. Numerical solutions of the Rayleigh-Bénard equations in two dimensions, from which the Lorenz equations are derived, by Moore and Weiss (1973), are regular. This implies that chaotic solutions of the two-dimensional Rayleigh-Bénard problem are an artefact of truncation. This is in distinction to three-dimensional Rayleigh-Bénard convection for which turbulence is experimentally observed. Marcus (1981) has examined in considerable detail the effects of truncation for spherical convection, and concludes that the bifurcation sequence may be sensitive to the order of truncation and that the number of modes required for an accurate representation of the original problem tends to increase with r.

We can also view this problem in terms of the Navier-Stokes equations. It has been shown by Foias and Prodi (1967) that the two-dimensional solutions to the Navier-Stokes equations can be described in

the limit $t \to \infty$ by a finite number N_2 of Fourier modes. This result has been extended to the three-dimensional solutions, with $N_3 \alpha N_2^3$ (Foias and Treve (1981)). Hence for a fixed set of parameters and initial flow and for some minimum N_2 (or N_3), one is assured that the Gälerkin expansion will yield all physically relevant properties of the actual flow. Treve (1981) has put forward a numerical test to determine post facto whether the number of modes used exceeds the required value of N_2 (or N_3). As already mentioned, there is no procedure yet known to determine a priori the required value.

We conclude this section with the following quote from Yorke and Yorke (1979):

"Lorenz's severely truncated system seems similarly to have lost all of its wetness, all the properties of the fluid except chaos, the same equations could conceivably arise in many situations that have nothing to do with fluid dynamics".

2.6d THE HOWARD-MALKUS-WELANDER CONVECTION MODEL

The severe truncations for the description of Rayleigh-Bénard convection by the Lorenz equations raises the question of whether these equations have any direct physical relevance whatsoever. Systems have been established to which the Lorenz equations bear direct relevance. We examine a convection loop model from which the Lorenz equations can emerge in some circumstances. We follow the discussion in Yorke and Yorke (1979), since it is relatively general. See also Malkus (1972), Miles (1984) and Welander (1967). Welander (1967) had obtained numerical solutions for a convection loop model and these solutions exhibited bursts of periodic and aperiodic flow. The following model is a modified version of this, considered by Howard and Malkus (1972). We follow the derivation given in Yorke and Yorke (1979).

A toroidal tube of cross-sectional area A and mean radius ℓ that is filled with an incompressible fluid of density ρ_0 at temperature

T_0, is orientated vertically in a uniform gravitational field $\underset{\sim}{g}$. See Figure 2.7. We assume that the density of the fluid depends linearly on the temperature as:

$$\rho = \rho_0 [1 - \alpha(T - T_0)], \quad \alpha > 0 \tag{2.18}$$

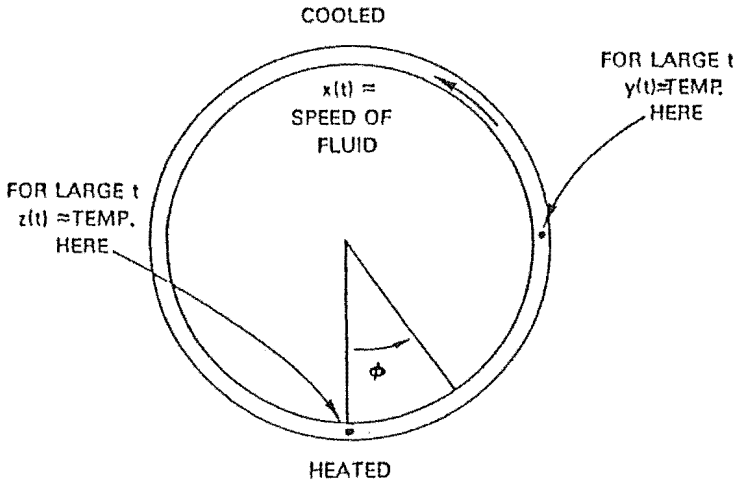

Figure 2.7 Fluid-filled tube, a physical model for the derivation of Lorenz's equations. (after Yorke and Yorke 1979)

where α is the coefficient of thermal expansion. Angular distance around the tube, ϕ, is measured clockwise from the direction of $\underset{\sim}{g}$. We shall maintain the walls of the tube at some time-independent, and angle dependant, temperature $T_W(\phi)$, which we shall specify. The bottom will be warmer than the top. Various approximations are now made (refer to Yorke and Yorke (1979) for these details).

The equation of motion of the fluid is:

$$\rho_0 \frac{\partial v_1}{\partial t} = - \nabla P + [\rho_0 + \alpha\rho_0(T_0 - T)]\underset{\sim}{g} + \underset{\sim}{f}_{fr} \tag{2.19}$$

where P is the pressure, $\underset{\sim}{v}$ is the fluid velocity, and $\underset{\sim}{f}_{fr}$ is the frictional force opposing the flow. The heat transfer equation, assuming thermal conduction is negligible in comparison to convection is:

$$\frac{\partial T(\phi,t)}{\partial t} + \frac{q}{n\ell}\frac{\partial T(\phi,t)}{\partial \phi} = k[T_W(\phi) - T(\phi,t)] \tag{2.20}$$

where $q(t)$ is the instantaneous flow rate and k a constant. Also the relation:

$$\frac{\partial q(t)}{\partial t} = \frac{A\alpha g}{2\pi}\int_0^{2\pi} T(\phi,t)\sin\phi d\phi - Rq(t) \tag{2.21}$$

can be derived (see Yorke and Yorke (1979)).

We now proceed to expand T_W and T in Fourier series in ϕ, noting that the coefficients in the expansion for T are time-dependent. The expansions are:

$$T(\phi,t) = C_0(t) + \sum_{n=1}^{\infty}[S_n(t)\sin n\phi + C_n(t)\cos n\phi] \tag{2.22a}$$

$$T_W(\phi) = W_0 + \sum_{n=1}^{\infty}[V_n \sin n\phi + W_n\cos n\phi] \tag{2.22b}$$

Now inserting these expansions into (2.21) and (2.20) and solving for the coefficients yields an infinite set of ODE's.

$$\frac{dq}{dt} = \frac{A\alpha g}{2} S_1 - Rq \tag{2.23}$$

$$\begin{cases} \dfrac{dS_1}{dt} - \dfrac{q}{A\ell} C_1 = k(V_1 - S_1) & (2.24a) \\ \dfrac{dC_1}{dt} + \dfrac{q}{A\ell} S_1 = k(W_1 - C_1) & (2.24b) \end{cases}$$

and

$$\begin{cases} \dfrac{dS_n}{dt} - \dfrac{nq}{A\ell} C_n = k(V_n - S_n) & (2.25a) \\ \dfrac{dC_n}{dt} + \dfrac{nq}{A\ell} S_n = k(W_n - C_n) & (2.25b) \end{cases}$$

Equations (2.23) and (2.24) are coupled to each other. These three equations determine the instantaneous flow rate q. The flow of the fluid is governed by the $n = 1$ Fourier components since q appears only as a time-dependent coefficient in (2.24). Fortunately in this case the Fourier series uncouple when using the common technique to approximate solutions of PDE's. The coefficients usually do not uncouple, and the infinite set of equations for the derivatives of any finite collection of the Fourier series coefficients involves other coefficients outside its collection. In this case we have the "closure problem" i.e., the question of how to obtain a closed set of equations.

Now non-dimensionalize (2.23)-(2.25) via the following change of variables: Let $Y = \dfrac{q}{2kR}$ and introduce the dimensionless variables $\sigma = \dfrac{R}{k}$, $\tau = kt$, $x = \dfrac{q}{kA\ell}$, $y = YS_1$, $r = YW_1$, $r' = YV_1$, and

$z = r - YC_1$. For $n \neq 1$, $y_n = YS_n$, $r_n = YW_n$, $r_n' = YV_n$, and $Z_n = YC_n$. The result is:

$$\begin{cases} \dfrac{dx}{d\tau} = \sigma(y - x) \\ \dfrac{dy}{d\tau} = -y + rx - zx + r' \\ \dfrac{dz}{d\tau} = xy - z \end{cases} \tag{2.26}$$

$$\begin{cases} \dfrac{dy_n}{d\tau} = n x z_n + r_n' - y_n \\ \dfrac{dz_n}{d\tau} = -n x y_n - z_n + r_n \end{cases} , \quad n > 1 \tag{2.27}$$

$$\frac{dz_0}{d\tau} = r_0 + z_0 \tag{2.28}$$

Now if $r' = 0$, (2.26) reduces to the Lorenz equations with $b = 1$. This parameter r', when non zero, breaks the clockwise versus counter-clockwise symmetry. A brief investigation of the situation when $r' \neq 0$, shows that the fluid circulates preferentially by rising on the heated side (determined by the sign of r'). For a small range of values of r' (and for $r > 2$), the solutions are sensitive to initial conditions, with a bias towards circulation in the preferred direction.

Thus the Lorenz equations have a direct correspondence to a laboratory-reproducible system without the uncertainties implied by truncation in Lorenz's original model. Other systems are known to share this property. For a mechanical model which is described by the Lorenz equations, see Coullet (1979). Also Professor W. Malkus has constructed a laboratory water wheel whose equations of motion are the Lorenz equations. The derivation can be found in Sparrow (1982), which incidentally is one of the leading monographs on the Lorenz system.

2.6e PROPERTIES OF THE LORENZ EQUATIONS

(i) Topological Structure

As shown in Figure 2.8(a), the Rossler attractor has the simple structure of a sheet that has been stretched, folded over once,

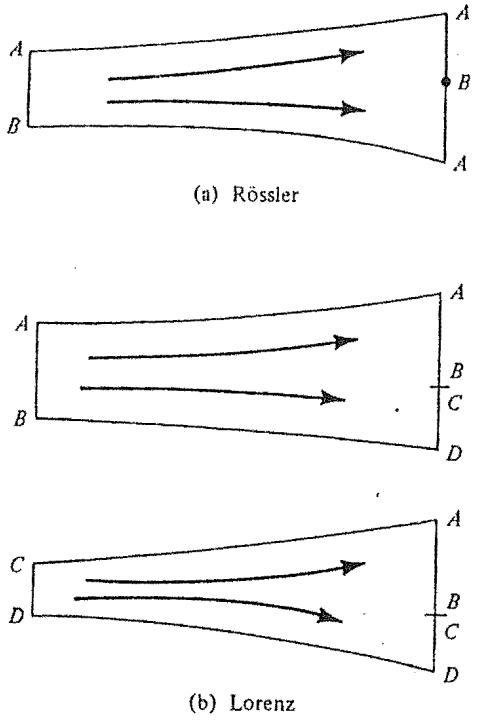

Figure 2.8 Topological structure of the Rössler and Lorenz attractors. All line segments with the same label (AB or CD) are joined together. (after Lichtenberg and Lieberman, 1982)

and joined from right to left edge. In contrast, the Lorenz attractor is more complicated, consisting of two such sheets, with the stretched edge of each sheet, on the right, divided into two parts, as shown in Figure 2.8 (b). The right edge of each sheet, joins both sheets on their left. Various other topological structures for strange attractors can also be imagined. Guckenheimer (1980) and Guckenheimer and Williams (1976) have argued convincingly that the topological nature of the Lorenz attractor is different for each value of r. i.e., attractors for different values of r are so different that even if they were made of rubber, one could not be squeezed or stretched into the shape of another. The fine structure of how the edges of the infinitely many sheets are interwound, changes with r. Guckenheimer and Williams (1976) have argued that for the Howard-

Malkus-Welander model which has the symmetry-breaking parameter r', even more topological types appear. It appears that for each r and r' (in the chaotic range) the topological type of the attractor is distinct. Small perturbations to the Lorenz equations can only produce strange attractors which are topologically equivalent to one of those already obtained. For more detail, see Sparrow (1982) or Guckenheimer and Holmes (1983).

(ii) Symmetry

The Lorenz equations have the symmetry $(x,y,z) \to (-x,-y,z)$ for all values of the parameters.

(iii) The z-axis

The z-axis is invariant. All orbits which start on the z-axis remain on it and tend toward the origin (0,0,0). All orbits which rotate around the z-axis, do so in a clockwise direction when viewed from above the plane $z = 0$. This follows from the fact that if $x = 0$ then $\frac{dx}{dt} > 0$ when $y > 0$, and $\frac{dx}{dt} < 0$ when $y < 0$.

(iv) Existence of a bounded globally attracting set of zero volume.

The divergence of the flow is:

$$\frac{\dot{dx}}{dx} + \frac{\dot{dy}}{dy} + \frac{\dot{dz}}{dz} = -(\sigma + b + 1) \qquad (2.29)$$

and hence a volume element V, is contracted by the flow into a volume element $Ve^{-(\sigma+b+1)t}$ in a time t. This contraction rate is very large for the parameter values usually chosen. For example, if $\sigma = 10$, $b = \frac{8}{3}$ then $\Lambda = -(\sigma + b + 1) = -13\frac{2}{3}$. In one unit of time, the volume contracts by a factor of $e^{\Lambda} \approx 10^{-6}$.

One can show that there is a bounded ellipsoid E, in R^3, given by:

$$rx^2 + \sigma y^2 + \sigma(z - 2r)^2 \leqslant c < \infty \qquad (2.30)$$

such that all solutions of the Lorenz equations enter E with finite time and thereafter remain in E. (See Appendix C in Sparrow (1982)). When the parameter r lies between 0 and 1, consideration of the *Lyapunov function* $V = x^2 + \sigma y^2 + \sigma z^2$ shows

that the origin (0,0,0) is globally stable. For all values of the parameters, the existence of the bounded ellipsoid E and the negative divergence, taken together show that there is a bounded set of zero volume within E towards which all trajectories tend. It is suggested in Sparrow (1982) that it is probably true, that this set lies completely in $z \geqslant 0$ for all values of the parameters. This result has yet to be proven in general but Sparrow (1982) has proven the result for $b < \sigma + 1$, which covers all the interesting cases studied so far.

(v) One-dimensional mappings

Lorenz (1963) first observed that the plot of z versus t appeared chaotic. He demonstrated remarkable insight by plotting the height of the (n+1)st maximum, z_{n+1}, against the height of the nth maximum, z_n. The points fall on a cusped curve like that of Figure 2.9. The peaks of z(t) approximately satisfy a difference equation of the form:

$$x_{n+1} = G(x_n) \tag{2.31}$$

Yorke and Yorke (1979) point out that it is possible to fit a curve G to the set of points so that $|G(z_n) - z_{n+1}| \leqslant 10^{-3}$; for all n. This error of 10^{-3} is difficult to determine precisely, but there is some point below which the error cannot be reduced. The existence of a functional relationship is somewhat illusory, The one-dimensional map is only approximate with the infinitely many leaves of the attractor being melded into one, although the approximation is very good due to the high volume contraction rate. Note that $\left|\frac{dG}{dx}\right| = 1$ everywhere. From this follows a useful property. If $\{z_n\}$ is an infinite sequence of peaks generated from the original differential equation, then there will exist an x_1 such that for $x_{n+1} = G(x_n)$ we have:

$$|x_n - z_n| \leqslant \varepsilon \quad \text{for all } n = 1,2,\ldots . \tag{2.32}$$

It is unlikely that the correct choice of x_1 would be exactly equal to z_1, and only a choice of x_1 would produce a good fit for all n. The existence

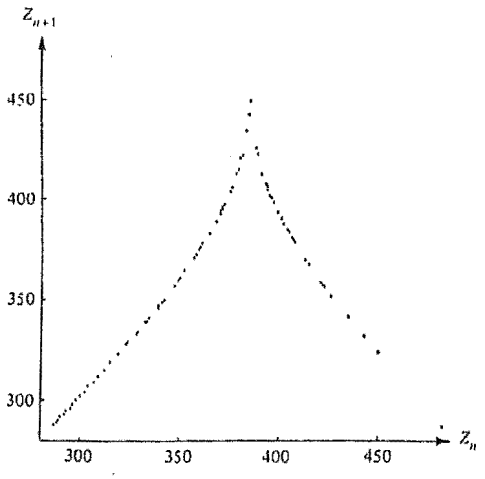

Figure 2.9 Maxima versus previous maxima of z for the Lorenz attractor of r = 28, illustrating the embedded one-dimensional map (after Lorenz, 1963)

of an approximate relation like (2.31) for the Lorenz system is useful in that it permits a less expensive study of the properties of the sensitive solutions. We explore the correspondence between strange attractors and one-dimensional maps more fully in chapter 4.

(vi) Stationary Points

The origin is a stationary point for all parameter values. If $0 < r < 1$ we know that it is stable and globally attracting. In fact in this parameter range, the origin is a hyperbolic sink and is the only attractor. At r = 1, the linearized system:

$$\begin{bmatrix} -\sigma & \sigma & 0 \\ r-z & -1 & x \\ y & x & -b \end{bmatrix}_{x=y=z=0} = \begin{bmatrix} -\sigma & \sigma & 0 \\ r & -1 & 0 \\ 0 & 0 & -b \end{bmatrix} \qquad (2.33)$$

has eigenvalues $\lambda_1 = 0$, $\lambda_2 = -b$ and $\lambda_3 = -(1+\sigma)$; with λ_2 and λ_3 being negative. A pitchfork bifurcation takes place at r = 1.

For all $r > 1$, the origin is a saddle point with a one-

dimensional unstable manifold. Also for $r > 1$, two nontrivial fixed points at:

$$c_1, c_2 = (x,y,z) = (\pm \sqrt{b(r-1)}, \pm \sqrt{b(r-1)}, r-1) \qquad (2.34)$$

are born. For $r > 1$, the linearized flow near the origin has the following three eigenvalues:

$$\lambda_1, \lambda_2 = \tfrac{1}{2}\{-\sigma - 1 \pm ((\sigma-1)^2 + 4\sigma r)^{\frac{1}{2}}\}, \quad \lambda_3 = -b \qquad (2.35)$$

where λ_2 and λ_3 are negative, and λ_1 is positive. We have $-\lambda_2 > \lambda_1 > -\lambda_3$ provided that:

$$r > 1 + \frac{b(\sigma+1+b)}{\sigma} . \qquad (2.36)$$

For $\sigma = 10$ and $b = \frac{8}{3}$ this condition is approximately $r > 4.644$.

The eigenvalues of the flow linearized near c_1 and c_2 are the roots of the equation:

$$a^3 + a^2(\sigma+b+1) + ab(\sigma+r) + 2\sigma b(r-1) = 0 . \qquad (2.37)$$

The condition for all three roots to be real is complicated and not important. All three roots are real when r is very close to one, but when $\sigma = 10$ and $b = \frac{8}{3}$, we have one real root and a complex conjugate pair of roots when $r > 1.34b$.

It is very important that if $r < \frac{\sigma(\sigma+b+3)}{(\sigma-b-1)}$, then all three roots have negative real part. Hence c_1 and c_2 are stable (sinks) for:

$$r \in \left[1, \frac{\sigma(\sigma+b+3)}{(\sigma-b-1)}\right) . \qquad (2.38)$$

For $\sigma = 10$ and $b = \frac{8}{3}$ the stable parameter range is $1 < r < \frac{470}{19} \approx 24.74$. This value of r is usually denoted by r_H.

At $r = r_H$, the eigenvalues of the linearized matrix are as follows:

$$\lambda_1 = -(\sigma+b+1) \qquad \lambda_2, \lambda_3 = \pm i\sqrt{\frac{2\sigma(\sigma+1)}{(\sigma-b-1)}} \qquad (2.39)$$

(following Lorenz, we assume $\sigma > 1 + b$, so that imaginary roots are possible). When $r > r_H$ the complex roots of (2.37) have positive

real part and c_1 and c_2 are non-stable (as is the origin). A single point attractor does not exist. The real root is negative for all r. At $r = r_H$, as the complex eigenvalues cross the imaginary axis, there is a Hopf bifurcation in which the points c_1 and c_2 lose their stability. As mentioned in chapter 1, there are two types of Hopf bifurcation, these being "*supercritical*" and "*subcritical*". It is subcritical if they lose their stability by absorbing a non-stable periodic orbit. In our case, we can show that the bifurcation is subcritical (Marsden and McCracken (1976)). It appears that the bifurcation is likely to be subcritical for all σ and b values for which the bifurcation occurs in $r > 0$ (Hassard et al., 1981)).

Hence for $r > r_s = 24.06$ there is a strange attractor on which chaotic motion takes place. In the narrow range $r_s < r < r_H$, three attractors coexist, two corresponding to regular motion and the third to chaotic motion. The system exhibits hysteresis; as r increases through r_H, the regular motion becomes chaotic; as r decreases through r_H, the chaotic motion becomes regular. Figure 2.10 shows the flow near c_1 for r near r_H. Also recall Figure 2.5, of the strange attractor.

Lorenz studied the value $r = 28$. In Figure 2.5, the trajectory first gets close to c_1 and then spirals away, finally being attracted to c_2. It then spirals away from c_2 and is attracted back close to c_1. The period of rotation near $c_{1,2}$ is 0.62, and the spiral radius expands by about 6% with each rotation. The number of consecutive rotations about c_1 or c_2 varies widely in a manner that is unpredictable in practice since it depends sensitively on initial conditions.

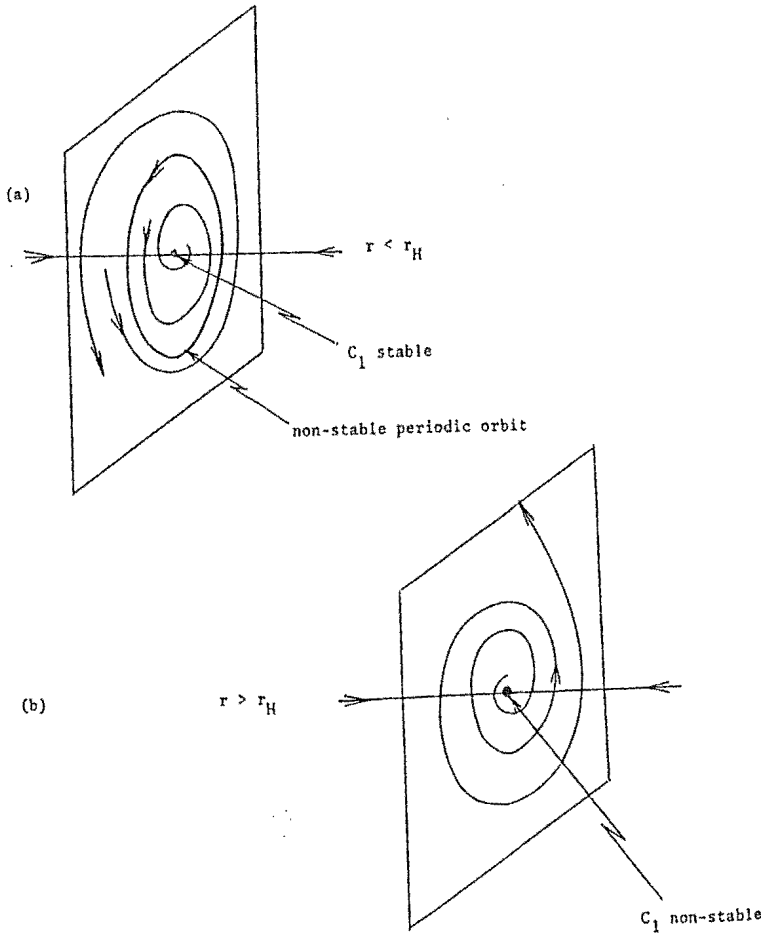

Figure 2.10 A schematic view of the flow near c_1 for r near r_H. (a) $r < r_H$, (b) $r > r_H$ (after Sparrow, 1982)

2.6f BIFURCATIONS INVOLVING PERIODIC ORBITS IN THE LORENZ SYSTEM

The theory in this section is based closely on the discussion in Sparrow (1982).

(i) The Homoclinic Bifurcation

From the last section it follows that the two non-stable periodic orbits which are required for the Hopf bifurcation at r_H, must come into existence somewhere in the parameter range $1 < r < r_H$. When r is only slightly larger than one, the stable manifold of the origin (the two-dimensional sheet of initial values in $\mathbb{R}^3$ from which orbits tend towards the origin) divides $\mathbb{R}^3$ into two

halves in the following manner. Orbits which start in one half-space tend towards c_1 and orbits started in the other half space tend towards c_2. Orbits started on the stable manifold of the origin tend towards the origin. As r increases towards $r_e \approx 13.926...$ the spirals formed by the orbits starting on the unstable manifold (the one-dimensional manifold of initial values in R^3 on which orbits tend in backwards time towards the origin) of the origin grow larger and larger. For $r > r_e$ they "swap over" and are attached to the other stationary point. See Figure 2.11. At $r = r_e$, orbits started on the unstable manifold of the origin will also lie in the stable manifold of the origin and therefore tend, in both forwards and backwards time, towards the origin. We say that there is a *homoclinic orbit* associated with the stationary point at the origin. Hence we can define a homoclinic orbit of a stationary point $\underset{\sim}{x}'$ as an orbit which tends to $\underset{\sim}{x}'$ in both forwards and reverse time.

Similarly we can define a *heteroclinic* orbit between stationary points $\underset{\sim}{x}'$ and $\underset{\sim}{y}'$ to be a trajectory which tends towards $\underset{\sim}{x}'$ in reverse time and towards $\underset{\sim}{y}'$ in forward time. The bifurcation which occurs as r passes through r_e, is called a *homoclinic bifurcation*. Sparrow (1982) calls these bifurcations "*homoclinic explosions*". There are two types of homoclinic bifurcations and the difference between them is important. Homoclinic bifurcations play an important role in the evolution of the Lorenz system. See Figure 2.12. The two simplest orbits born in this first homoclinic bifurcation are the orbits involved in the later Hopf bifurcation.

We can explain the presence of the strange attractor in terms of homoclinic bifurcations. There is a first homoclinic explosion which creates a "*strange invariant set*" (a set consisting

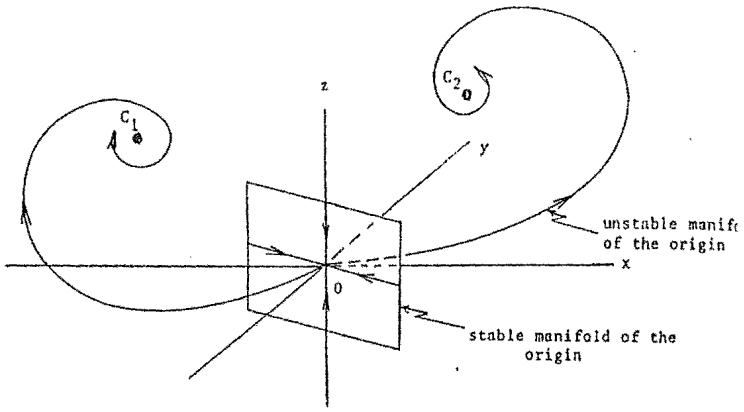

Figure 2.11a A schematic view of the flow in $1 < r < 13.926$.

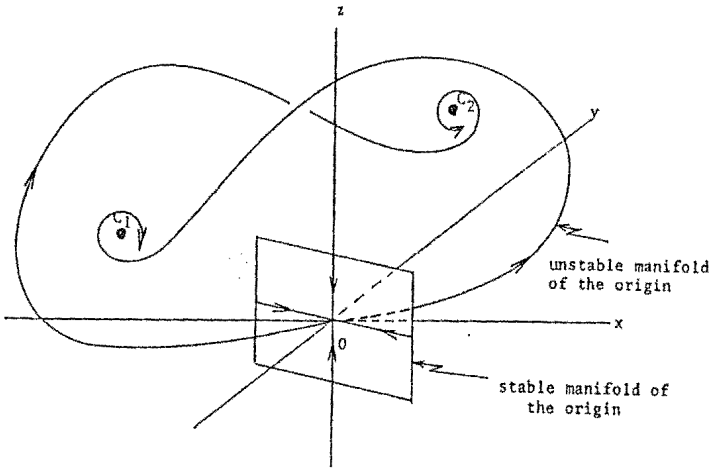

Figure 2.11b Behaviour of the unstable manifold of the origin for $r > 13.926$ (after Sparrow, 1982)

of a countable infinity of periodic orbits, an uncountable infinity of aperiodic orbits and an uncountable infinity of orbits which end in the origin). This set is initially non-stable. At $r_s \approx 24.06$ the original invariant set becomes attracting, and the unstable manifold of the origin is attracted to this set. An infinite sequence of homoclinic bifurcation begins which are all of one type (called type (a)). For $r_s < r < 30.1 = r_t$, the homoclinic bifurcations remove all periodic orbits from the non-wandering set. At this stage we have a strange attractor. At some r-value near r_t, homoclinic bifurcations (of both types) occur which add new periodic orbits to the non-wandering set.

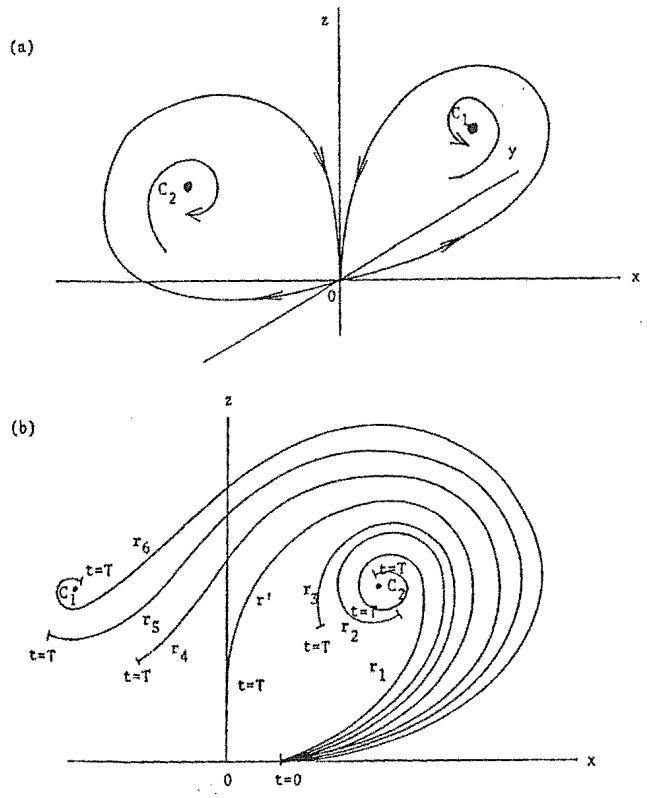

Figure 2.12 (a) Homoclinic orbits at $r = r'$.
(b) Trajectories with the same initial conditions for different values of r near r'.
(after Sparrow, 1982)

Some of these new periodic orbits are those required for the "period-doubling windows" which occur in $r > r_t$. Homoclinic bifurcations can be viewed as removing original periodic orbits from the non-wandering set in an indirect way. They do this by providing all the periodic orbits needed for a period-doubling window which ends with an original periodic orbit being annihilated in a saddle-node bifurcation.

(ii) The Saddle-Node Bifurcation

On one side of the bifurcation point $r = r'$, we have a non-stable periodic and a stable periodic orbit. As the parameter increases (or decreases) towards r', the two orbits move very close together and their periods tend towards a common value. On the other side of r' neither orbit exists. This bifurcation can occur between

two symmetric, or between two non-symmetric orbits. See Figure 2.13.

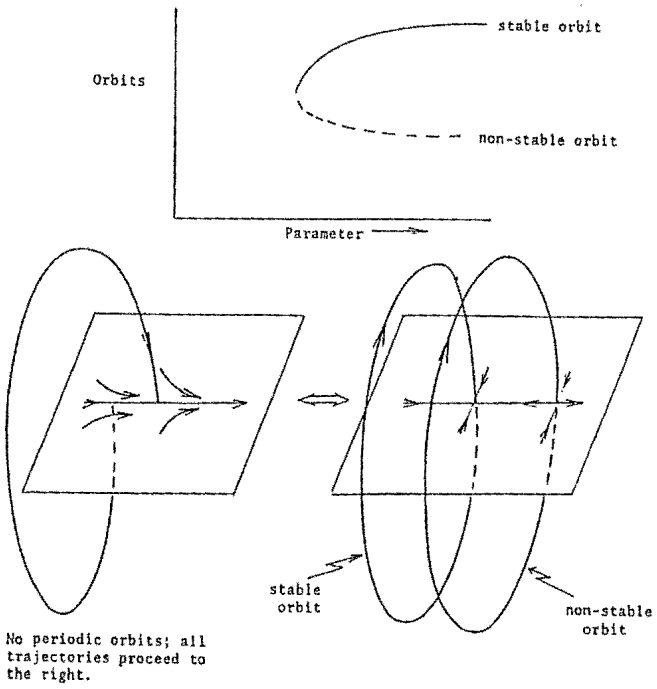

Figure 2.13 The saddle-node bifurcation (a) Bifurcation diagram, (b) schematic view of the flow; the periodic orbits can be both non-symmetric or both symmetric. (after Sparrow 1982)

(iii) The Symmetric Saddle-Node Bifurcation

This bifurcation is the periodic orbit analogue of the pitchfork bifurcation involving stationary points which occurred when $r = 1.0$. On one side of the bifurcation point, r', we have two non-symmetric orbits and a symmetric orbit. As r increases (or decreases) towards r', these three orbits move close together and their periods tend towards some common value. On the other side of r', there is only one symmetric orbit. This is called a *symmetric saddle-node bifurcation* or *symmetry breaking bifurcation* because if we disturb the symmetry slightly, we are left with a saddle-node bifurcation. In the Lorenz system this bifurcation has been observed only when it involves two stable non-symmetric orbits and a non-stable symmetric orbit coalescing to form a stable symmetric

orbit. See Figure 2.14.

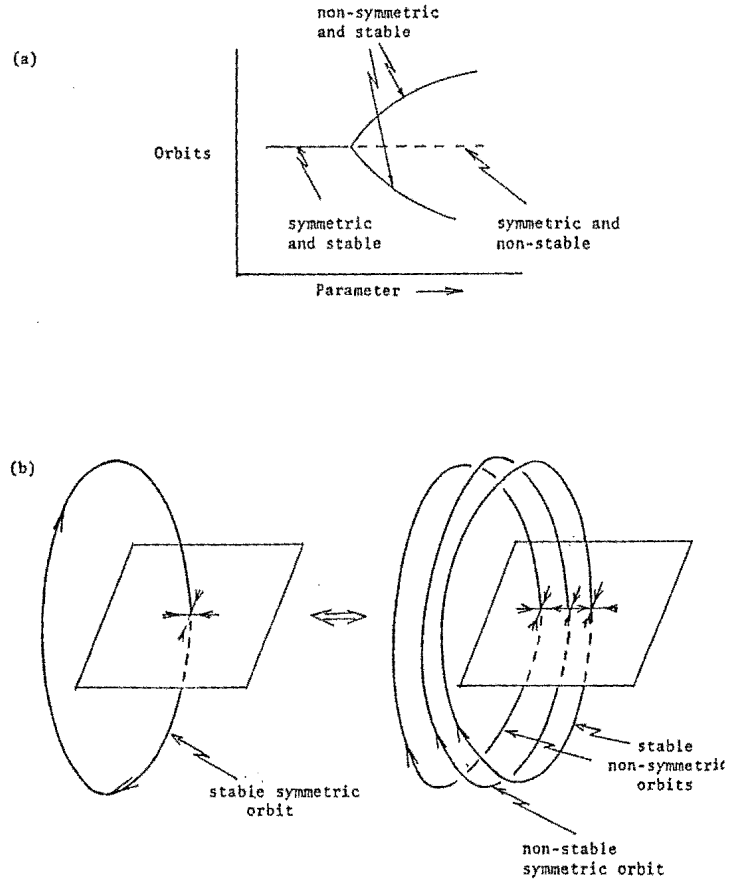

Figure 2.14 The symmetric saddle-node bifurcation. (a) Bifurcation diagram, (b) Schematic view of the flow. (after Sparrow, 1982)

(iv) The Period-Doubling Bifurcation

This is also known as the *flip bifurcation*. On one side of the bifurcation point, r', we have a periodic orbit and as r increases (or decreases) towards r', its period approaches some value T. On the other side of r' this periodic orbit continues to exist, but near it there is a periodic orbit of period 2T. See Figure 2.15. The period-doubling bifurcation can only occur in non-symmetric orbits. For it to work, orbits moving near the orbit of period T must "flip" half-way around it on each revolution, thus allowing the possibility of a periodic orbit of period 2T after two revolutions. This cannot occur near a symmetric orbit. In the Lorenz system this bifurcation has only

been observed when a stable periodic orbit becomes non-stable by throwing off a stable periodic orbit of twice the period. There is also the Hopf bifurcation which we have already discussed. These are the main bifurcations involved in the evolution of the Lorenz system.

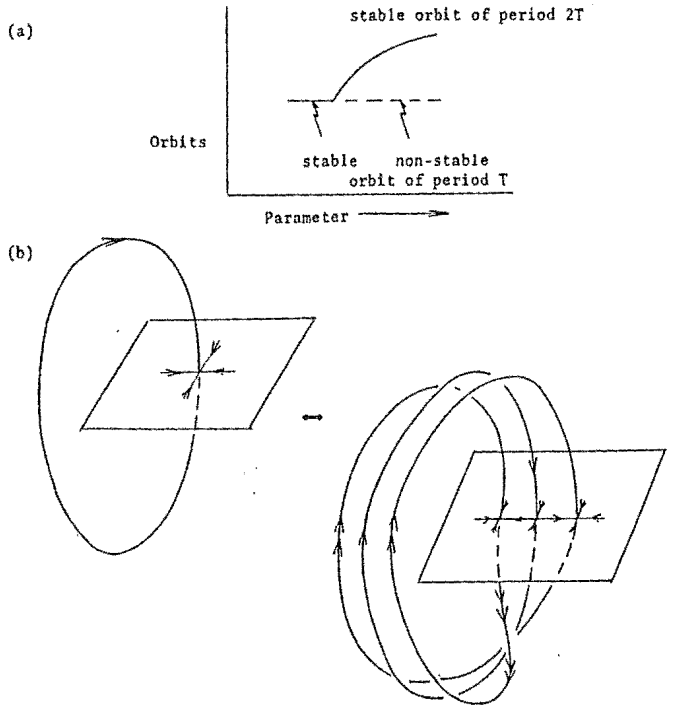

Figure 2.15 The period-doubling bifurcation
(a) bifurcation diagram, (b) schematic view of the flow; all orbits are non-symmetric.
(after Sparrow, 1982)

2.6g METASTABLE CHAOS

For certain ranges of parameter values for the Lorenz system, there is a substantial region of R^3 for which an orbit starting in this region appears to be of the chaotic type discussed so far. Eventually, with little warning, the orbit begins to spiral into one of the steady "convective" states. It is not possible to tell when this change from chaotic behaviour will occur. This phenomenon just described is known as "*preturbulence*" after Kaplan and Yorke (1979) or as "*metastable chaos*" after Yorke and Yorke (1979). As pointed out in Yorke and Yorke (1979),

for r slightly less than $r_s \approx 24.06$ ($b = \frac{8}{3}, \sigma = 10$), the mean number of chaotic oscillations before decay sets in, is approximately $300\ (r_s - r)^{-k}$, where $k \approx 4$. For $r = 23.5$, the time is approximately 3050 oscillations. The transient chaotic behaviour would most likely persist for longer than the time one observed the system. Thus chaotic behaviour would be improperly inferred. Hence the time spent wandering, by an orbit which wanders at all, tends to infinity as r increases towards r_s. At this r-value, the strange invariant set has become a strange attractor.

Not all orbits will show metastable chaotic behaviour in $r < r_s$. Orbits started close enough to c_1 or c_2 will tend to these stationary points without wandering near the strange invariant set. In fact, c_1 and c_2 are still stable at $r = r_s$. The value $r = r_s$ is a lower r-value than r_H - the Hopf bifurcation value - and there will still be some trajectories attracted to c_1 and c_2, even after we have a strange attractor. Also orbits started near the origin do not exhibit metastable chaotic behaviour. See Figure 2.16.

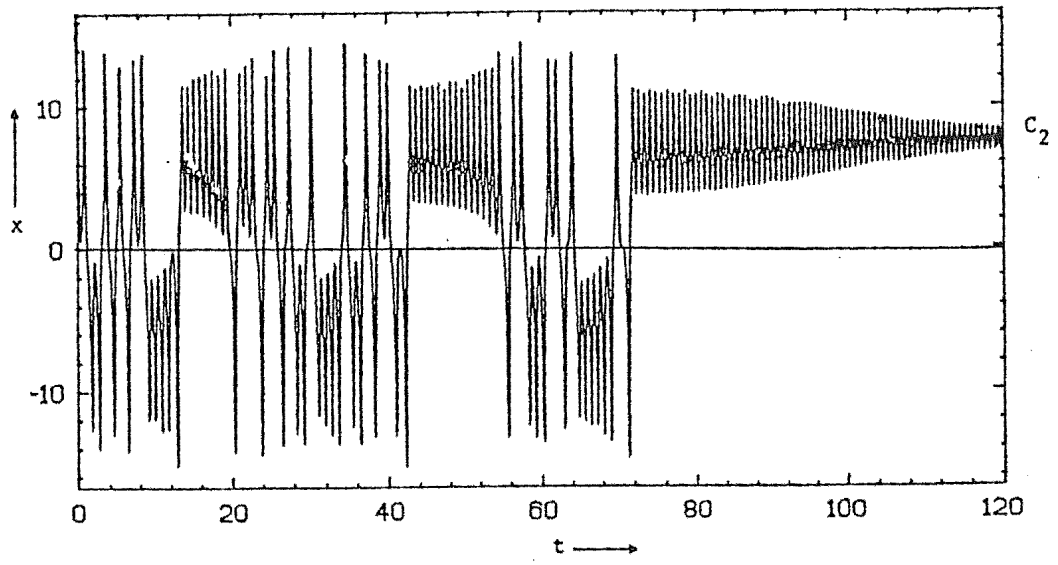

Figure 2.16 A typical "preturbulent" trajectory wanders chaotically near the strange invariant set before spiralling into c_2. ($r = 22.4$).
(after Sparrow, 1982)

2.6h SUMMARY OF THE EVOLUTION OF THE LORENZ SYSTEM

We now summarize the results found by varying the parameter r.

$0 < r < 1$ — The origin $(0,0,0)$ is the only fixed point (hyperbolic sink), and it is globally attracting. This corresponds to steady heat conduction in the Rayleigh-Bénard problem.

$1 < r < r_e \approx 13.926$ — The origin loses stability slightly above $r = 1$ and two new fixed points c_1, c_2 are born with $c_1, c_2 = (\pm[b(r-1)]^{\frac{1}{2}}, \pm[b(r-1)]^{\frac{1}{2}}, r-1)$. These points $c_{1,2}$ are attracting for $1 < r < r_H$, where $r_H \approx 24.74$. This corresponds to steady convection in the original Rayleigh-Bénard problem.

$r_e < r < r_s \approx 24.06$ — A homoclinic bifurcation occurs at $r = r_e$, which creates the original "strange invariant set". This parameter range shows metastable chaotic behaviour (preturbulence).

$r_s < r < r_H \approx 24.74$ — At r_s, the original invariant set becomes attracting, and the unstable manifold of the origin is attracted to this set. An infinite sequence of homoclinic bifurcations begins which will ultimately (at $r_t \approx 30.1$) remove all periodic orbits from the non-wandering set. In this range, three attractors coexist; two corresponding to regular motion and the third to chaotic motion.

$r_H < r < r_t \approx 30.1$ — At $r = r_H$, the subcritical Hopf bifurcation occurs in which c_1 and c_2 lose their stability by absorbing the two non-stable periodic orbits created in the first homoclinic bifurcation. At this point all three stationary points are non-stable and the non-wandering set now contains no periodic orbits

at all. We now just have the strange attractor present.

$r > r_t$ At an r-value slightly larger than r_t, homoclinic bifurcations occur which add new periodic orbits to the non-wandering set. Some of these periodic orbits are those required for the period-doubling windows. We observe for $r > r_t$. These period-doubling windows end with an original periodic orbit being annihilated in a saddle-node bifurcation. At the top of the period-doubling windows (r large) we find what is called "intermittent chaos". We shall look at this in detail in chapter 4. At the bottom of the windows (r small), we find "noisy periodicity". See Sparrow (1982) for a discussion on this.

r large Robbins (1979) has shown that in the limit as $r \to \infty$, the system becomes integrable, and using the exact solutions for that case, she was able to demonstrate the existence of a pair of attracting periodic orbits for sufficiently high r. As r decreases (in the range 100-200, for $\sigma = 10$, $b = \frac{8}{3}$) successive period-doubling bifurcations occur in which the flow becomes progressively more complex until ultimately a strange attractor appears. See Figure 2.17 which shows some of the behaviour observed as r increases.

We mentioned earlier that the Hopf bifurcation which occurs at r_H is subcritical, i.e. unstable periodic orbits, shrink down upon the sinks as r increases towards r_H and no closed orbits exist for the fixed points for $r > r_H$. In physical terms, the steady convection rolls

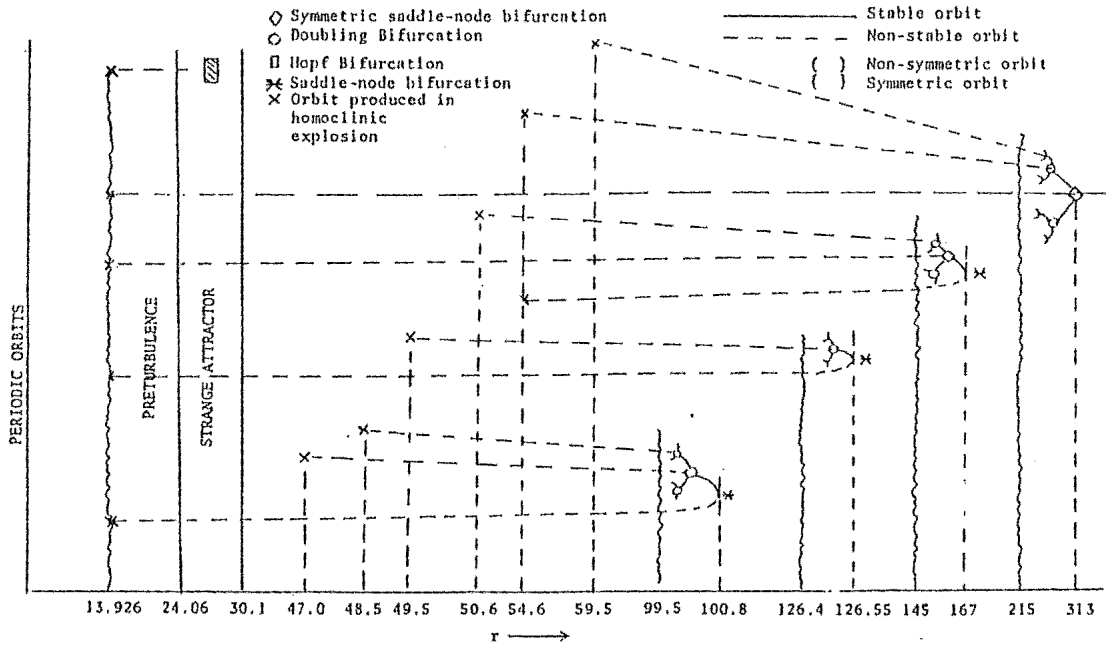

Figure 2.17 Bifurcation diagram showing a few of the shorter periodic orbits. (after Sparrow, 1982)

represented by the symmetric pair of nontrivial solutions become unstable and are replaced by some other large amplitude motion (turbulence). We stress that it is important not to assert that it is this subcritical Hopf bifurcation which results in an immediate transition to chaos (at r_s) for this is incorrect. As we have discussed, this is due to an infinite sequence of homoclinic bifurcations beginning at r_s. This concludes our detailed look at the Lorenz system.

2.7 NONAUTONOMOUS SYSTEMS

The only kind of nonautonomous systems studied in detail to date appear to consist of nonlinear oscillators driven by external force. Most periodically forced systems can be viewed as coupled systems of one nonlinear and one linear oscillator. This viewpoint allows for a more intuitive interpretation of various regimes of oscillation including period-doubling and chaos. Having the driving frequency as a control parameter enables one to reach very high frequency resolution by using various *stroboscopic sampling* techniques. These merits distinguish

the periodically driven equations from purely autonomous systems in numerical studies. Every autonomous system can be extended to a non-autonomous system through the addition of a periodic force. A non-autonomous system can be made autonomous by adding one or more variable. Hence most of this section is concerned with briefly presenting models under discussion in recent literature, and using them where possible to illustrate important concepts. Also it follows that at least two variables are required for a nonautonomous system to exhibit chaotic behaviour.

2.8 VAN DER POL'S EQUATION

The basic system can be written in the form:

$$\ddot{x} + \varepsilon\phi(x)\dot{x} + x = bp(t) \tag{2.40}$$

where $\phi(x)$ is even and $\phi(x) < 1$ for $|x| < 1$, $\phi(x) > 0$ for $|x| > 1$, $p(t)$ is T-periodic and ε, b are non-negative parameters. For the additional necessary constraints on $\phi(x)$, see Guckenheimer and Holmes (1983). The discovery of the chaotic properties of this equation were made by Cartwright and Little during experimental investigations of electrical circuits during World War 2.

A frequently used example is when $\phi(x) = x^2 - 1$ and $p(t) = \varepsilon\omega \cos \omega t$. We can rewrite this system as:

$$\begin{cases} \dot{x} = \varepsilon \left[y - \left(\frac{x^3}{3} - x \right) + b \sin \omega t \right] \\ \dot{y} = -\frac{1}{\varepsilon} x \end{cases} \tag{2.41}$$

To obtain an autonomous system from (2.41), we introduce another variable, θ, where $\theta = \omega t$. Hence (2.41) is replaced by:

$$\begin{cases} \dot{x} = \varepsilon \left[y - \left(\frac{x^3}{3} - x \right) + b \sin \theta \right] \\ \dot{y} = -\frac{1}{\varepsilon} x \\ \dot{\theta} = \omega \end{cases} \tag{2.42}$$

where $(x, y, \theta) \in \mathbb{R}^2 \times S^1$.

The map $T : \mathbb{R}^2 \to \mathbb{R}^2$ which follows orbits of (2.41) for a time $\frac{2\pi}{\omega}$ is independent of t. It is also given by the return map of the flow of (2.42) on a plane of constant θ. This map exhibits chaotic behaviour, but often in sets which are not attracting. Most points tend to stable periodic orbits but there are sheets of orbits on which the motion is chaotic. In this regard, the map is more like the logistic map (which we study in chapter 4), than the Lorenz equations. For more on the van der Pol oscillator see Guckenheimer (1979) and Guckenheimer and Holmes (1983).

2.9 PHASE LOCKING

When a nonlinear oscillator such as that described by the van der Pol equation is driven with a periodic forcing term, a phenomenon known as *phase locking* or *entrainment* often occurs. Phase locking means that the forced oscillator has a stable limit cycle whose period is an integer multiple n of the period T of the forcing term, the solutions are termed *subharmonic* because their frequency $\frac{2\pi}{nT}$ divides the frequency of the forcing term $\frac{2\pi}{T}$. The time T flow map Q has a stable periodic orbit of period n formed from n points along the limit cycle.

Cartwright and Littlewood observed that there are parameter values for which two different subharmonic solutions occur simultaneously with distinct periods. Along with these stable limit cycles come additional unstable chaotic orbits. The full extent of this additional chaotic behaviour has not yet been described, but its presence has been proved by Levinson (1949) for an equation which is very similar to the forced van der Pol equation.

2.10 OTHER SYSTEMS OF INTEREST

The Duffing equation takes the form:

$$\ddot{x} + k\dot{x} + f(x) = g(t) \qquad (2.43)$$

where $g(t)$ is a periodic function of t and $f(x)$ a nonlinear function of

x. This system is also well studied Moon and Holmes (1979) have shown that the Duffing equation in the form:

$$\ddot{x} + \delta\dot{x} - x + x^3 = \gamma \cos \omega t \tag{2.44}$$

provides the simplest possible model for the forced vibrations of a cantilever beam in the nonuniform field of two permanent magnets.

The forced mathematial pendulum:

$$\ddot{x} + k\dot{x} + \sin x = \alpha \cos \omega t \tag{2.45}$$

and the parametrically excited pendulum:

$$\ddot{x} + k\dot{x} + (A + \alpha \cos\omega t)\sin x = 0 \tag{2.46}$$

are representatives of another important class of physical models. For example, in describing Josephson junctions in a microwave cavity.

The forced Brusselator (forced limit cycle oscillator):

$$\begin{cases} \dot{x} = A - (B+1)x + x^2y + \alpha \cos \omega t \\ \dot{y} = Bx - x^2y \end{cases} \tag{2.47}$$

provides at the present time, the most thoroughly studied model by combined use of various numerical methods. This system describes a hypothetical three-molecular chemical reaction with autocatalytic step under far from equilibrium conditions. By introducing new variables z,u and fixing the initial conditions $z(0) = 1$, $u(0) = 0$, the periodically forced Brusselator is equivalent to the following system of autonomous differential equations

$$\begin{cases} \dot{x} = A - (B+1)x + x^2y + \alpha z \\ \dot{y} = Bx - x^2y \\ \dot{z} = -\omega U \\ \dot{U} = \omega z \end{cases} \tag{2.48}$$

which for numerical work is superior to (2.45) since it saves computer time by not having a cosine term. All well known routes to chaos and the U-sequence of Metropolis, Stein and Stein (which we study in chapter 4) have been shown to exist in this model. See Hao and Zhang (1982).

Our final model in this discussion is in a noteworthy paper by Gonzalez and Piro (1983). An exactly solvable nonlinear oscillator was subjected to periodic kicks. Using the known solution of the free oscillator, this model was transformed into a discrete mapping of two variables which enabled a detailed study using a reasonable amount of computer time. Hao (1984) claims that further exploration of this model may explain how the *Faray sequences* describing locking frequencies immersed in a quasiperiodic regime are replaced by the U-sequences describing periodicities embedded in the chaotic region when the non-linearity gets stronger.

2.11 TIME-DELAYED EQUATIONS

An example of a time-delayed equation is:

$$\tau\dot{\phi} = -\phi + A^2\{1 + 2B\cos[\phi(t - t_R) - \phi_0]\}. \qquad (2.49a)$$

This equation may possess a very complicated bifurcation and chaos structure depending on the value of the various parameters. This equation occurs in a model describing chaos in *optical bistability devices*. See Gibbs et al (1980), from which this example is taken. Another example, taken from Hao (1984) is:

$$\tau\,\dot{x}(t) + x(t) = \mu x(t-1)(1 - x(t-1)) \qquad (2.49b)$$

which has similar origins to (2.49a). The time-delay may be written as an infinite order differential operator acting on the function x(t):

$$x(t-1) = \exp\left(-\frac{d}{dt}\right) x(t) = \sum_{n=0}^{\infty} \frac{(-1)^n}{n!} \frac{d^n}{dt^n} x(t). \qquad (2.50)$$

From this one can see that a time-delayed equation in one variable may correspond to an infinite system of ODE's.

Time delays also arise in another important system; the *Belousov-Zhabotinskii reaction*. In this reaction, which involves more than 30 chemical constituents, an acidic bromate solution oxidizes malonic acid in the presence of a metal ion catalyst. The concentration of one of

more of the constituents is monitored. Chaotic behaviour is observed. See Roux et al (1983).

2.12 PARTIAL DIFFERENTIAL EQUATIONS

The study of chaotic behaviour in PDE's is still in its infancy; probably because of the time-consuming nature of numerical work on PDE's. The key reference on this topic is a recent paper by Moore et al (1983). In this study a system of PDE's for thermosolutal convection showed period-doubling and chaos. A finite difference scheme on a mesh replaced the equations in (t,x,z). An important result was that the essential nature of the solution was shown to not depend upon altering the mesh interval. Although nothing essentially new was reported compared to ODE's, Hao (1984) suggests we should expect some new features in chaotic behaviour in PDE's; in particular, the interplay between spatial structure and temporal chaos. See Hao (1984) for references on this.

2.13 TWO-AND-HIGHER DIMENSIONAL MAPPINGS

In using these mappings as models of physical systems, most "real world" complications are thrown away. These models are still very useful if they mimic reality with a minimum of computational effort. Higher-dimensional mappings may be conservative as well as dissipative and invertible as well as noninvertible. This depends on the parameter range in the model. We shall examine one such model in this section. The Hénon mapping.

2.14 THE HÉNON MAPPING

Lorenz inferred the Cantor set structure of the attractor from reasoning but could not observe it directly because the contracting ratio after one "circuit" was too small: 7×10^{-5}. A similar experience was reported by Pomeau (1976). In the Hénon mapping:

$$\begin{cases} x_{n+1} = 1 - ax_n^2 + y_n \\ y_{n+1} = bx_n \end{cases} \tag{2.51}$$

the contracting ratio after one iteration is b = 0.3, and one can easily observe a number of successive levels in the hierarchy. See Figure 2.18. From this figure one can observe the scale invariance of the attracting structure. Figure 2.18 (b)-(d) obtained by repeated magnification, all look identical. This similarity across the layer, corresponds to the structure of a Cantor set, as described earlier. The exponential divergence of initial, close trajectories has been verified computationally, strongly suggesting that the motion is chaotic on the attractor.

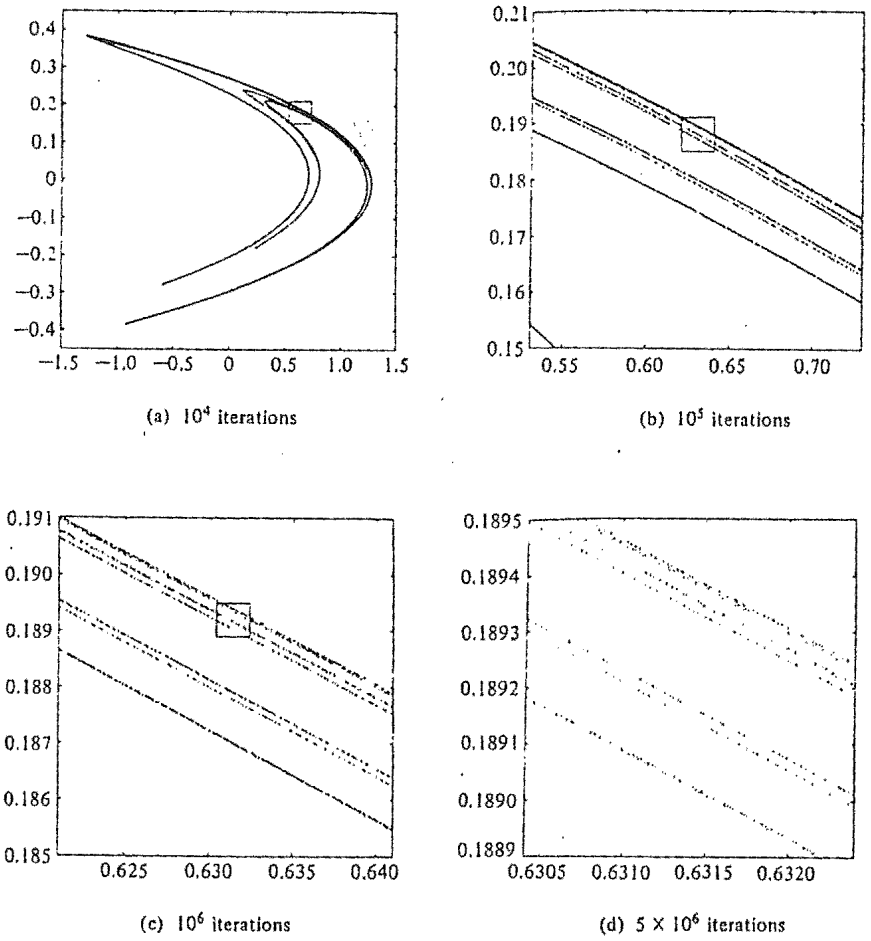

Figure 2.18 The leaves of Hénon attractor.
(a) Initial condition at the unstable fixed point x_0, y_0 ;
(b) enlargement of the small square in (a);
(c) enlargement of the small square in (b);
(d) enlargement of the small square in (c). Note the scale invariance of the leaved structure.
(after Hénon, 1976).

Hénon's idea was to take a "reductionist" approach in which he tried to find a model problem which was as simple as possible, yet exhibited the same essential properties of the Lorenz system. His aim was to

(i) make numerical exploration faster and more accurate, so that solutions could be followed for a longer time and more detailed explorations conducted, and

(ii) to provide a model which might lend itself more easily to mathematics.

Numerical results by Pomeau (1976) on the Lorenz system, show clearly how a volume is stretched in one direction, and at the same time folded over itself, in the course of one revolution. Hénon simulated the folding by the following chain of three mappings of the (x,y) plane onto itself. Considering a region elongated along the x-axis (see Figure 2.19 (a)), we begin the folding by:

$$T' : x' = x , \quad y' = y + 1 - ax^2 \tag{2.52a}$$

which produces Figure 2.19 (b), where a is an adjustable parameter. We complete the folding by a contraction along the x-axis:

$$T'' : x'' = bx', \quad y'' = y \tag{2.52b}$$

which produces Figure 2.19c, where b is another parameter which should be less than unity in absolute value. Finally we come back to the orientation along the x-axis by:

$$T''' : x''' = y'' , \quad y''' = x' \tag{2.52c}$$

which results in Figure 2.19d. Our mapping is now defined as the product:

$$T = T''' T'' T' . \tag{2.53}$$

Now write (x_i, y_i) for (x,y) and (x_{i+1}, y_{i+1}) for (x''', y'''), as a reminder that the mapping will be iterated. Finally we have:

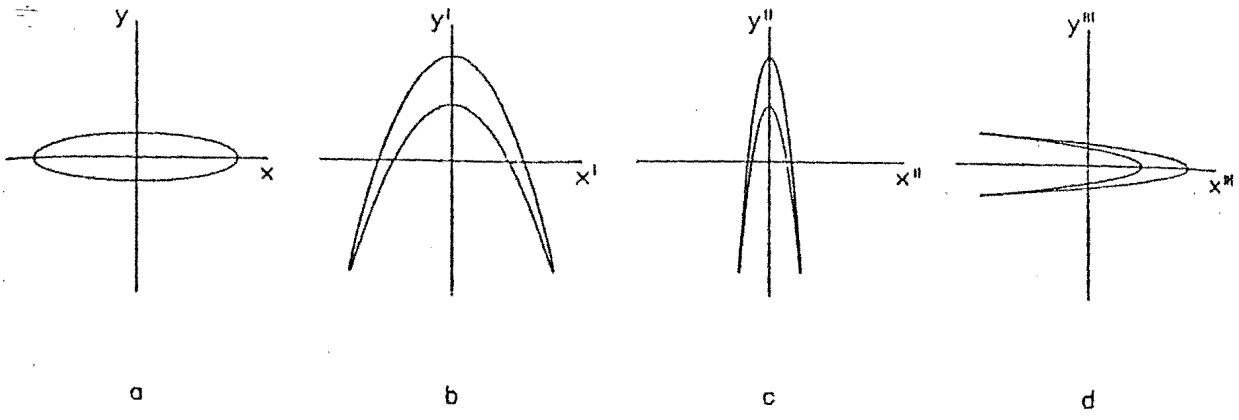

Figure 2.19 The initial area (a) is mapped by T' into (b), then by T'' into (c), and finally T''' into (d). (after Hénon, 1976).

$$T : x_{i+1} = 1 - ax_i^2 + y_i, \quad y_{i+1} = bx_i \tag{2.54}$$

as mentioned earlier in (2.51).

This map can be thought of as the Poincaré map for some three-dimensional flow. The Jacobian is constant:

$$\frac{\partial(x_{i+1}, y_{i+1})}{\partial(x_i, y_i)} = -b = \det M \, . \tag{2.55}$$

This property is the counterpart of the constant negative divergence in the Lorenz system. Hence, for one iteration the area contracts by the factor $|\det M|$. A polynomial mapping satisfying (2.55) is known as an *entire Cremona transformation*. The inverse mapping exists when $b \neq 0$ and is also given by polynomials:

$$T^{-1} : x_i = b^{-1} y_{i+1}, \quad y_i = x_{i+1} - 1 + ab^{-2} y_{i+1}^2 . \tag{2.56}$$

Thus T is a one-to-one mapping of the plane onto itself. This is the counterpart of the fact in the Lorenz system there is a unique trajectory through any given point. This mapping is in fact the most general quadratic mapping with constant Jacobian. It goes back to the logistic mapping when $b = 0$. It preserves area for $b = 1$ and corresponds to a dissipative system for $b < 1$. The case $b = 0.3$ was studied in great detail by Hénon and many others.

One difference with the Lorenz problem is that the successive points obtained by repeated application of T do not always converge towards an attractor. They sometimes escape to infinity. This is because the quadratic term in (2.56) dominates when the distance from the origin becomes large. For particular values of a and b it is still possible to prove the existence of a bounded "trapping region", R, from which points can never escape once they have entered it. i.e., for x_0 very large, the quadratic term makes $|x_n| \to \infty$, but for (x_0, y_0) within some finite area near the origin, the solution converges towards an attractor.

In contradistinction to one-dimensional mappings, even for one and the same parameter value, the character of the stationary output of (2.56) depends on the initial point taken. i.e., the (x,y) plane divides into basins, and starting from different basins one may be led to different periodic or aperiodic orbits. For one-dimensional unimodal mappings, there exists at most only one stable orbit. Also, for certain parameters and initial points, the interactions of (2.56) converge to an attractor with self-similar structure. In fact this was the first strange attractor known to have fractal dimension. Thirdly, it was proven that there exist intersections of stable and unstable manifolds in Hénon's model i.e., homoclinic points give rise to chaos. We shall examine homoclinic points etc., in more detail in the next section.

The diffeomorphism T has two invariant points given by:

$$x = (2a)^{-1}[-(1-b) \pm \sqrt{(1-b)^2 + 4a}], \quad y = bx . \tag{2.57}$$

These points are real for $a > a_0 = \frac{(1-b)^2}{4}$. When this is the case, one of the points is always linearly unstable, whilst the other is unstable for $a > a_1 = \frac{3(1-b)^2}{4}$. For $a_0 < a < a_1$, the attractor is the stable invariant point. When a is increased beyond a_1, the point attractor x_0 is numerically observed to undergo a cascade of period-doubling bifurcations. At first the attractor is still simple and consists of a

set of $p = 2^n$ points. This set is periodic. As $a \to a_2$, $p \to \infty$. For $a_2 < a < a_3$ the attractor is no more simple, and the behaviour of the points becomes erratic. Numerical evidence strongly suggests the presence of a strange attractor for most values of a in this range. The attractor appears to be unique for a given value of a. For $a > a_3$, most points escape to infinity.

To say that a strange attractor always exists for $a_2 < a < a_3$ is is an oversimplification there are many small subintervals within which the motion is periodic with period 3,4,5,... and the motions generally undergo period-doubling bifurcations. It has not been possible to prove mathematically the chaotic nature of the Hénon attractor, although the introduction of a discontinuity into the mapping makes this proof possible. Lozi (1978) has described such an attractor, replacing x_n^2 with $|x_n|$ in the map, which has been proved to be chaotic by Misiurewicz (1980).

We conclude by extolling some of the advantages of working with the Hénon mapping as opposed to a set of ODE's. The Hénon system appears to have the same basic properties of the Lorenz system. The numerical exploration is much easier, with much of the original work done on a programmable calculator. The solutions can be followed over a much longer time than in the case of a system of differential equations. The accuracy is also increased since there are no integration errors. Also, the mapping is much easier to handle analytically.

2.15 TRANSVERSE HOMOCLINIC ORBITS

The theory in this section is compiled from various parts of Guckenheimer and Holmes (1983). The Poincaré map associated with the forced Duffing equation with negative linear stiffness:

$$\ddot{x} + \alpha\dot{x} - x + x^3 = \beta\cos wt \qquad (2.58)$$

which is a nonlinear diffeomorphism of the plane, possesses a hyperbolic saddle point p whose stable and unstable manifolds intersect transversely.

A transversal intersection of manifolds in n-dimensional space is one for which the tangent spaces of the intersecting manifolds span n-space. One can see from Figure 2.20 that if there is one point $q \in W^u(p) \cap W^s(p)$, with $q \neq p$, then since $G^n(q) \to p$ as $n \to \pm \infty$ (where $G(x_n) = x_{n+1}$), and the approach is governed by the linear system for $|q - p|$ small, there must be an infinite set of such homoclinic points i.e., the existence of a single homoclinic point implies the existence of an infinite number of homoclinic points.

If the map is orientation preserving, then the two homoclinic points q, G(q) must be separated by at least one further point in $W^u(p) \cap W^s(p)$ (= $\hat{q}$ in Figure 2.20). The orbit $\{G^n(q)\}$ of q is called a homoclinic orbit and plays an important role in the global dynamics of the map G. In particular, the violent winding of the global manifolds $W^u(p)$ and $W^s(p)$ in the neighbourhood of p leads to a sensitive dependance of orbits $\{G^n(x_0)\}$ on the initial condition x_0. Hence the presence of homoclinic orbits tends to promote chaotic behaviour. If the stable and unstable manifolds $W^s(p_1)$, $W^u(p_2)$ of two distinct fixed points intersect then the resulting orbit is called heteroclinic. Homoclinic and heteroclinic points play the role of organizing centres for chaotic motion.

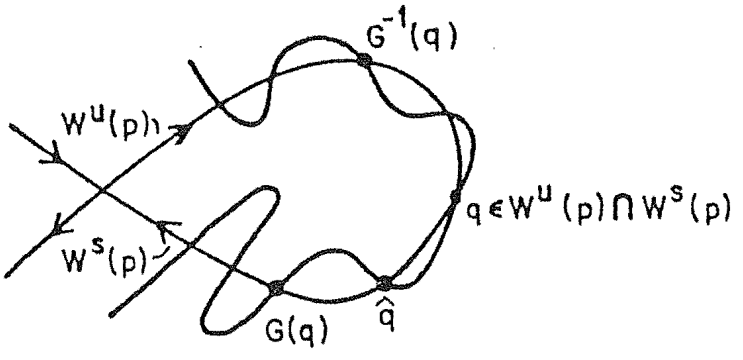

Figure 2.20 Homoclinic orbits (after Guckenheimer and Holmes, 1983)

In planar flows, all the possible non-wandering sets fall into

three classes (Andronov (1966)). They are:

(i) fixed points

(ii) closed orbits, and

(iii) unions of fixed points and the trajectories connecting them (homoclinic and heteroclinic orbits).

The fixed points in such cycles must all be saddle points (if they are hyperbolic), since sinks and sources necessarily have wandering points in their neighbourhoods. Observe from Figure 2.21 that in R^2, we are limited in how heteroclinic orbits are formed. In Figure 2.21 (b) the uniqueness of the solution is violated. Transverse saddle connections (or heteroclinic orbits) cannot exist at all in two dimensions, since the saddle points have one-dimensional stable and unstable manifolds and a connection $\gamma = W^u(p_1) \cap W^s(p_2)$ is necessarily an open interval on which $W^u(p_1)$ and $W^s(p_2)$ are identified. The tangent space to such a curve at any point $q \in \gamma$ is thus one-dimensional. See Figure 2.21 (a).

Let us now look at the situation in R^n, when $n > 2$. Let us consider a three-dimensional system with a pair of saddle points p_1, p_2 and dim $W^u(p_1)$ = dim $W^s(p_2)$ = 2. It is now possible for $W^u(p_1)$ and $W^s(p_2)$ to intersect transversely on an orbit γ, so that at any point $q \in \gamma$, the tangent spaces $T_q W^u(p_1)$, $T_q W^s(p_2)$ span R^3. See Figure 2.22.

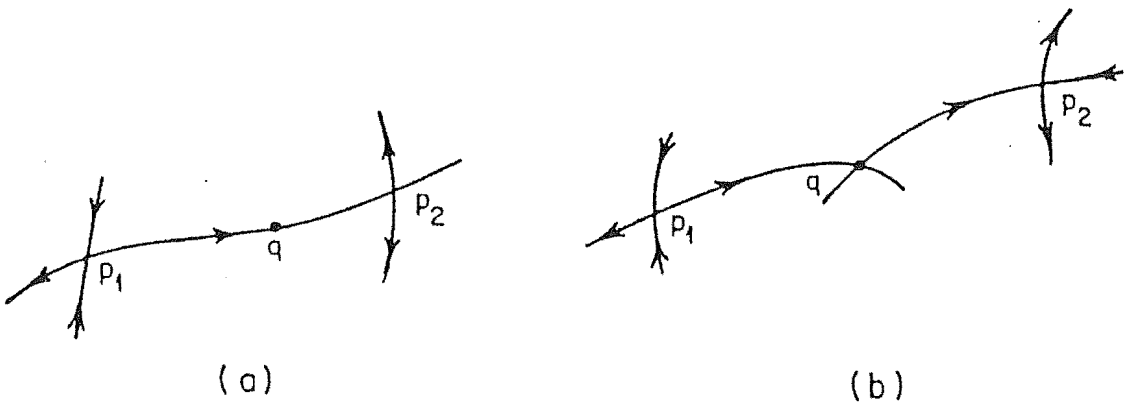

Figure 2.21 Heteroclinic points $q \in W^u(p_1) \cap W^s(p_2)$ for flows in R^2. (a) Admissible; (b) not admissible. (after Guckenheimer and Holmes, 1983)

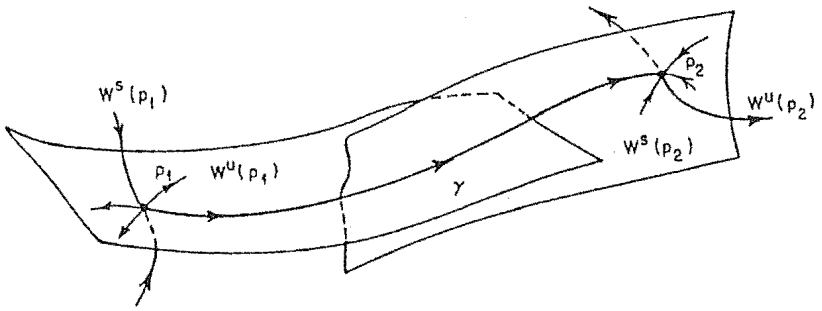

Figure 2.22 A transverse heteroclinic orbit in R^3.
(after Guckenheimer and Holmes, 1983)

If such a transverse heteroclinic orbit exists then it is structurally stable (cannot be removed by an arbitrary small perturbation). Transverse homoclinic orbits cannot exist, since dim $W^u(p)$ + dim $W^s(p) \leqslant n$ and for transversality we require dim $W^u(p_1)$ + dim $W^s(p_2) > n$. See Figure 2.23.

It is possible to test for the presence of transverse homoclinic orbits in a specific differential equation using a Melnikov function (seen Guckenheimer and Holmes (1983)). The presence of such orbits implies, via the Smale-Birkhoff theorem, that some iterate of the Poincaré map has an invariant hyperbolic set: A Smale horseshoe. A horseshoe contains a countable infinity of (unstable) periodic orbits, an uncountable set of bounded, nonperiodic orbits, and a dense orbit. Numerical evidence shows that solutions of differential equations and maps can depend sensitively on initial conditions when these complicated nonwandering Cantor sets are present. If the maps in question are Poincaré maps for flows, then similar observations apply to the solutions of the associated differential equations. Note that horseshoes are not attractors. We now examine the structure and properties of Smales horseshoe.

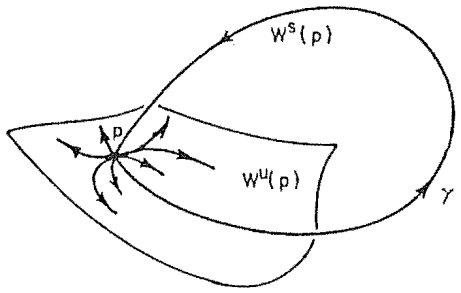

Figure 2.23 A nontransverse homoclinic orbit in R^3. (after Guckenheimer and Holmes, 1983).

2.16 SMALE'S HORSESHOE

The discussion in this section on Smale's horseshoe is based closely on that in Guckenheimer (1979). Consider a unit square S in the plane with two semicircular caps A and B at top and bottom respectively. The map f we consider is shown in Figure 2.24 (b). We are interested in S and the behaviour of f and its iterates on S. To make this study as simple as possible, assume that f is linear on the set $f^{-1}(S) \cap S$ of points in S whose images are also in S. The set $f^{-1}(S) \cap S$ consists of two horizontal bands cutting across S. On this set, assume f has the form $f(x,y) = (\pm ax + c_i, by + d_i)$ where a, b, c_i, d_i are numbers with $0 < a < \frac{1}{2}$, $b > 2$, and $i = 1$ or 2. This establishes the linear "hyperbolic" nature of f on the set $f^{-1}(S) \cap S$.

Consider successively the sets S, $S \cap f(S)$, $S \cap f(S) \cap f^2(S), \ldots,$ $\bigcap_{i=0}^{i=n} f^i(S)$. One can see that $\bigcap_{i=0}^{n} f^i(S)$ consists of 2^n vertical strips, each of width a^n, as shown in Figure 2.24 (c). It follows that $\bigcap_{i=0}^{\infty} f^i(S)$, is an uncountable collection of vertical segments. Now consider where points come from which map into S under successive iterates of f. We have seen that $f^{-1}(S) \cap S$ consists of two horizontal bands across S whose height is b^{-1}. The set $f^{-2}(S) \cap f^{-1}(S) \cap S$ consists of four horizontal bands across S whose height is b^{-2}. Inductively, one finds that $\bigcap_{i=-n}^{0} f^i(S)$ consists of 2^n horizontal bands of height b^{-n}. From this one concludes that $\bigcap_{i=-\infty}^{0} f^i(S)$ is an uncountable collection of horizontal segments crossing S. Putting this

together with our description of $\bigcap_{i=0}^{\infty} f^i(S)$, we find that the set

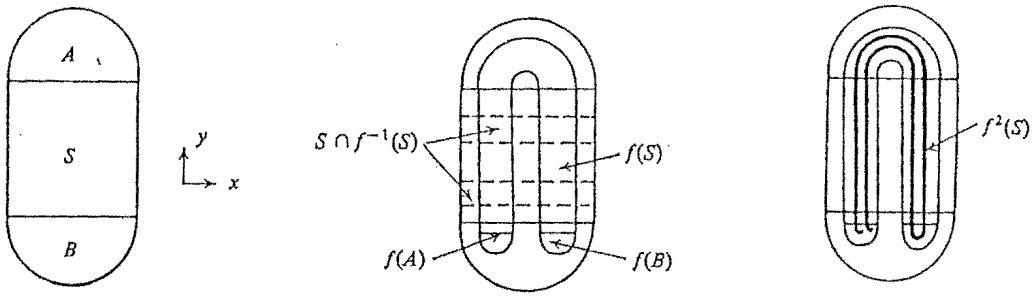

Figure 2.24 (a) the square with caps; (b) the image of the square with caps; (c) the second image of S under f. (after Guckenheimer, 1979)

$\Lambda = \bigcap_{i=-\infty}^{\infty} f^i(S)$ is an uncountable collection of points. These are the points which always remain in S and which are the images of points of S under arbitrarily high iterates of f.

We now attempt to obtain a description of the dynamics of f on the set Λ. We now introduce a "symbolic" description of what happens. Choose two symbols, say 0 and 1, to label the two pieces of $S \cap f(S)$. If we follow a point of Λ under the iterates of f, at each time it lies in one of the two pieces of $S \cap f(S)$. So corresponding to each point $p \in \Lambda$ is a sequence $\{a_t\}_{t=-\infty}^{\infty}$ of 0's and 1's determined by the rule:

$$a_t = \begin{cases} 0 & \text{if } f^t(p) \text{ is in rectangle } 0 \text{ of } S \cap f(S) \\ 1 & \text{if } f^t(p) \text{ is in rectangle } 1 \text{ of } S \cap f(S) . \end{cases} \qquad (2.59)$$

Smale proved that this is a one-to-one correspondence between the points of Λ and the set of sequences of 0's and 1's. This shows that the set of points in Λ is uncountable because the set of sequences of 0's and 1's is uncountable. Denote the set of sequences of 0's and 1's by Σ.

Now if $p \in \Lambda$, we want to follow its orbit under f, so we use the one-to-one correspondence we have established between Λ and Σ. If $\{a_t\}$ is the sequence associated to $p \in \Lambda$, what is the sequence associated to $f(p)$? If $f^t(p)$ lies in the rectangle a_t of $S \cap f(S)$, then $f^{t-1}(f(p))$ lies in the rectangle a_t of $S \cap f(S)$. Hence the sequence $\{b_t\}$ corres-

ponding to $f(p)$ has the property $b_{t-1} = a_t$. The map f looks like a map which just shifts the indices of sequences. Formally define the shift map:

$$\begin{aligned} &\sigma : \Sigma \to \Sigma \\ &\sigma(\{a_t\}) = \{b_t\} , \\ &b_{t-1} = a_t . \end{aligned} \tag{2.60}$$

To express the relationship between σ and f, let $\sigma : \Sigma \to \Lambda$ be the one-to-one correspondence between sequences and points of Λ. One then has the equation:

$$\phi\sigma = f\phi \tag{2.61}$$

or $\sigma = \phi^{-1} f \phi$. This implies:

$$\sigma^n = (\phi^{-1} f \phi)(\phi^{-1} f \phi) \ldots\ldots (\phi^{-1} f \phi) = \phi^{-1} f^n \phi . \tag{2.62}$$

Thus ϕ maps orbits of σ in Σ to orbits of f in Λ. We can use the map σ to study the map f on the set Λ, since it is much easier to study σ.

We now consider the problem of finding periodic orbits in f. We assert that there are exactly 2^n sequences $\{a_t\}$ of Σ such that $\sigma^n(p) = p$. Any "block" $(a_1, \ldots, a_n)$ of length n repeated infinitely often in both directions gives such a sequence. Since there are 2^n blocks of length n, we conclude that there are exactly 2^n points p in Λ such that $f^n(p) = p$. This implies that there are an infinite number of periodic orbits of f in Λ with arbitrarily long periods. One can also show that there is an orbit of f which is dense in Λ (see Guckenheimer and Holmes (1983)). This means that every point of Λ is the limit of a sequence of points selected from the orbit. We can also use this powerful "symbolic" analysis to predict the asymptotic behaviour of orbits in Λ. The conclusion is that after a certain time, one can say nothing about where in Λ the orbit of p goes. i.e., the limit set is not an attractor. This means that nost nearby initial conditions

have trajectories which lead away from the complicated limit set. We point out that this is a discrete time system.

We conclude this section with a few remarks. First, some mathematical results on one-dimensional mappings can be "lifted" to mappings on R^n. Higher-dimensional mappings are richer in their behaviour. For example, basin dependance and transitions from quasi-periodic motion to chaos may take place. Secondly, period-doubling bifurcations, do occur in area-preserving mappings in the plane, but the universal convergence rate happens to be $\delta = 8.7210....$. Thirdly we mention that complex mappings are now being studied and as yet no physical relevance is known.

2.17 METHODOLOGICAL CONCEPTS

There are very few analytical tools that mathematicians and physicists can use in studying higher-dimensional systems. As yet, there is no a priori criterion for chaos. A classification scheme for attractors is at this time unknown. However progress is being made in this field of study. We shall break methodological concepts into two types, analytic and numerical.

2.17a ANALYTIC METHODS

The two most useful analytical methods are those of *Melnikov* and of *Silnikov*. Both methods are centred on the existence of homoclinic points or homoclinic orbits.

Melnikov's method is based on consideration of the *Melnikov function*:

$$M(t_0) = \int_{-\infty}^{\infty} f(q^0(t - t_0)) \wedge g(q^0(t - t_0), t)dt \, . \qquad (2.63)$$

This function measures the distance between the stable and unstable branches of the trajectory. For example, the criterion to have the "homoclinic tangle" in Figure 2.25, is that the sign of the Melnikov function alternates. See Guckenheimer and Holmes (1983) for details.

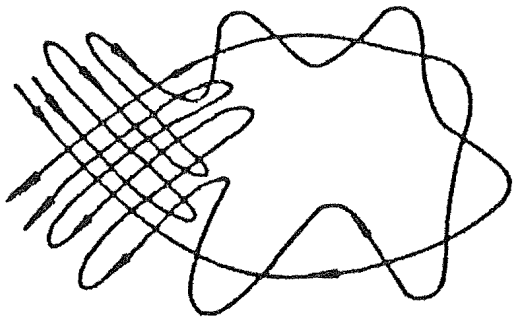

Figure 2.25 A homoclinic tangle.

This function is very important, since if $\frac{dM}{dt_0} \neq 0$ (simple zeros) then the intersections are transversal. Hence this method can be used to detect transversal homoclinic orbits. As we have discussed, these imply the presence of horseshoes in the Poincaré map and hence the presence of chaos in the system.

Silnikov's method applies to stationary points of the saddle-focus type, when there is a homoclinic trajectory passing through the saddle-focus. The saddle point has complex eigenvalues. Silnikov showed that if the real eigenvalue has larger magnitude than the real part of the complex eigenvalues then there are horseshoes present in the return map defined near the homoclinic orbit, i.e., there exists a set of chaotic trajectories near the original homoclinic trajectory. This criterion has been applied to the Rössler system, and such homoclinic orbits in flows have been found in phase portrait analysis for nerve axon equations.

2.17b NUMERICAL METHODS

We first mention a plausible objection against a numerical study of chaos using digital computers, put forward in Hao (1984). He suggests that it is impossible to realize even a quasi-periodic process, let alone chaotic orbits, since one works with a finite field of rational numbers representable on a digital computer of finite word length. He counters

this objection by stating that irrational numbers can be approximated by rationals and that chaotic regions are surrounded by periodic regimes. A very interesting discussion of numerical methods is presented in Hao (1984) and we summarize his discussion of the various methods in that which follows.

The main aim of numerical experiments in this context is to obtain high frequency resolution. Resolving power shall be compared in terms of the recognizable order p subharmonics with respect to the natural fundamental frequency of the system under study. For example $p = 2^n$ for period-doubling sequences etc.,

(i) the method with least resolution is direct observation. One advantage of this method is that a common sense veiwpoint can be adopted and physical intuition applied.

(ii) Poincaré maps are a common and effective means of observing the aspects of the motion under study. The Poincaré was discussed in Section 1.3. A practical problem involved matches the precision of the interpolation scheme used to locate the intersection point with that of the integration algorithm.

(iii) For periodically driven systems, stroboscopic sampling at fundamental and subharmonic frequencies is highly successful. Very high frequency resolution can be obtained at the expense of computing time. Various safeguards must be implemented when using subharmonic stroboscopic sampling to cope with factors such as round-off errors or to distinguish transient, or intermittent behaviour from chaotic behaviour. According to Hao (1984), period-doubling sequences up to p = 8192 have been identified in systems of ODE's using these methods.

Hao (1984) derives a rather useful relationship in his discussion of power spectrum analysis in the frequency domain which we shall present here. Let τ denote the sampling interval and $L = N\tau$ be the sampling

time for a single spectrum. Thus N equals the number of sampled points. These parameters, τ and L determine the two frequencies: $f_{max} = \frac{0.5}{\tau}$ is the maximal frequency one can measure using the given sampling interval; $\Delta f = \frac{1}{L}$ is the frequency difference between two adjacent Fourier coefficients. Now one has to take $f_{max} = kf_0$, where f_0 is the fundamental frequency of the physical system and k is a multiplier of the order 4 to 8, to eliminate effectively the aliasing phenomenon.

We want to resolve the p^{th} subharmonic of f, and want the subharmonic peak to be formed by s points in the spectrum i.e., $\frac{f_0}{p} = s\Delta f$. By combining all the above-mentioned relations we arrive at:

$$P = \frac{N}{2ks} \tag{2.64}$$

a relation which is independant of τ and f_0. The example Hao (1984) uses is, if: N = 8192, k = 4, s = 8, then p = 128, which is the limit of resolution in power spectrum analysis on most medium-size computers. Power spectrum analysis is the most effective method to tell different periods embedded in the chaotic bands.

This chapter is closed with a summary table from Hao (1984), which gives the main findings in computer experiments on various models. See Table 2.1.

Model	Method	Findings
Lorenz (5-4)	Poincaré map Power spectra Lyapunov exponents Dimension	Period-doubling Intermittency Transient chaos Strange attractor
Forced Brusselator (5-12)	Stroboscopic sampling Power spectra Lyapunov exponents Dimension	Period-doubling Intermittency Quasiperiodic to chaos Hierarchy of chaotic bands *U*-sequence and attractor
Rossler (5-6)	Power spectra Dimension	Period-doubling
Coupled Brusselator	Poincaré map Lyapunov exponents Dimension	Period-doubling Intermittency Metastable chaos Quasiperiodic to chaos Strange attractor
Double-diffusive convection	Trajectory	Period-doubling
3-wave coupling	Poincaré map Power spectra Lyapunov exponents Dimension	Period-doubling Strange attractor
5-mode truncat. Navier-Stokes	Poincaré map Power spectra	Period-doubling
6-mode truncat. Navier-Stokes	Poincaré map Power spectra	Quasiperiodic to chaos Hysteresis, Intermittency
7-mode truncat. Navier-Stokes	Poincaré map	Quasiperiodic to chaos Hysteresis
Duffing (5-9)	Poincaré map Power spectra	Period-doubling Quasiperiodic to chaos Strange attractor
Parametric pendulum	Stroboscopic sampling Power spectra Lynapunov exponents	Period-doubling Strange attractor
PDE's of thermo-solutal convection	Trajectory Time evolution of	Period-doubling Chaos

Table 2.1. Brief summary of computer experiments on differential equations (after Hao, 1984).

CHAPTER 3

CHARACTERIZING AND CLASSIFYING THE ATTRACTORS

We have seen that dissipative dynamical systems which exhibit chaotic behaviour often have an attractor in phase-space which is strange. Strange attractors are typically characterized by fractal dimensionality D, which is smaller than the number of degrees of freedom F, i.e., $D < F$. For example, the limit cycle attractor of the van der Pol oscillator (a two-dimensional dynamical system) appears one-dimensional. The simplest dynamical systems in three dimensions (such as those of Lorenz and Rössler) have attractors that appear locally two-dimensional.

We first examine why it is desirable to find some quantitative means to recognize, characterize and classify the attractors. Fractals and Cantor sets (since many attractors have a Cantor set like structure) are presented as geometrical objects having non-integer dimension. The various notions of dimension including Hausdorff, Kolmogorov capacity, information dimension and Lyapunov exponents are discussed and in each case methods for determining the particular quantity are looked at. Also some plausible conjectures are presented concerning the relationships between the various notions of dimension. In particular we look at the conjectures of Mori and of Kaplan and Yorke. Finally we briefly discuss reconstructing the attractors from experimental data.

Of paramount importance to the whole discussion is the concept of Lyapunov characteristic exponents (LCE's). Consequently much of the discussion will centre on LCE's, their determination and their interpretation. LCE's are also looked at in relation to one-dimensional mappings.

3.1 THE NEED TO DISTINGUISH

Let us consider a physical example. Couette flow experiments (see Appendix B) near the transition from laminar to turbulent flow

suggest that fluid motion in the weakly turbulent regime can be understood in terms of low-dimensional chaotic or strange attractors. In that case it is possible that weakly turbulent fluid flow, which in principle must be considered as an infinite-dimensional system, can be modelled by a system with relatively few phase-space dimensions. (This idea also arises with Rayleigh Bénard convection as discussed earlier). However, many natural phenomena, in contrast to this exhibit aperiodic behaviour that can only be explained by a model with a very large number of dimensions. An example from Froehling et al (1981) which illustrates this is that of a model of thermal noise in a resistor. This model must account for the motions of the individual electrons within the resistor. The number of electrons involved is so large that any signal derived from the system appears "noisy". As a first step in modelling systems exhibiting aperiodic behaviour then, we must distinguish between those having an underlying low-dimensional chaotic attractor, and those requiring a large number of phase-space dimensions for a dynamical description.

Both in the laboratory and on computers it is very difficult to distinguish a purely chaotic motion from a quasi-periodic one or from a motion perturbed by external noise by simply looking at the finite sequence of data. As pointed out by Hao (1984), mathematicians have prepared such nice notions as hyperbolic attractor, axiom A system and Smale's horseshoe. Unfortunately these are not always directly applicable to systems of physical interest. It is also desirable to measure the strangeness of strange attractors from the data available; in particular, from a single time series of sampled points.

Power spectrum analysis is useful in telling quasi-periodic motion from periodic, and in identifying higher order periodicities embedded in chaotic bands by the fine structure of the spectra. Power spectrum analysis characterizes aperiodic behaviour by the presence of broadband noise in the power spectrum. However, broadband noise can be produced by systems requiring either a small or large number of phase-space

dimensions. Thus the power spectrum fails to make this distinction. Low and high dimensional aperiodicity must instead be distinguished by a direct measurement of the number of coordinates needed to specify the state of the physical system under observation. References for papers on the scaling properties of power spectra are given in Hao (1984). So putting power spectra aside, we turn to the more sophisticated ways of characterizing attractors, among which are the various definitions of dimension and the Lyapunov characteristic exponents (LCE's).

We know that the phase-space volume of a dissipative dynamical system contracts in the process of evolution and that the motion is confined to a certain attractor in the long time limit $t \to \infty$. The dimension of the attractor D is lower than the dimension of the phase-space. Using any reasonable definition of dimension, the dimension of simple attractors can easily be calculated to be integers: $D = 0$ for fixed points, $D = 1$ for limit cycles, $D = 2$ for 2-tori etc. However, the dimension of strange attractors often turns out to have noninteger value. We now look at objects with noninteger dimension.

3.2 DIMENSION AND BOX-COUNTING ALGORITHMS

It is important to realize that a strange attractor cannot be generated merely by the contraction of the phase volume. The strange attractor has a sensitive dependence on initial conditions, i.e., solutions which start out together infinitesimally close, must eventually depart from each other. Exponential divergence of nearby trajectories within a compact object requires "folding" of sheets. A simple example of this process is illustrated in Figure 2.5 by Lanford. Trajectories diverge exponentially within a sheet, then the sheet folds and connects back to itself. In Lanford's description at a model strange attractor, it is the stretching property that ensures the eventual departure of adjacent solutions. Finally each member of the set of solutions comprising the strange attractor occupies zero volume in phase space. It is this

characteristic that forces the strange attractor to have noninteger dimensionality, or, in Mandelbrot's terms, *fractal measure*. The attractor is not simply a sheet with a single fold, but a sheet folded, and refolded infinitely by the flow. A line segment which cuts the attractor transverse to these sheets will intersect the attractor in a Cantor set. The attractor has *topological dimension* two but a *fractal dimension* greater than two.

A generalized definition of dimension was introduced by Hausdorff as early as 1919. It can be explained very simply in the following way. Take a usual "regular" geometrical object, say a cube, and double its linear size in each spatial direction. We get a cube whose volume is eight times larger than the original one, because $2^3 = 8$. In general, taking an object of dimension D_H and increasing its linear size in each spatial direction u times, one would have its volume increased to

$$v = u^{D_H} \tag{3.1}$$

times the original. By inverting this simple relationship we get a new definition for dimension:

$$D_H = \frac{\ell n\, v}{\ell n\, u}. \tag{3.2}$$

We have now freed ourselves from the restriction of D_H being an integer. A precise definition of *Hausdorff dimension* requires the notion of Hausdorff measure. We now look at the simplest example of a geometrical object having noninteger dimension: the *Cantor set*.

Recall how we constructed the "middle third" Cantor set by taking the interval $[0,1]$ and deleting the central one third $(\frac{1}{3}, \frac{2}{3})$, then repeating this operation with respect to the remaining segments again and again, ad infinitum. Let us calculate the dimension of the limiting set of points thus obtained. Let the points left in the interval $(0, \frac{1}{3})$ constitute our geometric object under consideration. Increasing its linear size by a factor $u = 3$ would yield 2 copies ($v = 2$) of the same object. Therefore:

$$D_H = \frac{\ell n 2}{\ell n 3} = 0.6309\ldots \quad . \tag{3.3}$$

We now examine some other interesting fractals.

The fractal idea as a description of turbulence precedes that of the dimensionality of the strange attractor and, in the geometric form put forward by Mandelbrot (1977), has considerable conceptual power. A *fractal curve* is a curve that is everywhere continuous but nowhere differentiable. An example of a fractal curve is the Brownian motion of a particle. Also before one sweeps the fractal idea of turbulence aside too quickly, they should recall that the Navier-Stokes equations can be considered as an ensemble average over a set of Brownian motion curves. To illustrate these curves and their properties, an example is given in Figure 3.1.

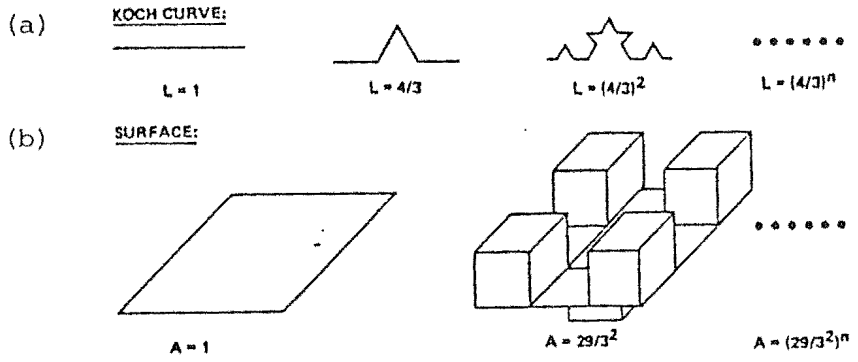

Figure 3.1 Examples of fractals (after Chapman and Tobak, 1985)

The simplest example is the *Koch curve* which is constructed in the following recursive manner. Take a line one unit long and divide it into three equal segments. Remove the Cantor segment and replace it with two equal segments to form a "hat". This process is repeated recursively on each of the new segments that are formed at successive steps. Now the length of the resulting curve increases without limit as the number of repetitions (n) increases without limit, but the curve does not fill up any space. Only a line with apparent texture results. A Koch curve is illustrated in Figure 3.1a. Another way to think of this

is to take three of these Koch curves and form an equilateral triangle. Now note that we have a finite enclosed area (an island) surrounded by a perimeter (coastline) that is infinitely large. The point is well described in Mandelbrot (1977) in the chapter entitled "How long is the Coast of Britain"? We can now form a relationship between the length of the line p and the length of the element used to construct p;q, at any point of the iteration:

$$p = q^{\alpha} . \tag{3.4}$$

Hence for the Koch curve we have: $\left(\frac{4}{3}\right)^n = \left[\left(\frac{1}{3}\right)^n\right]^{\alpha}$

or
$$\alpha = 1 - \frac{\ell n 4}{\ell n 3} \tag{3.5}$$

Now α can be interpretated as the difference between the *topological* (or *Euler*) *dimension*, D_T, of the element q, which in this case is 1, and the dimension of the line p, which is the fractal or Hausdorff dimension D_H; i.e., $\alpha = D_T - D_H$, or, for the Koch curve:

$$D_H = \frac{\ell n 4}{\ell n 3} = 1.262... \quad . \tag{3.6}$$

Note that if $D_T = D_H$, then the length of the line does not depend on the size of unit of construction, which is what one expects for smooth curves.

Another example, closely related to turbulence, illustrated in Figure 3.1b is that of a surface. This may be thought of as a surface of vorticity. It is distorted in the following recursive manner. Divide the unit square into nine small squares. Now remove the four corners and the center square and replace them by building a small square box over the open squares (center box down for convenience). With each of the 29 sides of the new figure, repeat the process. The surface becomes more and more distorted with each step, and the actual surface area increases without limit as the number of iterations increases. Hence, the surface in two dimensions becomes more and more distorted, but never fills up space in three dimensions. In a manner similar to

that used for the Koch curve, the fractal dimensions is found to be:

$$1 + \frac{\ell n 29}{\ell n 9} = 2.53\ldots \ . \tag{3.7}$$

For the direct numerical calculation of D based on (3.2), a box-counting algorithm may be employed. One divides that part of the phase space where the attractor lies into small cells of linear size ε, and counts the number $N(\varepsilon)$ of such cells that contain at least one point of the orbit. A list is kept throughout of these boxes containing at least one point on the attractor. Each newly generated point is checked to see if its box is on the list and if not, it is added to the list. After many iterations, the number of boxes approaches $N(\varepsilon)$. For small ε, we expect:

$$N(\varepsilon) \approx k\varepsilon^{-D} \ . \tag{3.8}$$

We define the quantity:

$$D_c = \lim_{\varepsilon \to 0} \frac{\ell n\ N(\varepsilon)}{\ell n \left(\frac{1}{\varepsilon}\right)} \ . \tag{3.9}$$

This is called the *Kolmogorov capacity* of the limiting set of points. One can see that:

$$D_c - D \approx \frac{\ell n\ k}{\ell n \left(\frac{1}{\varepsilon}\right)} \ . \tag{3.10}$$

It is difficult to make $D_c - D$ small by making ε small since the dependance is logarithmic. Note however, that for small ε, a plot of D_c versus $\left[\ell n \left(\frac{1}{\varepsilon}\right)\right]^{-1}$ will be approximately linear. This is in fact observed numerically. Our "measured" values of D are determined by least squares fitting a straight line to D_c versus $\left[\ell n \left(\frac{1}{\varepsilon}\right)\right]^{-1}$ for several small values of ε, and then extrapolating the result to $\varepsilon \to 0$. The accuracy of the result is estimated from the standard deviation of the points from the fitted line. For a plane, D_c is two by this construction, the same as the topological dimension D_T. The simplest strange attractors (those lying in three-dimensional phase spaces have fractal dimension

between 2 and 3. D_c then measures how "closely packed" the sheets of the attractor are. Several different box-counting algorithms have been presented and it turns out that it is very difficult to compute D whenever $D \gtrsim 2$. A possible reason for much interest in D_c for a strange attractor is that it says something about the amount of information necessary to specify the attracting set to within an accuracy ε. For more details on this point, see Russel et al (1980).

So far in counting $N(\varepsilon)$, no attention has been paid to the possible inhomogeneity of the attractor. i.e., no matter how many times the orbit travels through a given cell, the cell is counted only once. To correct this inexactitude one introduces a weight according to how frequently a cell is visited. If the i-th cell is visited with a probability P_i, then the definition (3.8) is replaced by:

$$D_I = \lim_{\varepsilon \to 0} \frac{I(\varepsilon)}{\ell n \left(\frac{1}{\varepsilon}\right)} \tag{3.11a}$$

where

$$I(\varepsilon) = - \sum_{i=1}^{N(\varepsilon)} P_i \ell n P_i \tag{3.11b}$$

and $N(\varepsilon)$ is the total number of cells visited. If every cell is visited with equal probability i.e., $P_i = \frac{1}{N(\varepsilon)}$, then (3.11b) reduces to: $I(\varepsilon) = \ell n\, N(\varepsilon)$ and $D_I = D_c$. In general

$$D_I \leqslant D_c . \tag{3.12}$$

D_I is called the *information dimension*. There exists several different ways to define dimension. See especially the review by Froehling et al (1981). It is conjectured that the Hausdorff dimension is equal to D_c and some other definitions are equivalent to D_I. Numerical calculations seem to support this conjecture.

3.3 CORRELATION INTEGRAL

Another useful notion is that put forward by Grassberger and Procaccia (1983). They suggest a different measure for the strangeness of attractors, a measure which can easily be obtained from any time

series without resorting to Poincaré maps, and which is closely related to the fractal dimension. The measure is obtained by considering correlations between points of a long-time series on the attractor. Denote the N points of such a long-time series by $\{\vec{X}_i\}_{i=1}^{N} \equiv \{\vec{X}(t+i\tau)\}_{i=1}^{N}$, where τ is an arbitrary but fixed time increment. The definition of the *correlation integral* is:

$$c(r) \equiv \lim_{N\to\infty} \frac{1}{N^2} \sum_{i,j=1}^{N} \theta(r - |\vec{X}_i - \vec{X}_j|) = \int_0^r dr^1\, c(\vec{r}^1) \qquad (3.13)$$

where $\theta(x)$ is the Heaviside function and $c(\vec{r})$ is the standard correlation function. Now $c(r)$ behaves as a power of r for small r:

$$c(r) \propto r^{\alpha} . \qquad (3.14)$$

Moreover, the exponent α is closely related to D as well as the *information theoretic entropy*.

Shown in Figure 3.2a,b are the logarithms of the correlation integrals for the Hénon map and the Lorenz model as a function of log r. Equally convincing power laws were obtained for the Kaplan-Yorke map, the Rabinovich-Fabrikant equations, and the logistic map at the onset of chaos. For the Zaslavskii map no clear power law is obtained even for longer runs. One can see from Table 3.1 that α is in all cases very close to D, but is never greater than D, with the exception of Zaslavskii's map where no good power law is seen. The errors quoted are "educated guesses". Grassberger and Procaccia (1983) argue that the value $\alpha = 1.21$ obtained for the Hénon map is wrong as a result of systematic errors, and an improved estimate yields $\alpha = 1.25 \pm 0.02$ so that $\alpha = D$ within the errors.

An estimate of the information content of the strange attractor in question can be made using:

$$\alpha \leqslant D_I \leqslant D . \qquad (3.15)$$

Note that when the covering of the attractor is uniform, the inequalities in (3.15) are realized. The fact that $\alpha \neq D$ in the logistic map shows

that in this case the coverage is not uniform. Certain neighbourhoods have higher "seniority" in the sense that they are visited more often than others. The fractal dimension is ignorant of seniority. It has only

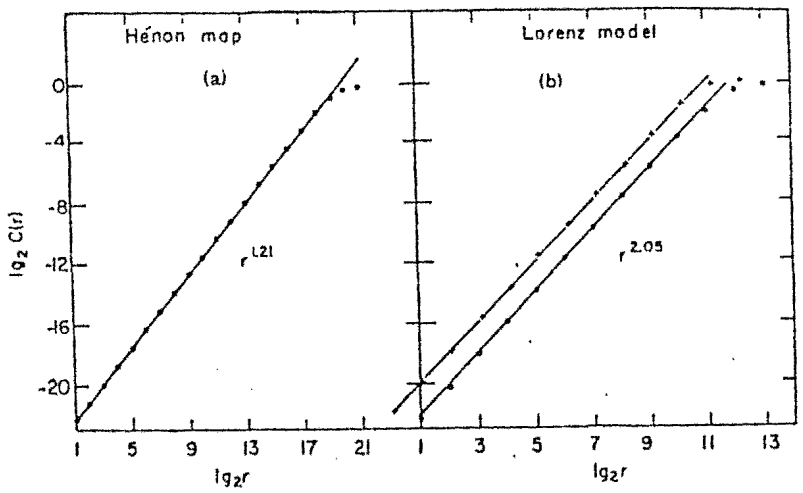

Figure 3.2 Correlation integrals for (a) Hénon map and (b) Lorenz model on doubly logarithmic scales. In (b) the upper line was computed from a single variable time series. In both panels the scale of r is arbitrary. (after Grassberger and Procaccia, 1983)

	α	No. of iterations, time increment τ	D
Hénon map,	1.21 ± 0.01	15 000	1.26
$a = 1.4$, $b = 0.3$	1.25 ± 0.02	20 000	
Kaplan-Yorke map,			
$\alpha = 0.2$	1.42 ± 0.02	15 000	1.431
Logistic equation,	0.500 ± 0.005		
$b = 3.569\,945\,6\ldots$	$0.4926 < \nu < 0.5024$	25 000	0.538
Lorenz equation	2.05 ± 0.01	15 000; $\tau = 0.25$	2.06 ± 0.01
Rabinovich-Fabrikant equation	2.18 ± 0.01	15 000; $\tau = 0.25$	...
Zaslavskii map	(~1.5)	25 000	1.39

Table 3.1 Maps used in evidence with values of corresponding parameter. (after Grassberger and Procaccia 1982)

to do with the geometrical structure of the attractor. Regions of the attractor which are rarely visited contribute to D with equal weight as regions of high visiting weight. The correlation integral is however, sensitive to this effect. In this sense α may be a more relevant

measure of the attractor than D because it is sensitive to the dynamical process of coverage of the attractor. The difference between α and D gives a measure of the importance of different seniority of different neighbourhoods.

3.4 APPROXIMATE FRACTAL DIMENSION

In certain instances, particularly when trying to reconstruct an attractor from a time-series, it is important to know the *approximate fractal dimension*. i.e., the closest integer approximation to the fractal dimension. Several techniques have been proposed for calculating the approximate fractal dimension. See Crutchfield et al (1980) for example, and Takens (1981). Unfortunately these methods appear to be sensitive to instrumental noise, and they require an unduly large number of data points. An algorithm which is less sensitive to noise is presented in Froehling, et al (1981).

One collects N-dimensional phase-space points that presumably lie on an attractor with approximate fractal dimension N - 1 or less. It is required that the phase-space be partitioned so that each portion of the embedded attractor is approximately flat. This partition is accomplished by sorting the phase-space data into N-dimensional boxes according to their coordinate value in each dimension. If the phase-space points in each box lie close to a piece of manifold or branched manifold we can describe these points as lying approximately in a linear space at dimension less than N. Multilinear regression is the natural analysis to apply to these points. On N-dimensional phase-space points it finds the best hyperplane (dimension N - 1 or less) that fits the data. By using smaller dimensional phase-spaces we can fit smaller-dimensional linear subspaces. The goodness of fit in each box is measured by χ^2, the sum of the squares of the deviations from this hyperplane divided by the number of degrees of freedom. If the dimension of the hyperplane is too small the fit will typically be poor and χ^2 will be large. When the

dimension is increased so that the hyperplane gives a good fit to the data, χ^2 will drop sharply. The dimension of this hyperplane provides the approximate fractal dimension of the attractor (locally). Figure 3.3 displays the results of this Local Linear Regression (LLR) in a histogram of the logarithm of χ^2, showing the number of occurrences of ranges of χ^2 for regions of the attractor where the analysis is applicable. Figure 3.3 shows the χ^2 histograms for the Rössler attractor. The greatest number of occurrences of χ^2 for planes occurs lower by a factor of one million than the peak in occurrences for points and lines, indicating that the Rössler attractor looks locally planar. That some local regions have poor plane fits is due to the branched manifold structure.

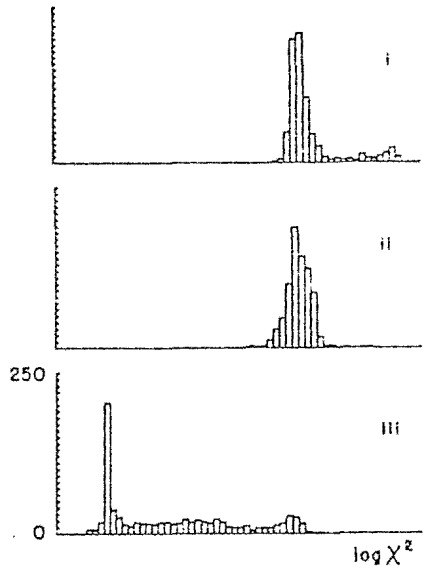

Figure 3.3 Chi-squared histograms for Rössler attractor using natural coordinates. $\Delta t = 0.2$, box size = 0.5, noise $\sigma = 0.01$ (= 0.1) added, 10,000 3-D points. (i)-(iii) best fit points, lines and planes. On these histograms, every five columns on the horizontal axis represent a factor of 10 difference in χ^2; every tick mark on the vertical axis represents 10 occurrences of a particular range of χ^2. (after Froehling et al, 1981)

There is another quantity arising in LLR which also characterizes the dimension of the attractor. If too many phase-space coordinates are chosen, the system of equations determining the hyperplane is over-determined: the resulting correlation matrix will be singular (with noise in the systems the correlation matrix will be approximately singular).

This fact can be used to determine the number of independent quantities needed to specify a physical system. It is worth mentioning data acquisition requirements. If we use D-dimensional boxes of diameter ε, the number of boxes required to cover the attractor is $N(R) \approx R^D$, where $R = \frac{1}{\varepsilon}$ is the resolution used in constructing the cover of boxes. Also the number of data points (n) that must be taken for the successful determination of the dimension of the best fit hyperplane is:

$$n \approx (D+1)N \approx (D+1)R^D \qquad (3.16)$$

for further details on LLR, see Farmer et al (1981).

As we have pointed out, the box-counting algorithms to computer dimension are very time-consuming and become impractical when the dimension of the original phase-space $N \geqslant 2$. Even the LLR method for determining approximate fractal dimension is limited to attractors of dimension less than about five. For example, using (3.16), if $R = 20$, $D = 5$, then $n \approx 2 \times 10^7$. It is often impractical to gather or process this many data points. Also, the dimension reflects only one aspect of dissipative dynamics, namely, the contraction of phase volume. We know that a strange attractor cannot be generated by contraction alone and that it must be stretched and folded as well. To describe those more subtle features we need the notion of Lyapunov characteristic exponents.

3.5 LYAPUNOV CHARACTERISTIC EXPONENTS: DERIVATION

Lyapunov characteristic exponents (LCE's) characterize the asymptotic orbital instability of dynamical systems. The following derivation is based on that in Shimada and Nagashima (1979) and Hao (1984).

The method employed to examine the time-dependant behaviour of small deviations from an orbit is Lyapunov's method which uses the first variational equation of orbits. Consider the following set of autonomous ordinary differential equations:

$$\dot{\underset{\sim}{x}} = \underset{\sim}{G}(\underset{\sim}{x}) \; . \qquad (3.17)$$

The solution of (3.17) under the initial condition $\underset{\sim}{x}(0) = \underset{\sim}{x}_0$ is written:

$$\underset{\sim}{x}(t) = T^t \underset{\sim}{x}_0 \tag{3.18}$$

where T^t is the map which describes time-t evolution of all phase points.

The time evolution equation for the first variation of the orbit obeys the following set of nonautonomous linear differential equations:

$$\dot{\underset{\sim}{dx}} = \frac{\partial \underset{\sim}{G}}{dx} (T^t \underset{\sim}{x}_0) \delta \underset{\sim}{x} \tag{3.19}$$

the solution of (3.19) may be written:

$$\delta \underset{\sim}{x}(t) = V^t_{\underset{\sim}{x}_0} \delta \underset{\sim}{x}_0 \tag{3.20}$$

where $V^t_{\underset{\sim}{x}_0}$ is the fundamental matrix of (3.19), and $\delta \underset{\sim}{x}_0$ is an initial deviation at $t = 0$. Also the fundamental matrix in (3.20) satisfies the following chain rule:

$$V^{t+s}_{\underset{\sim}{x}_0} = V^t_{T^s \underset{\sim}{x}_0} \circ V^s_{\underset{\sim}{x}_0} . \tag{3.21}$$

The eigenvalues of the fundamental matrix

$$V_{ij}(x_0) = \left. \frac{dG_i}{dx_j} \right|_{x=x_0} \tag{3.22}$$

determine the local stability of (3.17) in the vicinity of $\underset{\sim}{x}_0$. If the real parts of some eigenvalues happen to be positive numbers, then nearby trajectories will depart at an exponential rate. By averaging the real parts of all eigenvalues, we obtain a set of global characteristics. The Lyapunov characteristic exponents (LCE's). There is a more intuitive way to calculate n real numbers playing the same role.

From (3.21) one can see that the asymptotic behaviour of a small deviation is described by the asymptotic behaviour of the fundamental matrix for $t \to \infty$. The asymptotic behaviour of this matrix for $t \to \infty$ can be characterized by the following exponents:

$$\lambda(e^k, \underset{\sim}{x}_0) = \lim_{t \to \infty} \frac{1}{t} \log \frac{\| V^t_{\underset{\sim}{x}_0} \underset{\sim}{e}_1 \wedge V^t_{\underset{\sim}{x}_0} \underset{\sim}{e}_2 \wedge \ldots \wedge V^t_{\underset{\sim}{x}_0} \underset{\sim}{e}_k \|}{\| \underset{\sim}{e}_1 \wedge \underset{\sim}{e}_2 \wedge \ldots \quad \ldots \wedge \underset{\sim}{e}_k \|} \tag{3.23}$$

for $k = 1, 2, \ldots, N$. The symbols in (3.23) have the following meanings.

e^k is a k-dimensional subspace in the tangent space $\underset{\sim}{E}\underset{\sim}{x}_0$ at $\underset{\sim}{x}_0$, $\{\underset{\sim}{e}_i\}$ $(i = 1,2,\ldots, k)$ are a set of bases of e^k, $\wedge$ is an exterior product ($\wedge$ generalizes the vector product X to higher-dimensional spaces), and $\|\cdot\|$ is a norm with respect to some Riemannian metric.

The exponent defined by (3.22) represents an expanding rate of volume of the k-dimensional parallelipiped in the tangent space along the orbit which starts at $\underset{\sim}{x}_0$, and is called the k-dimensional Lyapunov characteristic exponent. From this definition it is clear that the exponent does not depend on a choice of a set of bases or norms, but depends only on the k-dimensional subspace e^k. We now list some properties of the LCE's.

3.6 PROPERTIES OF THE LYAPUNOV CHARACTERISTIC EXPONENTS

(i) The one-dimensional exponent $\lambda(e^1,\underset{\sim}{x})$ may take, at most, N distinct values for an N-dimensional phase-space. The notation $\{\lambda_i\}_{i\leqslant 1\leqslant N}$ is used and the N real exponents are ordered as $\lambda_1 \geqslant \lambda_2 \geqslant \ldots \geqslant \lambda_N$, with $\lambda_1 = \lambda_{max}$ being the largest.

(ii) The k-dimensional exponent $\lambda(e^k,\underset{\sim}{x})$ may take, at most, ${}^NC_k$ distinct values, and each value is connected with a sum of k distinct one-dimensional exponents. For example in the case N = 3, the k-dimensional exponents $\lambda(e^k,\underset{\sim}{x})$ $(k = 1,2,3)$ may take the following values respectively:

$\lambda(e^1,\underset{\sim}{x})$ = one of the values in $\{\lambda_1,\lambda_2,\lambda_3\}$

$\lambda(e^2,\underset{\sim}{x})$ = one of the values in $\{(\lambda_1+\lambda_2),(\lambda_1+\lambda_2),(\lambda_2+\lambda_3)\}$

$\lambda(e^3,\underset{\sim}{x}) = (\lambda_1+\lambda_2+\lambda_3)$

(iii) If a set of bases $\{\underset{\sim}{e}_i\}$ $(i = 1,2,\ldots, N)$ is chosen at random in tangent space, then the k-dimensional exponents $\lambda(e^k,\underset{\sim}{x})$ for $k = 1,2,\ldots, N$ converge respectively, with probability one, to the maximal values among sets of values which are allowed to possess ${}^NC_k$ distinct values. (This proposition was proved by Benettin et al (1976) in the case of diffeomorphisms).

i.e., $\lambda(e^1, \underset{\sim}{x})$ converges to the length ratio λ_1

$\lambda(e^2, \underset{\sim}{x})$ converges to the parallelogram area ratio $\lambda_1 + \lambda_2$

$\vdots$

$\lambda(e^k, \underset{\sim}{x})$ converges to the k-dimensional hyperparallelepiped volume ratio $\lambda_1 + \lambda_2 + \ldots + \lambda_K$.

In the limit, the N-dimensional hyperparallelepiped volume ratio converges to the sum of all the Lyapunov exponents:

$\lambda_1 + \lambda_2 + \ldots + \lambda_N$.

(iv) The average volume contraction rate is:

$$\Lambda_0 = \sum_{i=1}^{N} \lambda_i \tag{3.24}$$

i.e., $\sum_{i=1}^{N} \lambda_i = -$ div $\underset{\sim}{G}$, where $\underset{\sim}{G} = (g_1, g_2, \ldots, g_N)$ in (3.17).

In practice this serves as a good check for the correctness of computation.

(v) The LCE's measure the average rate of exponential divergence of nearby trajectories within the attractor when positive. The magnitude of an attractors positive exponents is a measure of its "degree of chaos". Also, one of the exponents representing the direction along the flow is zero.

(vi) The LCE's and definitions of Λ_0 apply to maps as well as flows, including the Poincaré map for a given flow. The N - 1 LCE's, of the Poincaré map are proportional to the N LCE's of the flow with the zero exponent deleted.

(vii) For chaotic motion we must have $\lambda_1 > 0$. For dissipative flows, volume must contract. These two facts show that one- and two-dimensional flows cannot give rise to chaos. In two dimensions, N = 2, the Poincaré map is one-dimensional (and invertible) and (3.23) yields $\Lambda_0 = \lambda_1$. Such a map cannot be dissipative ($\Lambda_0 < 0$) and chaotic ($\Lambda_1 > 0$). The simplest dissipative systems displaying chaotic behaviour are thus three-dimensional flows and their

related two-dimensional maps. The maps must have $\lambda_1 > 0$ and $\lambda_1 + \lambda_2 < 0$ for the motion to be chaotic.

One-dimensional noninvertible maps arise in certain limiting cases from $N \geqslant 2$ invertible maps. We examine these in chapter 4. For these maps, the link between volume expansion and exponential divergence of nearby trajectories is broken. For $\lambda_1 > 0$, one observes bounded chaotic motion. In an approximate sense, these maps are embedded in higher-dimensional systems.

For an algorithm to calculate the LCE's, see Shimada and Nagashima (1979).

3.7 CONJECTURES

Kaplan and Yorke (1979) conjectured that the Kolmogorov capacity D_C is related to the spectrum of LCE's as follows:

$$D_C = j + \frac{\left(\sum_{i=1}^{j} \lambda_i\right)}{-\lambda_{j+1}} \tag{3.25}$$

where the LCE's are ordered as in Section 3.6 (i), and j is the number of LCE's which assures the nonnegativeness of the sum in (3.25).

i.e., $\sum_{i=1}^{j} \lambda_i > 0$.

In the extreme cases $j = 0$ or $j = n$, define $D_C = 0$ or n respectively.

In fact the fractal dimension used by Kaplan and Yorke in their conjecture is the information dimension, which is bounded from above by the Kolmogorov capacity.

Another relation between dimension and LCE's has been put forward by Mori (1980):

$$D_C = M_0 + M_+\left(1 - \frac{\lambda_+}{\lambda_-}\right); \quad \lambda_+ = \frac{1}{M_+}\sum_{\lambda_i>0} \lambda_i, \quad \lambda_- = \frac{1}{M_-}\sum_{\lambda_i>0} \lambda_i \tag{3.26}$$

where M_-, M_0, M_+ denote the number of negative, zero, and positive exponents respectively. For sufficiently large n, (3.26) differs from (3.25) significantly, because all negative exponents contribute to (3.26), whereas only a finite number of them enter (3.25). Numerical experiments

seem to be in favour of (3.24).

Table 3.2, after Russel et al (1980), shows a comparison of the direct calculation of D_c using (3.9) and the value determined indirectly using (3.25). The comparison is for three different two-dimensional maps and one three-dimensional flow. The maps are as follows:

System tested	d from Lyapunov numbers	d from program based on Eq. (3.9)
Henon map, $a = 1.2$, $b = 0.3$	1.200 ± 0.001	1.202 ± 0.003
Henon map, $a = 1.4$, $b = 0.3$	1.264 ± 0.002	1.261 ± 0.003
Kaplan and Yorke map, $\alpha = 0.2$	1.430 676 6	1.4316 ± 0.0016
Zaslavskii map, $\Gamma = 3.0$, $\varepsilon = 0.3$, $\nu = 10^2 \times 4/3$	1.387 ± 0.001	1.380 ± 0.007
Ordinary differential equations	2.317 ± 0.001	2.318 ± 0.002

Table 3.2 Summary of test data (after Russel et al, 1980)

(a) The Hénon map:

$$\left.\begin{aligned} x_{j+1} &= y_j + 1 - ax_j^2 \\ y_{j+1} &= bx_j \end{aligned}\right\} \qquad (3.27)$$

(b) The Kaplan-Yorke map:

$$\left.\begin{aligned} x_{j+1} &= 2x_j \pmod 1 \\ y_{j+1} &= \alpha y_j + \cos 4\pi x_j \end{aligned}\right\} \qquad (3.28)$$

and (c) The Zaslavskii map:

$$\begin{aligned} x_{j+1} &= [x_j + \gamma(1 + \mu y_j) + \varepsilon\gamma\mu \cos 2\pi x_j \pmod 1 \\ y_{j+1} &= \exp(-\Gamma)(y_j + \varepsilon \cos 2\pi x_j) \end{aligned} \qquad (3.29)$$

where $\mu = [1 - \exp(-\Gamma)]\Gamma^{-1}$.

For two-dimensional maps with $\lambda_1 > 0 > \lambda_1 + \lambda_2$ representing one expanding direction with area contraction, (3.25) reduces to:

$$D = 1 - \frac{\lambda_1}{\lambda_2}. \qquad (3.30)$$

Also for three-dimensional flows with $\lambda_1 > 0 > \lambda_3$, $\lambda_2 = 0$ and $\lambda_1 + \lambda_3 < 0$:

$$D = 2 - \frac{\lambda_1}{\lambda_2} . \tag{3.31}$$

The system of three ODE's studied describes the saturation of a linearly unstable plasma wave via cubicly nonlinear coupling to linearly damped waves. For further details, see Russel et al (1980).

To find the LCE's for the Henon and Zaslavskii maps, λ_1 is numerically calculated and λ_2 is determined using the known area contraction for these maps:

$$\lambda_1 + \lambda_2 = \ell n \, |\det M| . \tag{3.32}$$

For the Hénon map, det M = -b and for the Zaslavskii map det $M = e^{-\Gamma}$. For the Kaplan and Yorke map, λ_1 and λ_2 are found analytically to be: $\lambda_1 = \ell n\, 2$ and $\lambda_2 = \ell n\, \alpha$. For the flow system studied, $\lambda_1 + \lambda_3$ is known analytically and λ_1 is calculated numerically.

Numerically, the calculation of D_C from the conjecture (3.25) is much less castly than the box-counting techniques because the LCE's converge fairly rapidly. As one can see for Table 3.2, agreement between (3.9) and (3.25) is good in all cases. The Kaplan-Yorke conjecture is not yet proven.

3.8 SIGNATURES

The spectrum of LCE's yields a useful quantitative classification of attractors. Recall that the LCE's measure the average rate of exponential convergence of trajectories onto the attractor when negative, and the average rate of exponential divergence of nearby trajectories within the attractor when positive.

We can classify the attractors according to the signature of the LCE's. For example, in a three-dimensional system:

(a) (-,-,-) corresponds to a fixed point with D = 0

(b) (0,-,-) corresponds to a limit cycle with D = 1

(c) (0,0,-) corresponds to 2-tori with D = 2

(d) (+,0,-) corresponds to a strange attractor with $D = D_C$.

In the case (+,0,-) for a chaotic attractor, the positive exponent indicates exponential spreading within the attractor in the direction transverse to the flow and the negative exponent indicates exponential contraction onto the attractor. Under the action of such a flow, phase-space volumes evolve into sheets. See Figure 3.4, after Froehling et al (1981).

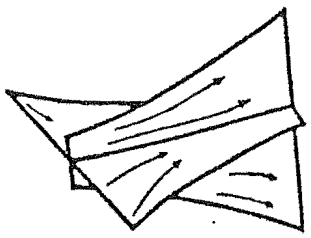

Figure 3.4 Under the action of 3-dimensional flows with local exponential spreading transverse to the flow and exponential contraction in the other dimension, phase-space volumes evolve into sheets. (after Froehling et al, 1981)

The spectrum of LCE's gives a rough measure of dimension for attractors in three dimensions. As a first step towards dimensional classification of attractors we can identify the dimension of an attractor with the number of non-negative LCE's as in the example given in the last paragraph.

By this classification scheme, a signature (+,+,0,-) would correspond to a strange attractor displaying *hyperchaos*. As example is the system by Rössler (1979):

$$\left.\begin{aligned} \dot{x} &= -y - z \\ \dot{y} &= x + 0.25y + w \\ \dot{z} &= 3 + xz \\ \dot{w} &= -0.5z + 0.05w \end{aligned}\right\} . \qquad (3.33)$$

It has fractal dimension $D_c = 3.006$, which can be calculated from (3.25), knowing the characteristic exponent spectrum: (0.121,0.021,0.005,-23.7).

Finally we mention that since the signature changes with control parameters, they provide also a means to classify transitions between various regimes.

3.9 ONE-DIMENSIONAL MAPPINGS

For one dimension, there is only one LCE, commonly called the *Lyapunov number*:

$$\lambda(k) = \lim_{\ell \to \infty} \frac{1}{\ell} \sum_{i=0}^{\ell-1} \ell n \left| \frac{dG}{dx_i} \right| \tag{3.34}$$

where $x_{i+1} = G(x_i, k)$. Following the discussion in Lichtenberg and Lieberman (1982) we present a list of the properties of the Lyapunov number for the map G.

(i) We can see from Figure 3.5 that $\lambda > 0$ if the slope G' has magnitude greater than unity when averaged over an orbit.

(ii) λ is independant of the initial condition x_0 (except for a set of measure zero).

(iii) For $\lambda > 0$, we have a chaotic orbit.

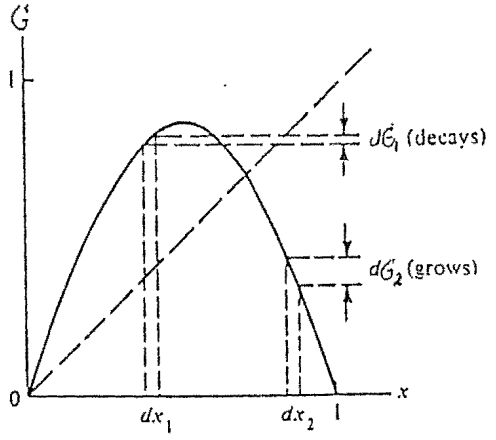

Figure 3.5 Relationship between the slope $\frac{dG}{dx}$ of a one-dimensional map and the Lyapunov exponent. The exponent is the average of $\ell n \left| \frac{dG}{dx} \right|$ over the orbit. (after Lichtenberg and Lieberman, 1982)

(iv) For $\lambda > 0$, a stable (attracting) cycle exists and after an initial transient, the orbit is periodic.

(v) The curve of λ versus k is highly convolved since the stable

cycles are dense in parameter space. This is shown in Figure 3.6, which are the result of a numerical experiment on the quadratic map. The number λ has been evaluated using (3.3). Each of the 300 equally spaced points in k from which the curve is composed represents 100,000 iterations. The low-period attracting orbits have relatively wide parameter windows. These are visible as regions where $\lambda < 0$. Other high-period attracting orbits which densely fill the k-interval, are invisible, because their parameter windows are narrower than the spacing of the points along k.

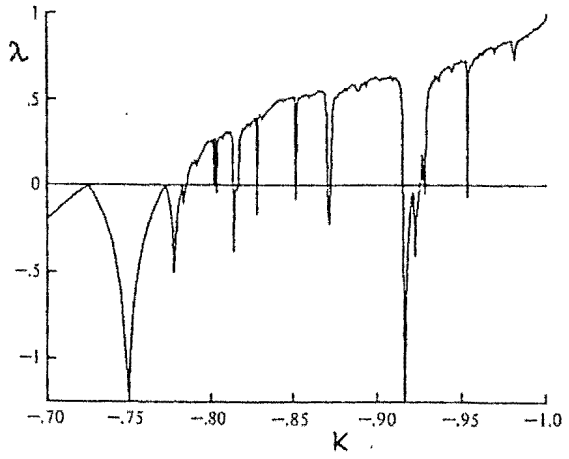

Figure 3.6 Graph of the Lyapunov exponent λ versus k for the quadratic map $x_{n+1} = 2kx_n + 2x_n^2$. This numerically generated graph has been smoothed, being composed of 300 points equally spaced in k. For $\lambda > 0$, the motion is chaotic, for $\lambda < 0$, the motion is periodic. (after Shaw, 1981)

(vi) As we have mentioned already, the chaotic orbits are found in regions where $\lambda > 0$. Near the critical parameter k_∞ where λ turns positive, it has been shown by Huberman and Rudnick (1980), that λ scales as:

$$|k - k_\infty|^\beta, \quad \text{where} \quad \beta = \frac{\ell n 2}{\ell n 8} \approx 0.4498 \tag{3.35}$$

(vii) $\lambda = 0$ at every bifurcation point, at the accumulation point k_∞ of the period-doubling cascade, and at tangent bifurcations (to

be discussed more fully in chapter 4).

(viii) It has been shown by Grassberger (1981), that at k_∞, where we have a Cantor set structure, the dimension is universal with $D_c = 0.538$ .... . No matter how long the bifurcation is being carried on, one always gets a cluster of points near every finite bifurcation point, due to critical slowing down. It has been shown by Wang and Chen (1984) that this cluster acquires an "operational" dimension $D = \frac{2}{3}$ if measured by a box-counting algorithm. The true dimension of a periodic orbit, however, must be zero. A scaling function relating these two values $D = \frac{2}{3}$ and $D = 0.538...$ does exist.

(ix) λ is independent of the specific form in which the map is written. Let us make an invertible coordinate transformation

$$\bar{x} = r(x) \ , \ r' \neq 0 \ . \tag{3.36}$$

Then the original map:

$$x_{n+1} = G(x_n) \tag{3.37}$$

is transformed to the new map:

$$\overline{x_{n+1}} = \bar{G}(\bar{x}_n) \ . \tag{3.38}$$

The Lyapunov exponent for the new map is:

$$\bar{\lambda} = \lim_{\ell \to \infty} \frac{1}{\ell} \sum_{i=1}^{N} \ell n \left| \frac{d\bar{G}}{dx_i} \right| \tag{3.39}$$

But $d\bar{G} = d\overline{x_{n+1}}$, and the chain rule applied to (3.36) gives:

$$\frac{d\overline{x_{i+1}}}{dx_i} = \left(\frac{dr}{dx_{i+1}} \right) \frac{dx_{i+1}}{\left(\frac{dr}{dx_i} \right) dx_i} \tag{3.40}$$

when (3.40) is used in (3.39), we obtain (3.34); i.e., $\bar{\lambda} = \lambda$.

3.10 RECONSTRUCTION OF ATTRACTORS

The problem of reconstructing a finite-dimensional phase-space picture that gives a faithful representational of the original phase-space is not yet settled. Packard et al (1980) mention as possibilities

time derivatives, time delays and even spatially separated sampling. Roux et al (1980) reconstructed a chaotic attractor from chemical turbulence using one time-varying signal and its derivatives.

A technique for reconstructing an N-dimensional phase-space from a single time series with time delay of between samples is presented in Froehling et al (1981). This technique equates the reconstructed phase-space point with N successive points of the time series separated by a delay $n\Delta t$. The next phase-space point is found by advancing each previous point by a time Δt. Unfortunately choices for N,n, or Δt may grossly distort the phase-space portrait of the original attractor. Figure 3.7 shows the Rössler attractor (which has signature (0.075,0,-5.372)), which has been reconstructed from a single time series using this method. Froehling et al (1981) show that this attractor and the Rössler attractor have the same approximate fractal dimension (D_C = 2.014). As an example of an unfortunate choice of variables, if the time delay Δt were simply rationally related to the average period of this system, the reconstructed attractor would be unrecognizable.

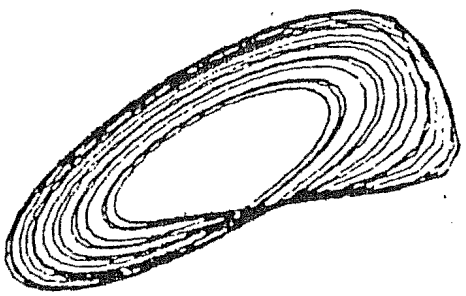

Figure 3.7 x - y projections of the Rössler attractor reconstructed from a time series: $\Delta t = 0.2$, N = 3, n = 1. This reconstructed attractor fits in a three dimensional box roughly 20 units on a side. (after Froehling et al, 1981)

CHAPTER 4

ONE-DIMENSIONAL MAPPINGS

In this chapter, we consider the properties of one-dimensional mappings of the form:

$$x_{n+1} = B(x_n, k) \tag{4.1}$$

where k is a parameter. As we have seen in chapter 2, such maps are often embedded in n-dimensional dissipative dynamical systems. Studies have shown that the very simplest nonlinear difference equations can possess an extraordinary rich spectrum of dynamical behaviour from stable points, through cascades of stable cycles, to a regime in which the behaviour (although fully deterministic) is in many respects "chaotic".

We are primarily interested in changes in the system behaviour as some parameter of the system is varied. Presented are qualitative explanations for the birth and consequent development of the various periodic regimes in the course of the evolution of the system. The methods for calculating the ordering of the periodic orbits are looked at. Also, the concepts of scaling, universality and Feigenbaum renormalization are discussed. Explanations for intermittency in one-dimensional maps are given. Finally we discuss Lyapunov exponents for one-dimensional mappings, and invariant distributions.

We approach these equations with the viewpoint that irregularities and chaotic oscillations of complicated phenomena may sometimes be understood in terms of a simple model, even if that model is not sufficiently sophisticated to allow accurate numerical predictions. Much of the theory in this chapter is based on the discussion in May (1976), Hao (1984 Lichtenberg and Lieberman (1982).

4.1 RELEVANCE TO CHAOS

In physics, one-dimensional models are usually too trivial or too specific to be extended to higher dimensions. Chaos in dissipative systems is a useful exception. The reason for this is that dissipation plays a global stabilizing role against local orbital instability and causes the volume representing the initial states in phase-space to contract in the process of evolution. As the geometric structure of strange attractors has been made clear, a qualitative picture has emerged in which an important feature is the close correspondence between motion on a strange attractor and motion described by non-invertible one-dimensional mappings. The contraction makes the phase-space volume approach one-dimensional objects in some of its solutions and this enables higher dimensional systems to enjoy the universal properties of one-dimensional systems. Hence one-dimensional mappings do not arise directly from dissipative flows, but they are still important examples of simple systems exhibiting chaotic behaviour. They also arise naturally as simple models of system behaviour.

Noninvertible maps undergo a sequence of bifurcations as a parameter is varied such that the period of an attracting periodic orbit (repeatedly) doubles, accumulating at a critical parameter value beyond which the behaviour is chaotic. Feigenbaum has shown this process to have a universal nature.

There are many situations in many disciplines which can be described, at least to a crude first approximation, by a simple first order difference equation. Studies of the dynamical properties of such models usually consist of finding constant equilibrium solutions, and then conducting a linearized analysis to determine their stability with respect to small disturbances. Explicit nonlinear dynamical features are usually not considered.

One-dimensional mappings of an interval into itself, by virtue of their simplicity, lend themselves to certain analytical tools and are not

very time consuming in numerical studies. At the same time they are rich enough to show many of the scaling and universal properties of chaotic transitions observed in higher-dimensional systems. We now consider some examples.

4.2 EXAMPLES OF ONE-DIMENSIONAL MAPPINGS

One of the simplest mathematical situations occurs when the phenomenon under discussion is described by a single number. A simple example from Li and Yorke (1975) is the situation where the number of children susceptible to some disease at the beginning of a school year can be estimated purely as a function of the number for the previous year. i.e., when the number x_{n+1} at the beginning of the (n+1)st year can be written:

$$x_{n+1} = B(x_n) \tag{4.2}$$

where B maps an interval I into itself. This model for the yearly progress of the disease is perhaps over-simplistic, and would only contain certain aspects of the more complicated phenomenon. For other situations, this model might be much more accurate. Several examples from the discussion in May (1976) follow.

This model can be used by ecologists to study a seasonally breeding population in which generations do not overlap. Examples from economics include models for the relationship between commodity quantity and price, for the theory of business cycles, and for the temporal sequences generated by various other economic quantities. This model applies as well to social sciences in theories of learning (where x may be the number of bits of information that can be remembered after an interval t), or in the propagation of rumours in variously structured societies. There are also examples in genetics and epidemiology. Perhaps the most interesting application (from Li and Yorke (1975)) is with respect to the model of the distribution of points of impact on a spinning bit for oil

well drilling. Knowing this distribution is helpful in predicting uneven wear of the bit.

Let us now look at a specific example. If a population of insects has discrete generations, the size of the (n+1)st generation will be a function of the nth. A suitable model would then be:

$$L_{t+1} = L_t(a - bL_t). \tag{4.3}$$

This nonlinear difference equation is called the "*logistic*" difference equation. This equation is quite possibly the simplest of its type. When b = 0, it describes a purely exponential population growth (for a > 1). When b ≠ 0, the quadratic nonlinearity generates a growth curve with a "*hump*". The steepness of this hump is tuned by the parameter a. The canonical form of (4.3) is:

$$x_{t+1} = a\, x_t(1 - x_t) \tag{4.4}$$

which is obtained by substituting $x = \frac{bL}{a}$ in (4.3). Through a simple linear transformation this equation can be converted to another well known version:

$$x_{t+1} = 1 - a'x_t^2. \tag{4.5}$$

Although extremely simple, (4.4) has the disadvantage that x must remain in the interval $0 < x < 1$. If x exceeds unity, the subsequent iterations diverge towards $-\infty$. Also since B(x,a) in (4.4) attains a maximum of $\frac{a}{4}$ at $x = \frac{1}{2}$, the equation therefore possesses non-trivial dynamical behaviour only if $a < 4$. For non-trivial dynamical behaviour we require $1 < a < 4$, since if $a < 1$ then all trajectories are attracted to x = 0 (otherwise the population becomes extinct). For more examples see May (1976) and Metroprolis et al (1973), and May and Oster (1977). Although these models are very simple, they exhibit surprisingly complex behaviour. For example, see Figure 4.1, which shows iterations for the logistic equation $x_{n+1} = r\, x_n\left[1 - \frac{x_n}{k}\right]$. We now narrow down the type of

one-dimensional mapping we shall discuss, and discuss some relevant background concepts.

4.3 PRELIMINARIES

We will confine ourselves to functions $B(x,k)$ which are non-invertible and only have one maximum on the interval I. Without loss of generality we can rescale $B(x,k)$ and x in such a way that:

(i) the maximum is located at $x = m$, so $B'(m,k) = 0$ and $B(m,k) = 1$.

(ii) $B(x,k)$ is monotonically increasing for $x < m$, and monotonically decreasing for $x > m$.

(iii) In the neighbourhood of $x = m$, $B(x,k)$ can be expanded as:

$$B(x,k) = 1 - a(x-m)^z + \ldots \qquad (4.6)$$

where $z = 2,4,6,\ldots$, etc.

These sort of mappings have been called *unimodal*.

The reason we have restricted ourselves to $B(x,k)$ of the above form is as follows. If $B(x,k)$ is linear in x, then the solution of (4.1) is trivial. The case where $B(x,k)$ is invertible (monotonic in x) is also simple; the steady state solutions are periodic and do not have a sequence of period-doubling bifurcations or chaotic behaviour.

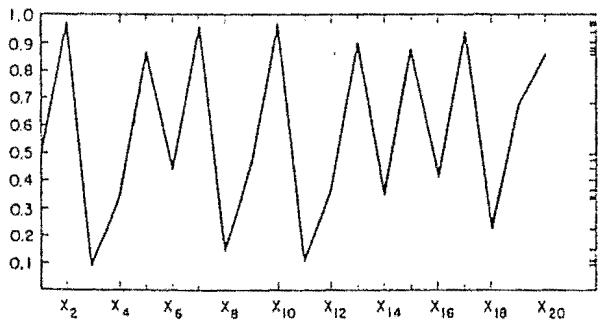

Figure 4.1 For $k = 1$, $r = 3.9$, with $x_1 = .5$ the above graph is obtained by iterating the logistic equation 19 times. At right the 20 values are repeated in summary. No value occurs twice. While $x_2 = .975$ and $x_{10} = .973$ are close together, the behaviour is not periodic with period 8 since $x_{18} = .222$. (after Li and Yorke, 1975)

As we shall see, such behaviour is associated with a local region of x

near $B(x,k) = 0$. In the generic case for which $B' = 0$ and $B'' \neq 0$ at the extremum, the map is locally quadratic. A Taylor series expansion about the extremum leads to consideration of the general quadratic map:

$$x_{n+1} = p + q x_n + r x_n^2 . \tag{4.7}$$

For $p = 1$, $q = 0$ and $r = -a$, we obtain the logistic mapping (4.5).

Note that with this mapping, even when x runs over the whole interval $I = [-1,+1]$, $B(x,k)$ does not necessarily fill up the interval I. For example in the Hénon mapping when $b = 0$, the map reduces to: $f(y) = 1 - ay^2$, which is just (4.5). For $0 < a < 2$, the interval $I = \left[-\frac{1}{2a}(1+\sqrt{1+4a}), \frac{1}{2a}(1+\sqrt{1+4a}) \right]$ is mapped into itself. This sort of mapping is called an *endomorphism*.

We can choose an arbitrary initial point $x_0 \in I$ and iterate it using $B(x,k)$:

$$x_n = B(k,x_{n-1}) \quad n = 1,2,3,\ldots . \tag{4.8}$$

This may be written as:

$$x_n = B^{(n)}(k,x_0) \quad n = 1,2,3,\ldots \tag{4.9}$$

where $B^{(n)}$ denotes the nth iterate of B. Alternative notations are:

$$B(n,k,x) \equiv B^{(n)}(k,x) \equiv B(k,B(k,\ldots, B(k,x),\ldots)). \tag{4.10}$$

The evolution of x starting initially at x_0 is found by iterating (4.1). We can graphically determine the evolution as follows (after Lichtenberg and Lieberman (1982)):

(i) Starting at x_0 move vertically to $x_1 = B(k,x_0)$
see Figure 4.2 and Figure 4.3.

(ii) Transfer x_1 to the x-axis by moving horizontally to the 45° line $B = x$.

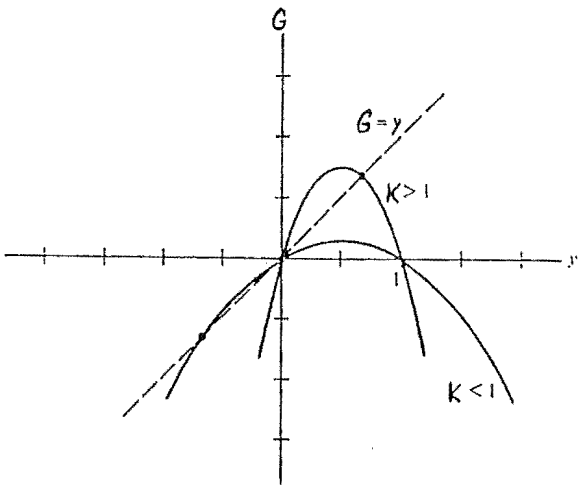

Figure 4.2 The logistic map $G = kx(1-x)$ for $0 < k < 4$; the interval $0 < x < 1$ is mapped into itself (after Lichtenberg and Lieberman, 1982)

(iii) Determine x_2, x_3, x_4 etc. by repeatedly applying (i) and (ii).

Figure 4.3 illustrates the procedure for initial conditions x_0 or x_0'. It is clear that B is invertible. The two values x_0 and x_0' generate the same B value and therefore a single value x_1 for the following iteration. Therefore, the map cannot be uniquely inverted to give x_0 (or x_0') once x_1 has been generated. (This sort of construction will be helpful later).

The normalized form of (4.7) is:

$$x_{n+1} = 2kx_n + 2x_n^2 \tag{4.11}$$

which is obtained by using a linear transformation. Following Lichtenberg and Lieberman (1982), we examine the various parameter ranges, two of which are of interest. For $0 < k < 2$, the interval $-k < x < 0$ is mapped into itself. See Figure 4.4a,b. For $-1 < k < \frac{1}{2}$, the interval $-\frac{1}{2} < x < \frac{1}{2} - k$ is mapped into itself. This range of k is illustrated in Figure 4.4 (c) - (f). Observe that the parameter ranges overlap, as shown by Figure 4.4 (b), (c) which are similar except for the interval in x which maps into itself. The extremum in B, at $x' = -\frac{k}{2}$ is of particular importance. Also, substitution of $x = \left(\frac{k'}{2}\right)y$ and $k = \frac{k'}{2}$ in

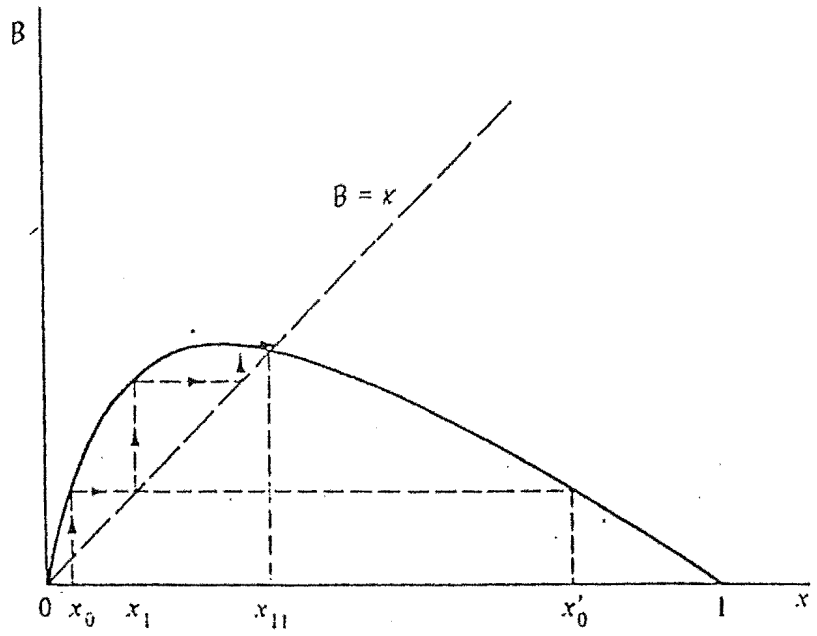

Figure 4.3 A typical one-dimensional noninvertible map (after Lichtenberg and Lieberman, 1982)

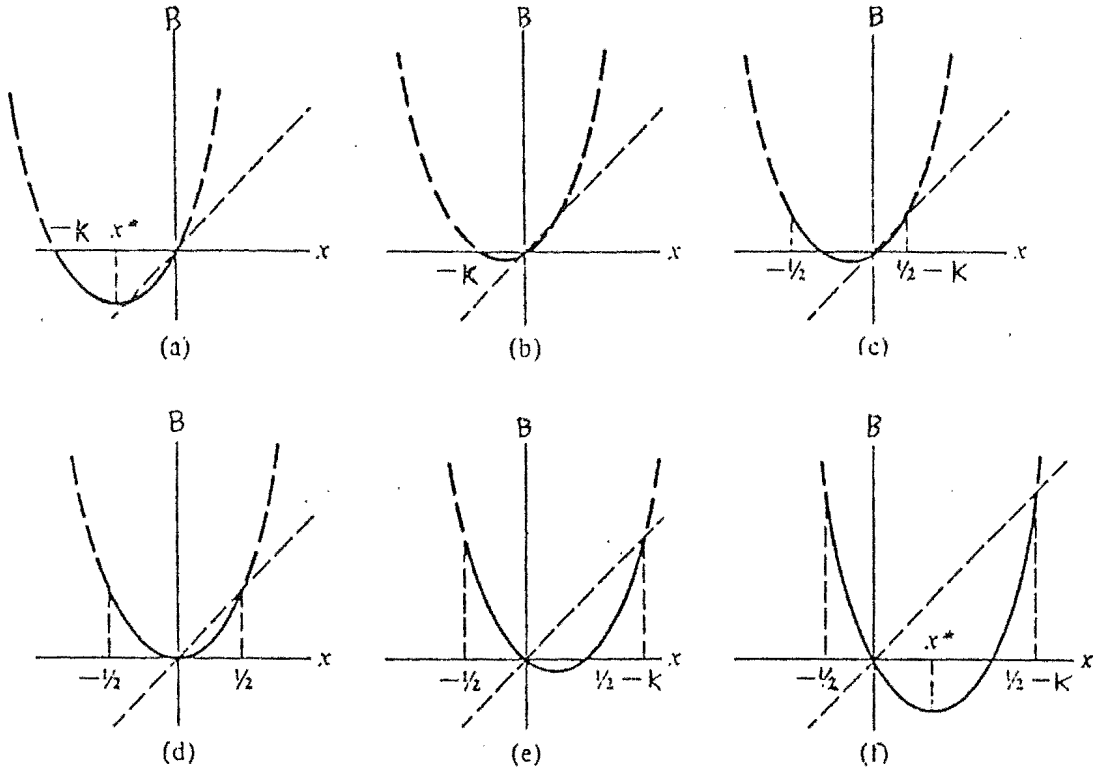

Figure 4.4 Parameter ranges for the quadratic map $x_{n+1} = 2kx_n + 2x_n^2$. The region that is mapped into itself, is shown by a solid line. Case I: $-k < x < 0$; (a) $k > \frac{1}{2}$; (b) $0 < k < \frac{1}{2}$. Case II: $-\frac{1}{2} < x < \frac{1}{2} - k$; (c) $0 < k < \frac{1}{2}$; (d) $k = 0$; (e) $-\frac{1}{2} < k < 0$; (f) $-1 < k < -\frac{1}{2}$ (after Lichtenberg and Lieberman, 1982).

(4.11) yields: $y_{n+1} = k'y_n(1 - y_n)$. We now examine some of the properties of the quadratic map (4.11).

4.4 PROPERTIES OF THE QUADRATIC MAPPING

We introduce some important definitions and discuss simple properties of (4.11) in this section.

4.4a MIRROR SYMMETRY

If we substitute the linear transformation:

$$x = \bar{x} + \frac{1}{2} - k \tag{4.12}$$

into (4.11), we obtain

$$\overline{x_{n+1}} = 2k'\bar{x}_n + 2\bar{x}_n^2 \tag{4.13}$$

where the new parameter is:

$$k' = 1 - k\ . \tag{4.14}$$

From this we can see the symmetry property of quadratic maps. Identical behaviour is obtained for two different parameter values. Since (4.13) and (4.11) have the same form, it follows that the properties of the quadratic map with parameters k and $1-k$ are identical. All phenomena occur twice at k values symmetric about $\frac{1}{2}$. Similarly by putting

$$y = (1 - \ell^{-1}) - (1 - 2\ell^{-1})\bar{y} \tag{4.15}$$

into the logistic mapping $y_{n+1} = \ell y_n(1 - y_n)$ yields:

$$\overline{y_{n+1}} = \bar{\ell}\ \bar{y}_n\ (1 - \bar{y}_n) \tag{4.16}$$

where

$$\bar{\ell} = 2 - \ell \tag{4.17}$$

that is, the logistic mapping is symmetric about $\ell = 1$.

4.4b PERIODIC BEHAVIOUR

Let us now discuss the sequence of iterations $\{x_i,\ i = 0,1,2,\ldots\}$. Usually after a few hundred transient points, the iterates settle into one of two kinds of stationary patterns: periodic or aperiodic. A periodic pattern of period p: $x_{i+p} = x_i$, $x_{i+k} \neq x_i$ for all $k < p$ and all i larger than a certain N, is called an orbit of *period p* or a *p-cycle*

for the mapping B. We shall assume in what follows that all transients have died away.

The case p = 1 corresponds to a fixed point for B.

$$x^* = B(x^*,k) \tag{4.18}$$

By definition, all points from a p-cycle of B must be fixed points of the pth iterate of B, i.e.,

$$x_i = B(p,k,x_i) \quad i = 1,2,\ldots, p . \tag{4.19}$$

The fixed points of (4.1) may be found algebraically by substituting $x_i = x_{i+1} = x^*$ and solving the resulting equation which is just (4.18). For example we can solve (4.5) algebraically to find the trivial fixed point $x^* = 0$ and the nontrivial fixed point $x^* = 1 - \frac{1}{a}$. These fixed points can also be obtained by an equivalent graphical approach. The fixed points are the points where the curve $B(x,k)$ that maps x_i to x_{i+1} intersects the 45° line. For example, using this method we would obtain the period 1 fixed points of (4.11) as $x^*_{10} = 0$ and $x^*_{11} = \frac{1}{2} - k$. See Figure 4.3.

A very important concept associated with a fixed point is stability. If x_1 is chosen very close to the fixed point x^* then:

$$x_i = x^* + \delta_i . \tag{4.20}$$

The following iterate is:

$$x_{i+1} = x^* + \delta_{i+1} . \tag{4.21}$$

If:

$$\left| \frac{\delta_{i+1}}{\delta_i} \right| < 1 \tag{4.22}$$

then we say that the fixed point x^* is *stable*. Linearize the mapping by substituting:

$$x_n = x_1 + \Delta x_0 \tag{4.23}$$

into (4.11), and keep only the linear terms. This yields:

$$\Delta x_n = \lambda_1^n \Delta x_0 \tag{4.24}$$

where the eigenvalue $\lambda_1 = B'(x_1)$. In this case, we see that provided $|\lambda_1| < 1$, x_1 is a stable (attracting) fixed point. Similarly if $|\lambda_1| > 1$, then x_1 is an *unstable* (repelling) fixed point. Hence the stability condition (4.22) is equivalent to:

$$|B'(x^*,k)| < 1 . \tag{4.25}$$

For example, the slope for (4.5) is $\lambda_1 = \left[\frac{dB}{dx}\right]_{x=x^*} = 2 - a$, and hence the fixed point is stable and attracts all trajectories originating in the interval $0 < x < 1$ if and only if $1 < a < 3$.

We can extend the stability relation by using the chain rule of differentiation. As p-cycle is stable if:

$$|B'(p,k,x_i)| = \left| \prod_{j=1}^{p} B'(k,x_j) \right| < 1 \quad i = 1,2,\ldots, p . \tag{4.26}$$

We can now see that our fixed point x_{11}^* of (4.11):

$$x_{11}^* = \frac{1}{2} - k \tag{4.27}$$

is stable for: $|B'(x_{11}^*,k)| = |2 - 2k| < 1$, or when k lies in the range $\frac{1}{2} < k < \frac{3}{2}$. Similarly, the fixed point x_{10} is stable provided: $|B'(x_{10},k)| = |2k| < 1$, or when $-\frac{1}{2} < k < \frac{1}{2}$. There is also the following stronger notion of stability.

For any function $B(x,k)$ a point $y \in J$ with period ℓ is said to be *asymptotically stable* if for some interval $I = (y - \delta, y + \delta)$ we have:

$$|B^{\ell}(x) - y| < |x - y| \quad \forall x \in I . \tag{4.28}$$

If B is differentiable at points $y, B(y),\ldots, B^{\ell-1}(y)$, there is a simple condition that will guarantee this behaviour, namely:

$$\left| \frac{d}{dx} B^{\ell}(x) \right| < 1 . \tag{4.29}$$

By the chain rule:
$$\begin{aligned} \frac{d}{dx} B^{\ell}(y) &= \frac{d}{dx} B(B^{\ell-1}(y)) \cdot \frac{d}{dx} B^{\ell-1}(y) \\ &= \frac{d}{dx} B(B^{\ell-1}(y)) \times \frac{d}{dx} B(B^{\ell-2}(y)) \times \ldots \times \frac{d}{dx} B(y) \\ &= \prod_{n=0}^{\ell-1} \frac{d}{dx} B(y_n) \end{aligned} \tag{4.30}$$

where y_n is the nth iterate of $B^n(y)$. Therefore y is asymptotically stable if:

$$\left| \prod_{i=0}^{\ell-1} \frac{d}{dx} B(y_i) \right| < 1, \quad \text{where} \quad y_i = B^i(y) . \tag{4.31}$$

This condition imparts no information about the limiting behaviour of points which do not start "near" the periodic point or one of its iterates. The function in Figure 2.9 which was studied by Lorenz, can be seen to have the opposite behaviour, i.e., where the derivative exists, we have $\left|\frac{d}{dx} B(x)\right| > 1$. For such a function, every periodic point is unstable since for x near a periodic point y of period ℓ, the ℓth iterate $B^{\ell}(x)$ is further from y than x is. To make this more clear, approximate $B^{\ell}(x)$ by:

$$B^{\ell}(y) + \frac{d}{dx} B^{\ell}(y)[y - x] = y + \frac{d}{dx} B^{\ell}(y)[y - x] . \tag{4.32}$$

Thus for x near y, $|B^{\ell}(x) - y|$ is approximately $|x - y| \left|\frac{d}{dx} B^{\ell}(y)\right|$. From (4.31), $\left|\frac{d}{dx} B^{\ell}(y)\right|$ is greater than 1. Therefore $B^n(x)$ is further from y than x is.

A particularly interesting case of stability occurs when

$$B'(p,\bar{k},x_i) = 0 \quad i = 1,2,\ldots, p . \tag{4.33}$$

In this case, one has quadratic convergence towards the fixed point. The stability condition (4.26) holds for a finite interval called a periodic window on the k-axis. The situation described by (4.33) takes place at one particular value $\bar{k}$ somewhere in the middle of the periodic window. This value $\bar{k}$, corresponds to a *superstable period*, which serves as the representative of all p-cycles from the same periodic window. It follows that any cycle containing the point $x = 0$ must be superstable, since $B'(k,0) = 0$ leads to $B'(p,k,0) = 0$ for all p.

The first few periodic windows for the logistic mapping (4.5), can easily be worked out on a calculator:

$p = 1$ $\qquad 0 < k < k_1 = 0.75$

$p = 2$ $\qquad k_1 < k < k_2 = 1.25$

$p = 2^2 = 4$ $\qquad k_2 < k < k_3 = 1.3680989...$

$p = 2^3 = 8$ $\qquad k_3 < k < k_4 = 1.3940461...$.

This is a period-doubling bifurcation cascade with period $p = 2^n$ which quickly converges to an aperiodic orbit at $n = \infty$, the value $k_\infty = 1.401155...$ being approached as a geometric progression, namely:

$$k_n \approx k_\infty - \frac{M}{\delta^n}, \quad \text{as } n \to \infty \tag{4.34}$$

where $\delta = 4.66920...$ is a universal (for unimodal quadratic maps) constant, first discovered by M.J. Feigenbaum (1978). It is the period-doubling windows we now examine.

4.5 PERIOD-DOUBLING BIFURCATION CASCADES

As we have already seen, the stability of the fixed point x^* depends on the slope of the $B(x,k)$ curve at x^*. Now as the relevant parameters are tuned so that the curve $B(x,k)$ becomes more and more steeply humped, this stability determining slope may change so $|\lambda_1| > 1$. At this point, the fixed point is no longer stable.

To see what happens next, let us consider the general quadratic map (4.11) as k decreases, starting from a value of $k > \frac{1}{2}$ for which x_{11} is stable and x_{10} is unstable. The argument presented now, is from Lichtenberg and Lieberman (1982). At $k_0 = \frac{1}{2}$, x_{11} becomes unstable, and x_{10} becomes stable, the latter root remains stable until k is decreased further to $k_1 = -\frac{1}{2}$. To see what happens as k is decreased below $-\frac{1}{2}$, we must consider the period 2 fixed points given by:

$$x_2^* = B(B(x_2^*)) . \tag{4.35}$$

These correspond to the intersection of the function:

$$B^{(2)}(x) = B(2,k,x) = B(B(x)) \tag{4.36}$$

with the 45° line, as shown in Figure 4.6 (a),(b) for $k > -\frac{1}{2}$ and $k \gtrsim -\frac{1}{2}$.

For $k \gtrsim -\frac{1}{2}$, the two intersections correspond to the period 1 fixed points

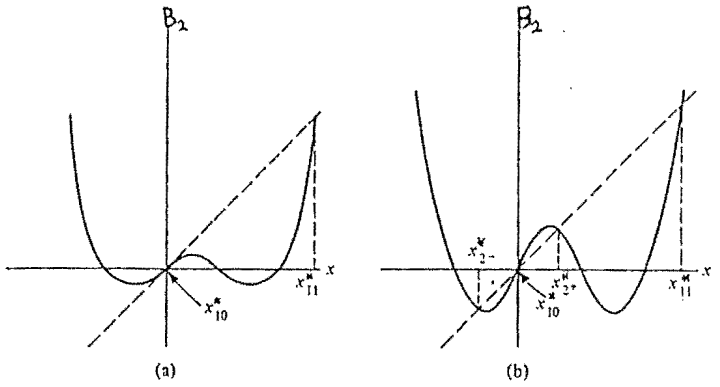

Figure 4.6 The creation of a pair of period 2 fixed points $x^*_2 \pm$ for the quadratic map. The graphs show $B_2(x) = B(B(x))$ versus x (a) $k > -\frac{1}{2}$; (b) $k \gtrsim -\frac{1}{2}$ (after Lichtenberg and Lieberman, 1982)

$x^*_{11} = \frac{1}{2} - k$ and $x^*_{10} = 0$, which obviously satisfy (4.35) i.e., the basic fixed point of period 1 is a degenerate case of a period 2 solution.

The slope of $B^{(2)}$ at x^*_{10} is less than unity, since the chain rule applied to (4.36) yields:

$$\left[\frac{dB^{(2)}}{dx}\right]_{x=x^*_{10}} = \lambda_1^2 = \lambda_2 \tag{4.37}$$

and $|\lambda_1| < 1$ for $k > -\frac{1}{2}$. As k is decreased below $-\frac{1}{2}$, the slope increases beyond 45° and a pair of period 2 fixed points are born as shown in Figure 4.6 (b). These points satisfy:

$$x^*_{2_+} = B(x^*_{2_-}) = B^{(2)}(x^*_{2_+}) \tag{4.38a}$$

$$x^*_{2_-} = B(x^*_{2_+}) = B^{(2)}(x^*_{2_-}) . \tag{4.38b}$$

The stability of the motion near $x^*_{2^\pm}$ can be obtained by writing:

$$x_{2,n} = x^*_{2^\pm} + \Delta x_{2,n} \tag{4.39}$$

and linearizing the mapping. We find that near $x^*_{2_-}$,

$$\Delta x_{2,n} = \lambda^n_{2_-} \Delta x_0 \tag{4.40}$$

where by the chain rule applied to (4.36):

$$\lambda_{2^-} = B^{(2)'}(x^*_{2^-}) = B'(x^*_{2^-})B'(x^*_{2^+}) \ . \tag{4.41}$$

Similarly, for the motion near $x^*_{2^+}$;

$$\lambda_{2^+} = B'(x^*_{2^+})B'(x^*_{2^-}) = \lambda_{2^-} \tag{4.42}$$

Hence the slopes (eigenvalues) are the same at each of the pair of period 2 fixed points.

For k just below $k_1 = -\frac{1}{2}$, it is clear from Figure 4.6 (b) that the slope λ_2 at $x^*_{2^-}$ (and $x^*_{2^+}$) satisfies $|\lambda_2| < 1$. Thus just after the period 1 fixed point $x^*_{10} = 0$ goes unstable, a pair of stable period 2 fixed points (a period 2 cycle) appears. The situation is illustrated in Figure 4.7, in which the locations of the fixed points are plotted versus the parameter k, with a solid line indicating stability and a dashed line indicating instability. The birth of the pair of stable period 2 fixed points as k decreases below $-\frac{1}{2}$ is an example of a pitchfork bifurcation with x^*_{10} the handle, and $x^*_{2^-}$, $x^*_{2^+}$ the tines of the pitchfork. The *mirror pitchfork bifurcation* which occurs for a certain parameter range, is also depicted in Figure 4.7.

As before, the stability of this period 2 cycle depends on the slope of the curve $B^{(2)}(x)$ at the two points $x^*_{2^+}$ and $x^*_{2^-}$. As we have seen, this slope is the same at both points, and in general is the same for all ℓ points on a period ℓ cycle. Furthermore, it is clear by imagining the intermediate stages between Figure 4.6 (a) and Figure 4.6 (b) that this stability-determining slope has the value $\lambda = +1$ at the birth of the 2-point cycle, and then decreases through zero towards $\lambda = -1$ as the hump in B(x,k) continues to steepen. Beyond this point, the period 2 points will in turn become unstable, and bifurcate to give an initially stable cycle of period 4. This in turn gives way to a cycle of period 8, and thence to a hierarchy of bifurcating stable cycles of periods $16, 32, 64, \ldots, 2^n$. In each case, the way in which a stable cycle of

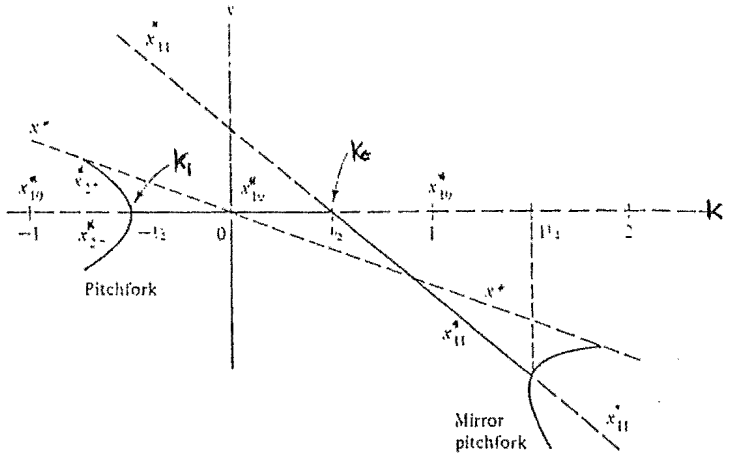

Figure 4.7 The fixed points x^*_{10}, x^*_{11}, $x^*_{2^+}$, and $x^*_{2^-}$ versus k. Stable fixed points are shown as solid lines, unstable fixed points, as dashed lines. The light dashed line shows the extremum of B at $x^* = -\frac{k}{2}$. (after Lichtenberg and Lieberman, 1982)

period ℓ becomes unstable, simultaneously bifurcating to produce a new and initially stable cycle of period 2k, is basically similar to the process just explained for k = 1. This process is generic to most functions B(x) with a hump of tunable steepness. Metropolis et al, (1973) refer to this hierarchy of cycles of period 2^n as the *harmonics* of the fixed point x^*.

Although this process produces an infinite sequence of cycles with periods $2^n (n \to \infty)$, the "*window*" of parameter values wherein any one cycle is stable progressively diminishes, so that the entire process is a convergent one, being bounded above by some critical parameter value. This is true for most, but not all functions B(x). For an exception, see May(1976). This critical point is a point of accumulation of period 2^n cycles. For (4.5), this value is $a_\infty = 3.57000...$, and for (4.11) the point of accumulation is $k_\infty = -0.7497...$.

Beyond this point there are an infinite number of fixed points with different periodicities, and an infinite number of different periodic cycles. Also there are an uncountable number of totally

aperiodic bounded orbits. These are regions of chaotic behaviour. See Figure 4.8, which is the bifurcation diagram for (4.5).

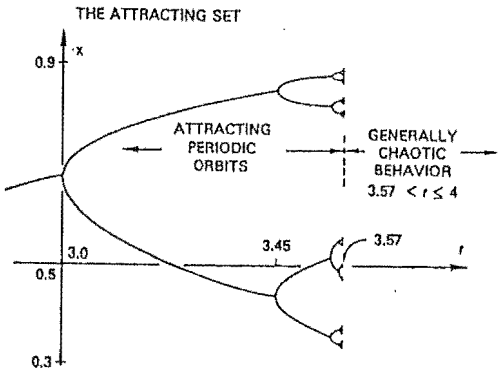

Figure 4.8 An infinite cascade of bifurcations on the way to chaos.
(after Yorke and Yorke, 1979)

4.6 RENORMALIZATION THEORY

Behind any *renormalization group* arguments there always features some fractal geometry, or geometry with an infinitely nested self-similar structure. In order to understand the period-doubling sequence quantitatively, we consider the renormalization of a unimodal map as we pass from one bifurcation to the next.

An exact renormalization theory exists for all unimodal maps. This exact theory was developed by M.J. Feigenbaum (1978), in terms of functional equations, which are independent of a specific B, and whose solution yields the exact scaling of the period-doubling bifurcations. Functional equations are rather difficult to deal with, so we give here a rather cursory explanation of this approach.

To obtain the scaling factors, we approximate the unimodal map by the quadratic map (4.11) and use an algebraic approach, which was put forward by Helleman (1980).

4.6a FEIGENBAUM'S METHOD

The functions considered all have a unique differentiable maximum $\bar{x}$, with

$$B(\bar{x}) - B(x) \approx |x - \bar{x}|^z \quad \text{(for } |x - \bar{x}| \text{ sufficiently small)} \qquad (4.43)$$

where $z > 1$, and the universal details depend only on z.

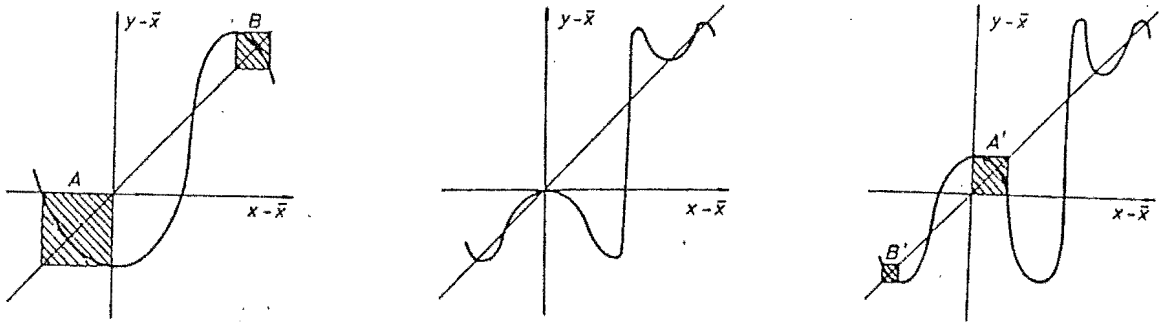

(a) (b) (c)

Figure 4.9 (a) A segment of $B^{(2^{n-1})}(\tilde{k}_n, x)$, $\tilde{k}_n$ is the superstable point for $B^{(2^n)}$; (b) A segment of $B^{(2^n)}(\tilde{k}_n, x)$; (c) A segment of $B^{(2^n)}(\tilde{k}_{n+1}, x)$ to be rescaled and inverted to get (a) again. (after Hao, 1984)

The diagrams in Figure 4.9 are a real modification of the Feigenbaum sketches, done by Hao (1984). They only show the vicinity of certain fixed points. A part of $B^{(2^n)}$ at the exact superstable parameter k_n is shown in Figure 4.9 (b). A sketch of $B^{(2^{n-1})}$ at the same parameter value k_n, represents the period-doubled regime shown in Figure 4.9 (a), where locally one has a few superstable 2-cycles as outlined by the square boxes. We now increase k_n from the situation of Figure 4.9 (b), until a new period-doubled superstable regime appears at the next parameter value k_{n+1} as shown by the smaller boxes in Figure 4.9 (c). Comparison of the two hatched boxes in Figure 4.9 (a) and Figure 4.9 (c) shows what happened was a rescaling and change of signs in both the x and y directions. This process repeats itself as k increases.

Now let us put this geometrical observation into analytical terms. Define an operator Q to represent this period-doubling, k-shifting and rescaling procedure starting from some fixed k_n:

$$Q\,B(k_n,x) = -\alpha B(k_{n+1}, B(k_{n+1}, -\frac{x}{\alpha})) = -\alpha B(2,k_{n+1}, -\frac{x}{\alpha}) = g_1(x)$$

$$Q^2 B(k_n,x) = (-\alpha)^2 B(2^2,k_{n+2}, \frac{x}{(-\alpha)^2}) = g_2(x)$$

$$\vdots$$

$$Q^{\ell} B(k_n,x) = (-\alpha)^{\ell} B(2^{\ell},k_{n+\ell}, \frac{x}{(-\alpha)^{\ell}}) = g_{\ell}(x) \qquad (4.44)$$

Feigenbaum showed that this hierarchy of universal functions g_{ℓ} exists, each descriptive of the same local structure but at levels of a cluster of 2^{ℓ} points. Feigenbaum also conjectured the existence of a universal limit:

$$\lim_{\ell\to\infty} (-\alpha)^{\ell} B(2^{\ell},k_{n+\ell}, \frac{x}{(-\alpha)^{\ell}}) = \lim_{\ell\to\infty} g_{\ell}(x) = g(x) . \qquad (4.45)$$

This result was proved later by Collet et al (1980). The hierarchy above obeys:

$$g_{\ell-1}(x) = -\alpha g_{\ell}(g_{\ell}(\frac{x}{\alpha})) . \qquad (4.46)$$

Taking the limit as $\ell \to \infty$, one finds that $g(x)$ obeys:

$$g(x) = -\alpha\, g(g(-\frac{x}{\alpha})) . \qquad (4.47)$$

This is the renormalization group equation of Feigenbaum. The solution of this equation determines both g and α.

The normalization of $B(k,0) = 1$ and the superstable condition (4.33) imply the following boundary conditions for (4.47):

$$g(0) = 1 \quad g'(0) = 0 . \qquad (4.48)$$

These conditions alone do not determine the solution of (4.47) uniquely. At least the behaviour of $g(x)$ near $x = 0$ should be given. For example, the series expansion:

$$g(x) = 1 + ax^z + bx^{2z} + cx^{3z} + \ldots \qquad (4.49)$$

will give different solutions to (4.47) for different choices of z. The renormalization group equation (4.47) can be generalized to period-n-tupling sequences:

$$\frac{1}{\alpha} g(\alpha x) = -g^{(n)}(-x) . \qquad (4.50)$$

Equation (4.47) defines a saddle point in the space of all functions leading to g(x). See Feigenbaum (1978). Therefore, one must be careful in devising a numerical procedure to calculate g(x), because the approximation may get away from the true solution after converging to it initially. The simplest way to solve (4.47) or (4.50) is by substituting the expansion (4.49) and then solving the resulting equations for α,a,b, etc. by combined use of algebraic manipulation and numerical methods.

We now look at the various scaling parameters. The *rescaling ratio* α, for successive bifurcations was determined by Feigenbaum to be:

$$\alpha = 2.5029078... \tag{4.51}$$

for z = 2 in (4.43). For the class of B's considered, there exists a k_n such that a 2^n-point stable limit cycle including $\bar{x}$ exists:

$$k_\infty - k_n \approx \delta^{-n} \quad (\delta = 4.669201... \text{ for } z = 2) . \tag{4.52}$$

The constant δ is called the *Feigenbaum constant*, and it determines the convergence rate of period-doubling bifurcation sequences for quadratic mappings i.e., z = 2 in (4.43). There is a smooth dependance of δ on z and its values for z = 4,6,8 are 7.248, 9.296 and 10.048 respectively. For references on this dependance see Hao (1984).

For ℓ asymptotic:

$$g_\ell \approx g - \delta^{-\ell} h \tag{4.53}$$

where $\delta > 1$ and h are determined as the associated eigenvalue and eigenvector of the operator $\mathcal{L}$:

$$\mathcal{L}[\psi] = -\alpha[\psi(g(\frac{x}{\alpha})) + g'(g(\frac{x}{\alpha}))\psi(-\frac{x}{\alpha})] . \tag{4.54}$$

Strictly speaking, δ is defined as the unique eigenvalue in excess of 1 of (4.54). Different solutions of the renormalization group equation lead to different α's and δ's for various period-n-tupling sequences. We now present an algebraic approach, to determining these scaling parameters.

4.6b AN ALGEBRAIC APPROACH

The argument of Helleman (1987), presented here is taken directly from Lichtenberg and Lieberman (1982). As mentioned already, we locally approximate a unimodal map by the quadratic map:

$$x_{n+1} = 2kx_n + 2x_n^2 . \tag{4.11}$$

We have already found that the stable period 1 solution $x^*_{10} > 0$ is first created with decreasing k at $k_0 = \frac{1}{2}$, and that the stable period 2 solution is created at $k_1 = -\frac{1}{2}$. The period 2 orbit is found by solving (4.38) to obtain

$$x^*_{2^\pm} = p \pm q \tag{4.55a}$$

where

$$2p = -\tfrac{1}{2} - k \tag{4.55b}$$

$$4q^2 = (k + \tfrac{1}{2})(k - \tfrac{3}{2}) \tag{4.55c}$$

where $q > 0$ in the range where the period 2 orbits exist. Now substituting:

$$x = x^*_{2^\pm} + \Delta x \tag{4.56}$$

into (4.11) we obtain (exactly); $\Delta x_{n+1} = r\Delta x_n + 2\Delta x_n^2$ (4.57a)

$$\Delta x_{n+2} = s\Delta x_{n+1} + 2\Delta x_{n+1}^2 , \tag{4.57b}$$

where:

$$r = 2k + 4x^*_{2^+} \tag{4.57c}$$

$$s = 2k + 4x^*_{2^-} \tag{4.57d}$$

and the initial conditions are chosen such that even subscripts in Δx give the motion near $x^*_{2^+}$, and the odd subscripts give the motion near $x^*_{2^-}$. Now eliminate Δx_{n+1} and keeping up to quadratic terms in Δx, for n even:

$$\Delta x_{n+2} = rs\Delta x_n + 2(r + s^2)\Delta x_n^2 . \tag{4.58}$$

Rescale by putting:

$$x' = \alpha\Delta x \tag{4.59}$$

into (4.58). We obtain:

$$x'_{n+2} = 2k'x'_n + 2x'^2_n \tag{4.60a}$$

with
$$k' = \frac{rs}{2} = -2k^2 + 2k + 2 \tag{4.60b}$$

$$\alpha = r^2 + s = 16q^2 - 12q \tag{4.60c}$$

with q given by (4.55c). Since (4.60a) has the same form as the original mapping (4.11), its fixed points undergo a period-doubling bifurcation at $k' = -\frac{1}{2}$. Using (4.60b) this corresponds to:

$$k_2 = \frac{1-\sqrt{6}}{2} \approx -0.72474\,, \tag{4.61}$$

the value of k for creation of a stable period 4 solution. At this value of k, using (4.55), $x^*_{2^+} \approx 0.466$ and $x^*_{2^-} \approx -0.241$. We note that one root, $x^*_{2^+}$, lies near the extremum in B at $x^* = -\frac{k}{2}$, a fact which we use below in calculating the rescaling of bifurcations of the plus and minus tines.

The cascade of bifurcations will accumulate at the value $k' = k = k_\infty$. Using (4.60b):

$$-2k_\infty^2 + 2k_\infty + 2 = k_\infty$$

or
$$k_\infty = \frac{1-\sqrt{17}}{4} \approx -0.781\,. \tag{4.62}$$

Iteration of the quadratic map, gives numerically the accumulation point: $k_\infty \approx -0.78497$ which is in good agreement with the renormalized value.

We can also find an approximate convergence of k to k_∞ by assuming an asymptotic expansion in the form of a geometrical series:

$$k_i \approx k_\infty + A\delta^{-1}\,. \tag{4.63}$$

Substituting this into (4.60b) and noting that when k bifurcations have taken place off the new orbit, then $k+1$ bifurcations have taken place off the old orbit, i.e.,

$$k_i = -k^2_{i+1} + 2k_{i+1} + 2 \tag{4.64a}$$

we find
$$\delta = -4k_\infty + 2 = 1 + \sqrt{17} \approx 5.12 \tag{4.64b}$$

The value obtained from solving the exact renormalization equation is

$\delta \approx 4.6692$. The geometric scaling law (4.63) can be expressed as:

$$\frac{k_{i+1} - k_i}{k_i - k_{i-1}} = \frac{1}{\delta} . \tag{4.65}$$

We now show that δ is independant of the parametrization by introducing an arbitrary parameter R given by: $R = m(k)$. (4.66) Assuming m is invertible near k, we can expand R in this neighbourhood:

$$R_i - R_\infty = m'(k_\infty)(k_i - k_\infty) . \tag{4.67}$$

Solving for k_i and inserting into (4.65)' yields the universal relation:

$$\frac{R_{i+1} - R_i}{R_i - R_{i-1}} = \frac{1}{\delta} . \tag{4.68}$$

Assuming that the asymptotic expansion (4.63) is valid even for $i = 0$ and $i = 1$, we find a useful estimate for the accumulation point in terms of the zero and first bifurcation

$$R_\infty = R_0 + \frac{\delta}{\delta - 1}(R_1 - R_0) = R_0 + (1.13)(R_1 - R_0) . \tag{4.69}$$

Finally, let us consider the rescaling parameter α in (4.59). From (4.60c) and (4.55c), we obtain α at the accumulation point k_∞ given by (4.62):

$$\alpha = 16q^2 - 12q \approx -2.24 \tag{4.70}$$

while exact renormalization theory yields $\alpha \approx -2.5029$ in agreement with numerical iteration of the map. Physically, α asymptotically rescales the variable x on successive bifurcations; i.e., if we magnify by α the x-interval near the extremum $x^* = -\frac{k}{2}$ and look at the next bifurcation, it will appear the same as the previous one. Thus the separation of the tines for successive bifurcation solutions near x^* scales as:

$$\frac{x_{i+} - x_{i-}}{x_{i+1,+} - x_{i+1,-}} = \alpha . \tag{4.71}$$

These are the solutions that grow out of $x^*_{2^+}$.

Since B is locally quadratic, the first iterates of a cluster of points near x^* must rescale as α^2; i.e., if the x_i's are the bifurcation

solutions near x^*, then their first iterates satisfy:

$$\frac{B(x_{i+}) - B(x_{i-})}{B(x_{i+1,+}) - B(x_{i+1,-})} = \alpha^2 \ . \tag{4.72}$$

These are the solutions that grow out of $x^*_{2^-}$. Thus half the elements of a period 2^k solution rescale as α and the other half as α^2.

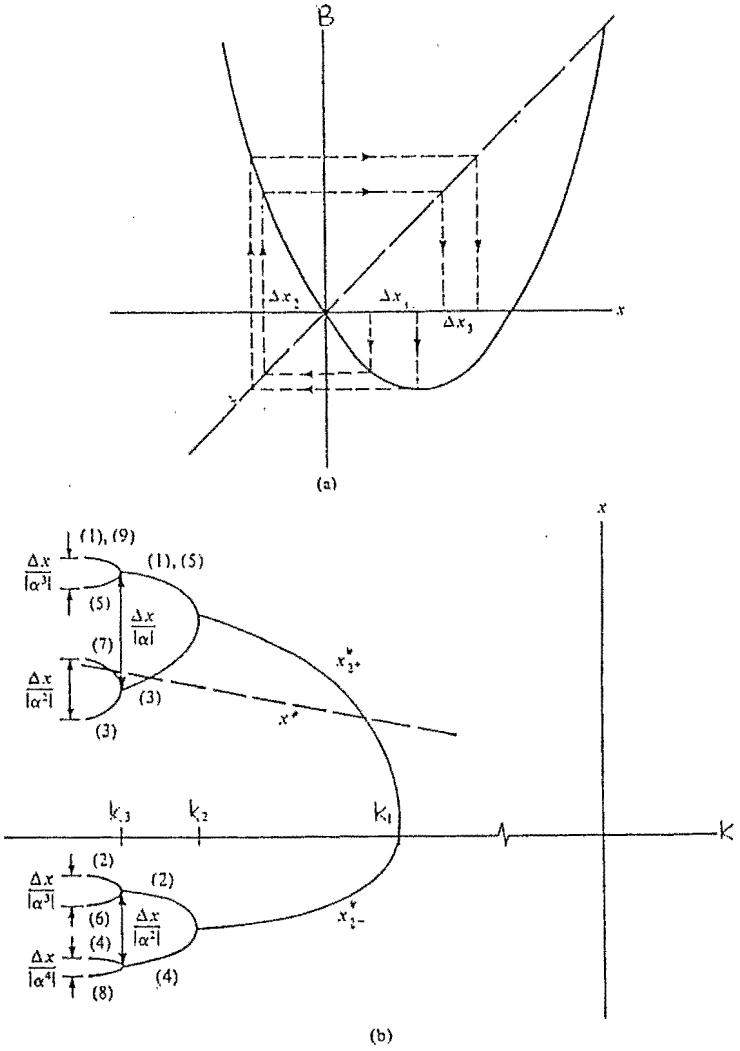

Figure 4.10 Illustrating the scaling of an interval in x for the quadratic map. (a) variation of an initial interval Δx_1 near the extremum of the quadratic map with successive iterations. Note that $\Delta x_2 \sim (\Delta x_1)^2$ but that $\Delta x_3 \sim \Delta x_2$. (b) The order of traversal and separation of the pitchfork tines for the first three bifurcations of the quadratic map. The order of traversal is shown in parentheses for a period 4 and a period 8 orbit. The alteration in the separation of the pitchfork tines from linear to quadratic scaling with α should be noted.
(after Lichtenberg and Lieberman, 1982)

This behaviour is illustrated in Figure 4.10 (a),(b). In Figure 4.10 (a), we note that a separation Δx_1 near the minimum of the map transforms to a separation $|\Delta x_2| \propto \Delta x_1^2$. However, Δx_2 then transforms back to an interval Δx_3 near the maximum with $|\Delta x_3| \propto \Delta x_2$. Thus the solution jumps back and forth between the tines of the pitchfork from linear to quadratic scaling in α. Note also the reversal of the sense of Δx on each traversal of the map. The resulting bifurcation structure for the first three bifurcations is shown in Figure 4.10 (b) indicating the widths of the various tines after each bifurcation. The order of traversing the tines for the period 4 and the period 8 cycles, starting on the upper tine, is shown in parentheses in the figure. We note the difference in the separation of the tines, with the separation of the $x^*_{2^+}$ tines (near x^*) being a factor of α greater than the separation of the $x^*_{2^-}$ tines. When another bifurcation takes place, the separations are as shown in the figure.

Any transformation which is invertible, from x to some new variable y preserves (4.71) and (4.72) with x replaced by y. Thus the constant α is also universal, in the same sense as δ.

As well as the bifurcation sequence which occurs when k decreases, the mirror bifurcation sequence also occurs. Here k increases from $\frac{1}{2}$ until the accumulation point is reached. The accumulation point for the mirror sequence is found from (4.12) and (4.62):

$$\overline{k_\infty} = \frac{(3+\sqrt{17})}{4} \approx 1.7808.$$

For the logistic map (4.4), the usual range of parameters considered is $0 < k < 4$. This corresponds to the mirror sequence for the quadratic map. Using $\bar{k} = 1 - k$ and noting $\ell = 2\bar{k}$, the first bifurcation occurs at $\bar{\ell} = 3$ and the accumulation point is $\overline{\ell_\infty} = \frac{(3+\sqrt{17})}{2} \approx 3.5616$, which compares well with the value found by direct iteration of the logistic map: $\overline{\ell_\infty} = 3.5700$.

The existence of period-doubling through very large periods is clearly shown in Figure 4.11, obtained by numerical iteration of the

quadratic map. The bifurcation sequence x_i versus k is plotted on a

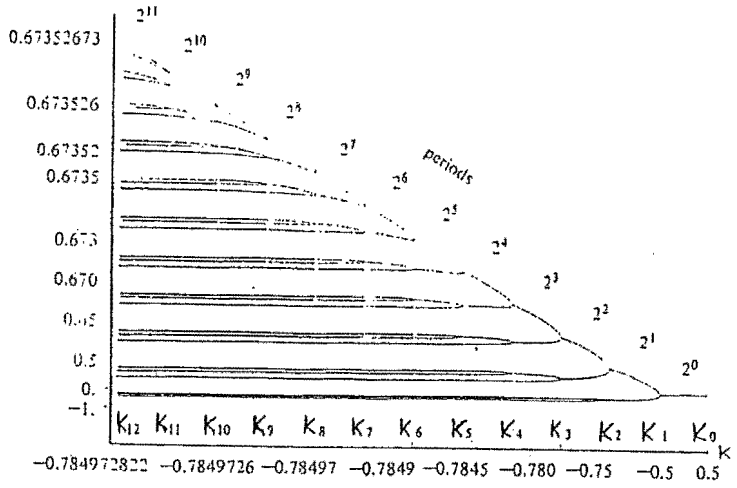

Figure 4.11 Period-doubling bifurcation sequence for the quadratic map. Vertically plotted are the x_ℓ of the attractor of period 2^ℓ, splitting off at k_ℓ from an attractor of period $2^{\ell-1}$, which continues as a repellor, not plotted here. Note the constant rates δ (at which the k_ℓ converge) and α (at which the orbits converge) in this doubly logarithmic plot. To the left of k_∞ an infinite number of repellors remain. (after van Zeyts, 1981; see Helleman, 1980)

doubly logarithmic scale. The constant rate of convergence δ along the k-axis, and the constant rate of convergence α of the bifurcation solutions along the x_i-axis are clearly seen.

There are many other universal constants related to one-dimensional unimodal mappings. For example, the height ratio of two adjacent period-doubled peaks in the power spectra is 13.2dB. For more details on this see Lichtenberg and Lieberman (1982). Also see Hao (1984) for references.

4.7 CYCLES OF PERIOD ℓ

We have seen how the original fixed point x^*_{10} gives rise to a cascade of pitchfork bifurcations as k decreases from k_0 to k_∞ i.e., the harmonics of period 2^n. For k less than k_∞ there exist other parameter regimes having periodic behaviour. These new cycles are born in pairs, one stable, the other unstable via *tangent bifurcations*. We now examine how new cycles of period ℓ arise, by considering the case $\ell = 3$.

To see graphically how these period 3 orbits arise, plotted in Figure 4.13 for the quadratic map is:

$$B^{(3)}(x,k) = B(B(B(x,k),k),k) \tag{4.73}$$

versus x, along with the 45° line for two parameter values. The period 3 roots satisfy:

$$x_3^* = B^{(3)}(x_3^*) \ . \tag{4.74}$$

For $k \geqslant k_0^{(3)}$, there are only two roots, corresponding to the period 1 roots x_{10}^* and x_{11}^*. If the hump in $B(x,k)$ is sufficiently steep then the threefold iteration will produce a function $B^{(3)}(x)$ with 3 "hills" as depicted in Figure 4.13(a) For $k \lesssim k_0^{(3)}$, the hump in B steepens and the hills and valleys in $B^{(3)}(x)$ become more pronounced until simultaneously the first valley and last two hills touch the 45° line. This can be made more plausible by observing Figure 4.13 which is $B^{(3)}(x)$ for (4.5)). $B^{(3)}(x)$ now intercepts the 45° line at 6 new points. Figure 4.13 (b) shows the curve $B^{(3)}(x)$ at this stage.

The stability-determining slope of $B^{(3)}(x)$ at three of these points has a common value, which is $\lambda^{(3)} = +1$ at their birth. It thereafter steepens beyond +1. Hence this period 3 cycle is never stable. This cycle is shown in Figure 4.13 (b) by the open circles. The slope of the other three points begins at $\lambda^{(3)} = +1$, and then decreases towards zero,

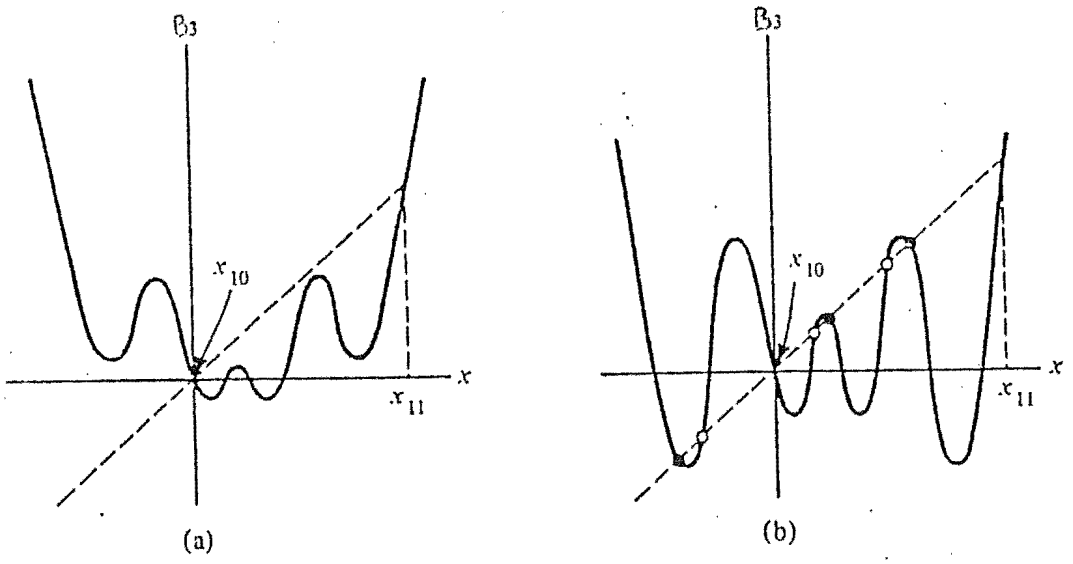

Figure 4.13 Birth of a pair of period 3 cycles by a tangent bifurcation. The solid circles show the stable period 3 orbit; the open circles show the unstable period 3 orbit: (a) $k \gtrsim k_0^{(3)}$, (b) $k \lesssim k_0^{(3)}$. (after Lichtenberg and Lieberman, 1982).

resulting in a stable limit cycle of period 3. This cycle is shown by the solid circles in Figure 4.13 (b).

As B(x,k) continues to steepen, the slope $\lambda^{(3)}$ for this initially stable 3 point cycle decreases beyond -1; the cycle becomes unstable and gives rise by the process of pitchfork bifurcations (since $B^{(3)}(x)$ is locally quadratic near the roots of this cycle), to stable cycles of period $6,12,\ldots, 3\times 2^n$. Solving (4.74) for x_3; we find that the two period three cycles are born at: $k_0^{(3)} = \frac{(1-\sqrt{8})}{2} \approx -0.9142$. The point of accumulation $k_\infty^{(3)}$, can be found by renormalization procedure of section 4.7b or by direct iteration. Iteration yields $k_\infty^{(3)} \approx -0.92475$. The mirror sequence period 3 cycle at $\bar{k} = 1 - k$ also exists.

We can now extend this result, knowing that there are two basic kinds of bifurcation processes for first order difference equations. New

cycles of period ℓ arise in pairs (one stable, one unstable) as the hills and valleys of high iterates B(x,k) move, respectively, up and down to intercept the 45° line. Such cycles are born at the moment when the hills and valleys become tangent to the 45° line, and the initial slope of $B^{(\ell)}$ at the points is $\lambda^{(\ell)} = +1$. This type of bifurcation is called a tangent bifurcation or a $\lambda^{(\ell)} = +1$ bifurcation. Conversely, an originally stable cycle of period ℓ may become unstable as B(x,k) steepens. This happens when the slope of $B^{\ell}(x,k)$ steepens beyond $\lambda^{(\ell)} = -1$, whereupon a new and initially stable cycle of period 2ℓ is born. This type of bifurcation is called a *pitchfork bifurcation* or a $\lambda^{(\ell)} = -1$ bifurcation.

In summary, we conclude that as the parameter in B(x,k) is varied the fundamental stable dynamical units are cycles of basic period ℓ, which arise by tangent bifurcation, along with their associated cascade of harmonics of periods $\ell \cdot 2^n$, which arise by pitchfork bifurcation. Hence the case $\ell = 1$ (the fixed point x^*_{11}) and the subsequent hierarchy of stable cycles of periods 2^n is merely a special case of a general phenomenon.

For all smooth and sensible functions B(x,k), there is a unique stable cycle for each value of the parameter. The entire range of parameter values may be thus regarded as made up of infinitely many windows of parameter values (some large, some unimaginably small, each corresponding to a single one of these basic dynamical units. These windows are divided from each other by points (the points of accumulation of the harmonics of period $\ell \cdot 2^n$) at which the system is truly chaotic, with no attractive cycle. Although there are infinitely many such special parameter values, they have measure zero on the interval of all values. The theory in this section is from May (1976).

4.8 CHAOTIC BEHAVIOUR

Beyond the point of accumulation (for (4.4)) a_∞, there are an infinite number of fixed points with different periodicities, and an

infinite number of different periodic cycles. There are also an uncountable number of initial points, x_0, which give totally aperiodic (although bounded) trajectories. The stable cycles, which represent regular motion, are dense and occupy a finite fraction of the parameter interval. The motion for the remaining parameter values is unstable and densely fills a finite interval in x for an arbitrary initial x_0. Nearby trajectories diverge exponentially and this motion is thus chaotic.

As the parameter increases beyond the critical value, at first all these cycles have even periods, with x_j alternating up and down between values above, and values below the fixed point x^*. These cycles may be very complicated, having a nondegenerate period of say 5726 points before repeating. To the casual observer, they would appear somewhat like a "noisy" cycle of period 2.

As we continue to increase the parameter, there comes a stage where the first odd period cycle appears. At first these odd cycles have very long periods. As the parameter value continues to increase, cycles of smaller and smaller odd periods are picked up until eventually the three point cycle appears. Beyond this point there are cycles with every integer period as well as an uncountable number of asymptotically aperiodic orbits. See Figure 4.14. Li and Yorke entitle their proof of this result "Period Three Implies Chaos".

Li and Yorke (1975) studied the behaviour of (4.1) where $B(x,k)$ is any continuous function defined on an interval. If there exists some initial point x_0 such that $x_1 > x_0$ and $x_2 > x_1$ but $x_3 \leqslant x_0$, then they show that there is an uncountable subset of initial conditions for which the resulting sequence never settles down to a constant periodic behaviour. Any two points in this subset lead to sequences which are in the long term very different, regardless of how close the initial two points are.

There can, in addition, be one or more stable periodic orbits but these seem to be somewhat rare, and when they do exist, they are totally

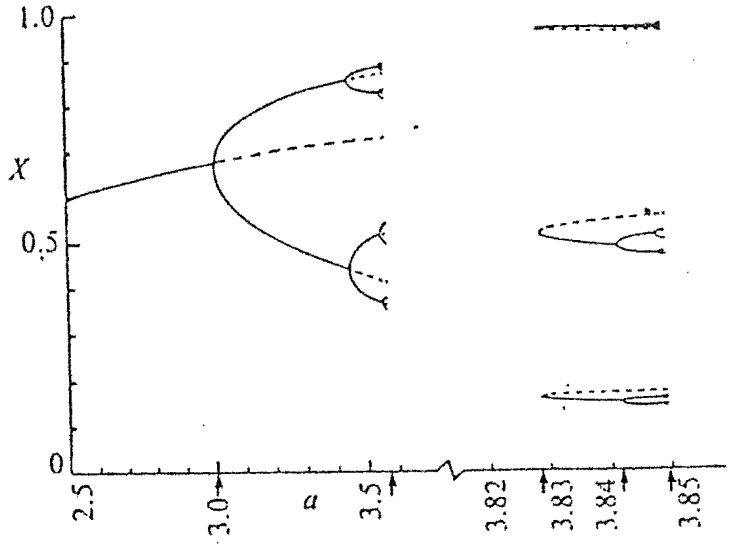

Figure 4.14 This figure illustrates some of the stable (——) and unstable (- - - -) fixed points of various periods than can arise by bifurcation processes in equation (4.1) in general, and equation (4.4) in particular. To the left, the basic stable fixed point becomes unstable and gives rise by a succession of pitchfork bifurcations to stable harmonics of period 2^n; none of these cycles is stable beyond $a = 3.5700$. To the right, the two period 3 cycles appear by tangent bifurcation: one is initially unstable: the other is initially stable, but becomes unstable and gives way to stable harmonics of period 3×2^n, which have a point of accumulation at $a = 3.8495$. Note the change in scale on the a-axis, needed to put both examples on the same figure. There are infinitely many other such windows, based on cycles of higher periods. (after May, 1976).

disrupted by small random perturbations. In fact, a unimodal mapping can have at most one stable period for each paramater value k. It may have no stable period at all for many k values. The necessary condition for B(x,k) to have at most one stable period was found by Singer (1978) and consists in the *Schwarzian derivative* SB of B being negative on the interval I :

$$SB(x) \equiv \frac{B'''(x)}{B'(x)} - \frac{3}{2}\left(\frac{B''(x)}{B'(x)}\right)^2 < 0. \qquad (4.75)$$

See Hille (1976) for more details on the Schwarzian derivative. This condition is not sufficient for a stable period to exist. It is just this insufficiency that allows the possibility of chaotic orbits to appear. Even when SB < 0 one can get different aperiodic sequences starting from different x_0, and never reaching a stable period.

For (4.4), Yorke and Yorke (1979) chose a = 3.83 and $x_1 = 0.16$ to test this fragile behaviour. There is also a stable period 3 orbit into which most trajectories of x_n will become locked (there is still an uncountable set of initial conditions whose trajectories do not get locked in). They found that the slightly noisy equation:

$$x_{n+1} = 3.83\, x_n(1 - x_n) \pm 0.001 \tag{4.76}$$

has a different behaviour when the signs ± are chosen randomly for each iteration. No sign of periodicity was observed. The orbits x_n will not stay near the original period 3 orbit, should x_n pass near (the stability is destroyed).

For sensible functions like B(x,k) in (4.4), for any specified parameter value there is one unique cycle that is stable, and that attracts essentially all initial points i.e., one cycle "owns" almost all initial points; the remaining infinite number of other cycles, along with asymptotically aperiodic trajectories, own a set of points which although uncountable, have measure zero.

The possibility of divergent but bounded trajectories arises because unimodal noninvertible maps act by first stretching the mapped interval and then folding a portion of this interval back on itself. Since folding cannot take place for one-dimensional invertible maps, such maps cannot display chaotic behaviour.

4.9 REVERSE BIFURCATION OF CHAOTIC BANDS

The stable period 1 motion for the quadratic map (4.11) bifurcates repeatedly as k decreases from $k_0 = \frac{1}{2}$ to $k_\infty = -0.78497...$ leading to the bifurcation tree shown in Figure 4.11. We now look at the nature of the motion as k becomes increasingly negative beyond $k = k_\infty$. The qualitative features are shown in Figure 4.15. The steady state x_n values ($1000 < n < 4000$) are shown as a vertical set of dots for each value of

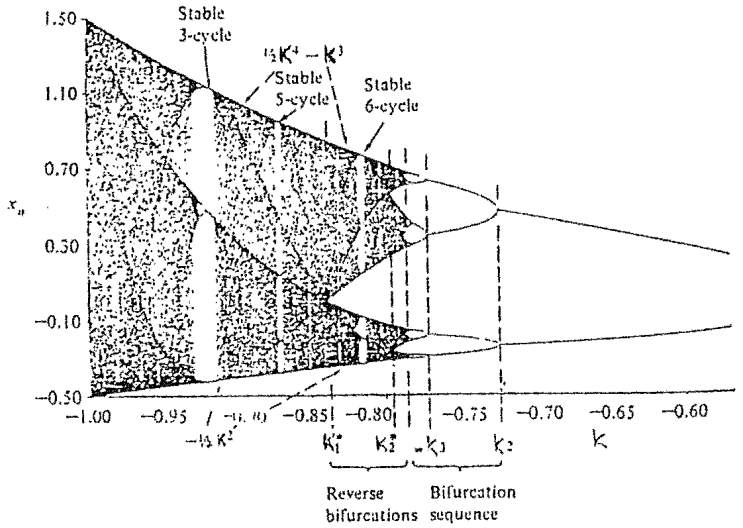

Figure 4.15 Numerical calculation of the reverse bifurcation sequence for the quadratic map. For each value of k, 3000 x_n's with $1000 < n < 4000$ have been plotted. The chaotic bands of motion for $k < k_\infty$ are clearly seen, with the band mergings occurring at k*. The stable 6,5 and 3 cycles (with decreasing k) embedded within the predominatly chaotic region of k are clearly seen. (after Collet and Eckmann, 1980).

k on the horizontal axis. Linear scales are used for both axes. We see clearly the presence of chaotic bands of motion for $k \leqslant k_\infty$.

As k becomes increasingly negative below k_∞ the bands merge, giving a reverse set of bifurcations at various values k_n^* noted on the figure. One can also see the presence of higher-period bifurcation trees embedded in the chaotic region, for $k < k_\infty$. The stable 6,5 and 3 cycles and their bifurcation trees (with decreasing k) are visible. The same scalings δ and α are found for the reverse bifurcations of the chaotic bands as for the bifurcations of the periodic attractors. These results, obtained by Grossman and Thomas (1977), can also be derived from the renormalization theory of the earlier section 4.6. This section is based on theory in Lichtenberg and Lieberman (1982).

4.10 LOCATING THE FIRST ODD PERIOD CYCLE

A simple graphical method for locating the parameter value in the chaotic regime at which the first odd period cycle appears is as follows. Let γ be the parameter which tunes the steepness of $B(x,k)$ (for example $\gamma = a$ in (4.5)). The fixed point of period 1 is $x^*(\gamma)$, and $x_{max}(\gamma)$ the maximum value attainable from iterations of (4.1) i.e., the value of $B(x,k)$ at its stationary point. The first odd period cycle appears for the value of γ which satisfies

$$x^*(\gamma) = B^{(2)}(x_{max}(\gamma)). \tag{4.77}$$

This result is due to Hoppensteadt and Hyman (1975).

Another important parameter value is where the period 3 cycle first appears. This critical value may be found numerically from the solutions of the third iterate of (4.1). For (4.5) it is $a = 1 + \sqrt{8}$.

4.11 COUNTING THE ORBITS

We present a rather simple approach from May (1976) which uses first principles. The problem may be phrased as follows. How many points of period ℓ are there? This is equivalent to finding the number of distinct solutions of:

$$x_\ell^* = B^{(\ell)}(x_\ell^*) . \tag{4.78}$$

When $B(x,k)$ is sufficiently steep, each successive iteration doubles the number of hills so that $B^\ell(x,k)$ has $2^{\ell-1}$ hills. For large enough parameter values, all these hills and valleys intersect the 45° line, producing 2^ℓ fixed points of period ℓ. See Table 4.1 (first row).

This list includes degenerate points (superstable) of period ℓ, whose period is a submultiple of ℓ. These degenerate points can be subtracted out, to leave the total number of nondegenerate points of basic period ℓ, as listed in the second row of Table 4.1. (We show how to calculate these points later). The 2^ℓ period ℓ points are arranged

k	1	2	3	4	5	6	7	8	9	10	11	12
Possible total number of points with period k	2	4	8	16	32	64	128	256	512	1,024	2,048	4,096
Possible total number of points with non-degenerate period k	2	2	6	12	30	54	126	240	504	990	2,046	4,020
Total number of cycles of period k, including those which are degenerate and/or harmonics and/or never locally stable	2	3	4	6	8	14	20	36	60	108	188	352
Total number of non-degenerate cycles (including harmonics and unstable cycles)	2	1	2	3	6	9	18	30	56	99	186	335
Total number of non-degenerate, stable cycles (including harmonics)	1	1	1	2	3	5	9	16	28	51	93	170
Total number of non-degenerate, stable cycles whose basic period is k (that is, excluding harmonics)	1	–	1	1	3	4	9	14	28	48	93	165

Table 4.1 Catalogue of the number of period points, and of the various cycles (with periods k = 1 up to 12), arising from equation (4.1) with a single-humped function B(x). (after May, 1976).

into various cycles of period ℓ, or submultiples thereof, which appear in succession by either tangent or pitchfork bifurcation as the parameters in B(x,k) are varied. The third row in Table 4.1 catalogues the total number of distinct cycles of period ℓ which so appear.

In the fourth row of Table 4.1, the degenerate cycles are subtracted out, to give the total number of non-degenerate cycles of period ℓ. These numbers must equal those of the second row divided by ℓ. This fourth row includes the (stable) harmonics which arise by pitchfork bifurcation, and the pairs of stable-unstable cycles arising by tangent bifurcation. By subtracting out the cycles which are unstable from birth, the total number of possible stable cycles is given in the fifth row.

Finally, we may subtract out the stable cycles which arise by pitchfork bifurcation, as harmonics of some simple cycle; to arrive at the final row in Table 4.1, which lists the number of stable cycles of basic period ℓ. For further details, including an example, see May (1976).

4.12 ORDERING OF THE ORBITS

In this section we examine how the various cycles are arranged along the interval of relevant parameter values. This question has been answered by several groups of people. The way in which these basic

cycles are arranged along the interval of parameter values is universal for all unimodal quadratic maps. For example, through to period 6, the basic cycles are ordered with k decreasing from k_0 as having periods 1,6,5,3,5,6,4,6,5,6. We present two results, both of which can be used to establish the ordering of the orbits.

4.12a SARKOVSKII THEOREM

This theorem first appeared in Sarkovskii (1964) in 1964, which is in Russian. Stefan (1977) has translated his work and corrected several mistakes in his argument. Consider an order relation $<$ on the set N of all integers $\geqslant 1$, defined as follows.

Let $N = A \cup B$, $A = \{2^n \ell : n \leqslant 0, \ell \leqslant 3, \text{ odd}\}$ and $B = \{2^m, m \leqslant 0\}$. Order A lexicographically with increasing n and ℓ; order B with decreasing m, and let A precede B. We have

$$3 > 5 > 7 > 9 > \ldots > 3.2 > 5.2 > 7.2 > 9.2 > \ldots > 3.2^2 > 5.2^2 > 7.2^2 > 9.2^2 > \ldots > 3.2^n > 5.2^n > 7.2^n > 9.2^n > \ldots 2^m > \ldots > 32 > 16 > 8 > 4 > 2 > 1 . \qquad (4.79)$$

The main result is as follows:

Theorem: Let $T : R \to R$ be a continuous mapping which has a period orbit of order n. Then T has a periodic orbit of period m for every $m \in N$ such that $n > m$.

Proof: See Stefan (1977).

In simple terms: if $B(x,k)$ is a unimodal mapping and has a point x leading to a n-cycle, then it must have a point leading to a m-cycle for every $m < n$ in the sense of the above ordering.

It is important to realize that the Sarkovskii theorem is only a statement concerning different x's at a fixed parameter value k. It says nothing about the stability of the periods, nor about the measure (the observability of these periods). Unaware of the work of Sarkovskii, many equivalent formulations or corollaries of this theorem were suggested in the intervening years, among which is the Li-Yorke theorem "Period 3 Implies Chaos" and the Oono's statement "Period $\neq 2^n$ Implies Chaos", etc. We now look at an important result by Metropolis, Stein and Stein.

4.12b THE U-SEQUENCE

The *U-sequence* (U stands for "universal") is on application of symbolic dynamics. It is also known as a *M.S.S. sequence* or *kneading sequence* according to the procedure by which it is constructed.

Let us take $x = \bar{x}$ (the x value for which B has a maximum) as the "centre" and initial point of the mapping and follow the subsequent iterations. To a point we assign the letter R or L according to whether it falls to the right or left of the centre. Hence, each periodic sequence corresponds to a word of finite length of R's and L's. Metropolis, Stein and Stein (1973), found that it is possible to introduce an ordering for all admissible words, i.e., to compile a dictionary of the words and there is a correspondence between the position of a word in the dictionary and the place of occurrence of a period on the parameter axis for a wide class of unimodal mappings. In particular, if the word P corresponds to a period, we can construct another word:

$$H(P) = P_x P \tag{4.80}$$

where $x = R$ if there is an even number of R's in P and $x = L$ otherwise. H is called the *harmonic* of P and represents the period-doubled orbit adjacent to P. All admissible words corresponding to periods less than or equal to 11 are given in the Appendix of Metropolis, Stein and Stein (1973).

Given the complete U-sequence for $k \leqslant K$, one generates the sequence for $k + 1$ by inserting the appropriate pattern of length $k + 1$ between every two (non-harmonic) adjacent patterns whenever the theorem permits it. The pattern R $(k = 2)$ remains the lowest pattern, as is easily shown, for any k, the last pattern is always of the form RL^{k-2}, and this is simply appended to the list.

As is pointed out in Hao (1984), the construction of harmonics happens to be a particular case of a more general composition rule, introduced and denoted by * in the paper by Derrida et al, (1978). Using the composition one can express the harmonic of P as $P*R$, and a period-doubling sequence starting with P corresponds to the symbolic sequence $P*R^{*n} = P*R* \ldots *R$ (n times R etc.). In particular, one can select a period tripling sequence $(RL)^{*n}$, period-quadrupling sequence $(RL^2)^{*n}$ etc. from the infinite number of periods embedded in the chaotic bands. Periods in these sequences are not adjacent on the parameter axis, but they have their own scaling factors and convergence rates.

By examining the properties of the * composition, Derrida et al (1978), succeeded in proving the self-similarity of the U-sequence, i.e., part of it appears to be similar to the whole sequence. This important result is the mathematical manifestation of the hierarchy structure of chaotic bands, seen in bifurcation diagrams. The U-sequence has been observed in real and computer experiments. See Hao (1984) for references.

4.13 DETERMINING THE SUPERSTABLE VALUES

We follow the reasoning in Hao (1984). Define a sequence of polynomials $P_n(k)$ using recursive relations based on the original mapping $B(k,x)$:

$$P_0(k) = 0$$

$$P_n(k) = B(k, P_{n-1}(k)) \tag{4.81}$$

The $P_n(k)$'s as functions of k describe the dark lines seen in the chaotic region of bifurcation diagrams, because the iterates of $x = 0$

always correspond to extremes in islands of the chaotic bands. In fact, $P_n(k)$ is nothing but the nth iterate of B taken at point $x = 0$, i.e.,

$$P_n(k) \equiv B(n,k,0) \ . \tag{4.82}$$

Therefore, real zeros of $P_n(k)$ in the appropriate interval give the parameter values for superstable orbits of period n.

Example: $P_5(k)$ in the case of the logistic mapping (4.5) has three zeros; $k = 1.62541\ldots$, $1.86078\ldots$, and $1.98542\ldots$, which correspond to superstable orbits of types RLR^2, RL^2R and RL^3.

Most numerical algorithms to solve $P_n(k) = 0$ lose stability, which makes this method impractical. This loss of stability occurs when zeros get very close to each other. There does exist an effective method to calculate the superstable parameter values separately, given the corresponding word in the U-sequence.

Let us consider for example the word RLR^2 which represents the first superstable period 5 orbit. Write it as a 5-cycle starting and ending at $x = 0$, i.e.,

$$B_R(k,B_L(k,B_R(k,B_R(k,B(k,0))))) = 0 \tag{4.83}$$

where the subscript R or L indicates which branch, right or left, of the map has been used at each step (the first B maps into the centre and thus has no subscript).

Once the branches have been marked, we can invert (4.83) to give:

$$1 = B(k,0) = B_R^{-1}(B_R^{-1}(B_L^{-1}(B_R^{-1}(0)))) \ . \tag{4.84}$$

Now define

$$R(x) = B_R^{-1}(x), \ L(x) = B_L^{-1}(x) \tag{4.85}$$

and write (4.84) using the functional composition symbol $\circ$. Observe that the word RLR^2 has been "lifted" to an equation for k:

$$R \circ L \circ R \circ R(0) = 1 \tag{4.86}$$

which determines the superstable parameter k for RLR^2. In the case of

the logistic map (4.5), taking the square of (4.84) a few times to get rid of the radicals would bring us back to $P_5(k) = 0$ with all other zeros present, so we retain (4.86) and multiply it by k to get:

$$\sqrt{k + \sqrt{k - \sqrt{k - \sqrt{k}}}} = k \, . \tag{4.87}$$

H. Kaplan suggested to solve this equation by iteration. That is, let:

$$k_{n+1} = \sqrt{k_n + \sqrt{k_n - \sqrt{k_n - \sqrt{k_n}}}} \tag{4.88}$$

with suitable k_0, say, $k_0 = 2$. The general rule for the iteration equation for any word in the U-sequence follows from this.

4.14 INTERMITTENCY

Here we are interested in the onset of chaotic behaviour characterized by the occurrence of regular or laminar phases separated by intermittent bursts. This *intermittent transition* to chaos was discussed by Pomeau and Manneville (1980) in connection with the Lorenz model. See Figure 4.16. We shall define the term intermittency exclusively

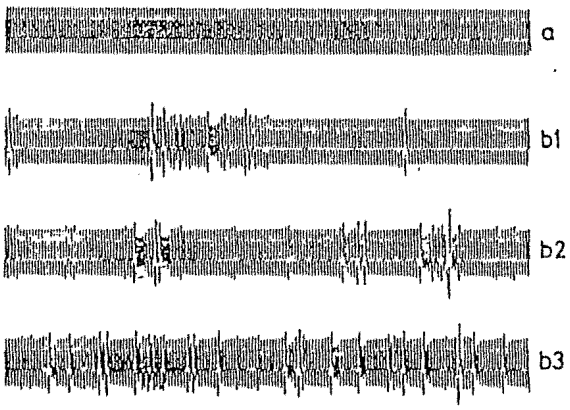

Figure 4.16 Time record of one coordinate (z) in the Lorenz model (a) stable periodic motion for r = 166. (b) Above the threshold the oscillations are interrupted by bursts which become more frequent as r is increased. (after Pomeau and Manneville, 1980)

to refer to random, alternations of chaotic and regular behaviour in time evolution without involving any spatial degrees of freedom. This is in contradistinction to the concept of intermittency in the hydrodynamical

theory of turbulence which refers to random bursts of turbulent motion on the background of laminar flows. This temporal intermittency is caused by spatially changing boundaries separating different flow regimes.

By inspection of the bifurcation diagram for a one-dimensional mapping or the phase diagram showing the bifurcation and chaos structure of a system of ODE's, one sees many chaotic regions contained in between pairs of type RL^{n-1} and RL^{n}. If one enters a given chaotic region from the RL^{n-1} side, then the transition takes place via a cascade of period-doubling bifurcations. If one approaches the same chaotic region from the RL^{n} boundary, the intermittent transition shows itself. In this sense we can say that among the various routes to chaos, period-doubling and intermittency are twin phenomena.

We shall illustrate this with an example from Hirsch, Huberman and Scalapino (1982): the logistic mapping (4.4). The attractor is in the region $3 \leqslant k \leqslant 4$ in Figure 4.17. Past the first period-doubling bifurcation cascade at k = 3.57, various open regions with odd numbers of fixed points appear which arise from tangent bifurcation. The 3-cycle region

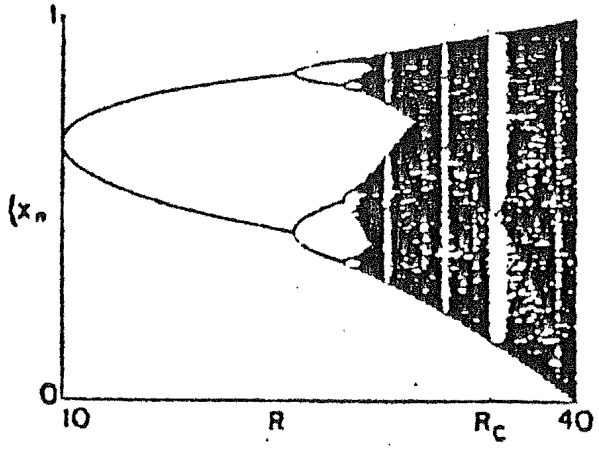

Figure 4.17 The attractor vs R for the logistic map $x_{n+1} = Rx_n(1 - x_n)$. The intermittent behaviour discussed in this review arises when R decreases below the threshold for an odd-limit cycle. In particular, we focus on the region just below $R_c = 1 + \sqrt{8}$ which is the threshold for three-cycle orbits. (after Hirsch et al, 1982)

appears last at $k_c = 1 + \sqrt{8}$. As k increases further, one can see that

this 3-cycle behaviour undergoes the usual bifurcation cascade to chaos. Now as k decreases below k_c, the system also enters a chaotic regime and it is this transition in which intermittency occurs. Figure 4.18 shows results of iteration of (4.4) for $k = k_c + 0.002$ and $k = k_c - 0.002$. For $k > k_c$, after an initial transient, the iterates settle down to a threefold limit cycle. However, for $k < k_c$, approximate threefold cycles are interrupted by irregular behaviour.

It is fair to say that the mechanism of intermittency in one-dimensional mappings has been fully understood. Pomeau and Manneville (1980) pointed out that it arises in the neighbourhood of tangent bifurcation just as period-doubling is related to pitchfork bifurcation. Once again let us view the logistic mapping. When the parameter k is kept very close to but still less than $k_c = 1 + \sqrt{8}$, its third iterate $B(3,k,x)$ has three humps or valleys that come very close to the bisector in the $B(3,k,x)$ versus x diagram, but do not touch it, thereby leaving very narrow corridors between the curve $B(3,k,x)$ and the bisector. See Figure 4.19.

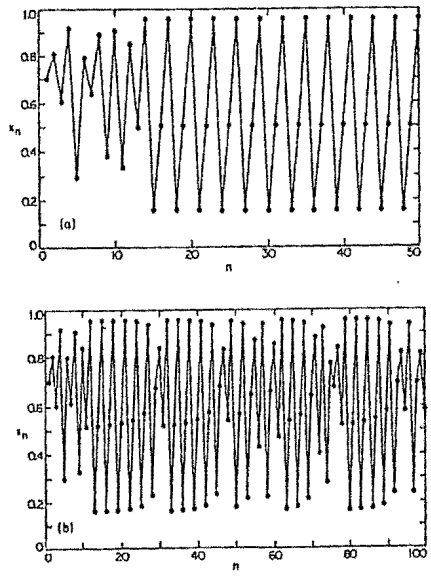

Figure 4.18 Iterates of the logistic map starting from $x = 0.7$; (a) in the stable three-cycle region $R_c - R = -0.002$ and (b) in the intermittent region $R - R_c = -0.002$. (after Hirsch et al, 1982)

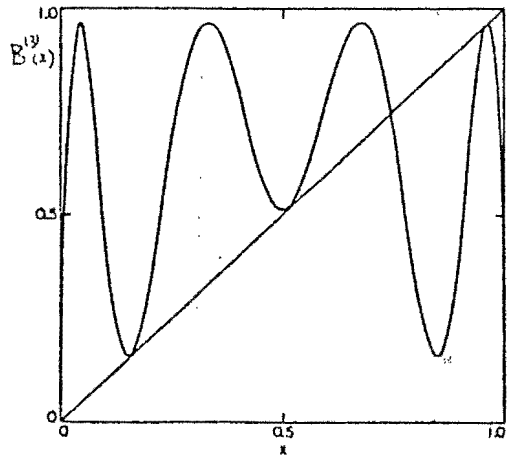

Figure 4.19 The threefold iterated map $B^{(3)}(x)$ vs x for $R = R_c$.
(after Hirsch et al, 1982)

Now whenever one iteration point falls near the entrance to one of the corridors, it will take many iterations to pass through the corridor when k is very close to k_c, this looks much like a segment of convergent iteration to the would be fixed point k_c and leads to the laminar phase of the iteration. See Figure 4.20 for this "staircase" structure. Having passed through one corridor, the point will make a number of large-step jumps before falling again, to the entry of one or another corridor. These jumps constitute the random bursts of the chaotic behaviour.

Pomeau and Manneville (1980) pointed out that as $k \to k_c$, the time of passage diverges as $(k_c - k)^{-\frac{1}{2}}$ (for the Lorenz system). In general, we can say that the nearer k is to k_c, the longer the averaged laminar time is. Simple mean-field arguments give the passage time t:

$$t \propto (k_c - k)^{-(1 - \frac{1}{z})} \qquad (4.89)$$

where z denotes the order of maximum in the mapping.

We briefly now mention an effective method to recognize intermittency in practice. One constructs the (P_i, P_{i+n}) map near a tangent bifurcation of period n, where P_i may be any of the variables under study. If there were an exact period n, one would get n points on the bisector on the

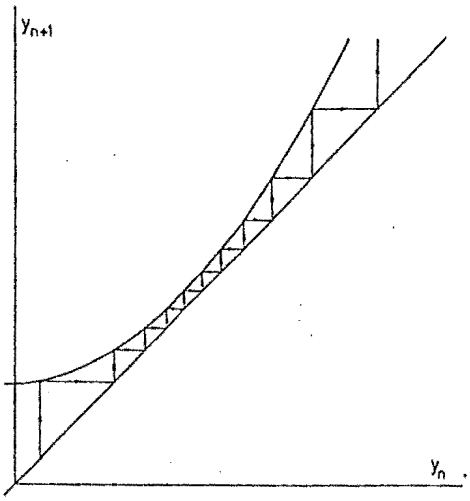

Figure 4.20 The motion through the channel corresponds to the laminar phase of the movement. The slow drift is quite imperceptible on the time record of (4.16b). (after Pomeau and Manneville, 1980)

(P_i, P_{i+n}) diagram, but at the intermittent transition we can only see what Hao (1984) calls the "spirit" of the would be fixed points, i.e., n clusters along the bisector together with a few points scattered away from it. Also in periodically forced systems, intermittency associated with tangent bifurcations of not very long period can be easily distinguished from chaotic or transient behaviour by their specific subharmonic stroboscopic sampling diagrams. Since there are an infinity of periodic windows born from tangent bifurcations embedded in the chaotic regions of the parameter space, the intermittent transitions are generic in numerical and laboratory experiments.

Finally we mention the renormalization group equation for intermittent transitions. We know that a periodic window in a one-dimensional mapping remains stable whenever the quantity: $|B'(x,k)| < 1$. In fact, the limit $B'(x,k) = -1$ corresponds to period-doubling bifurcations, whereas $B'(x,k) = +1$ indicates an intermittent transition. Therefore, it is not surprising that intermittent transitions can be described by the same renormalization group equation of Feigenbaum (4.47), with changed boundary conditions:

$$g(0) = 0 \quad \text{and} \quad g'(0) = 1 \tag{4.90}$$

Note that Hirsch et al (1982) have found an exact solution to (4.90). Their solution has been extended to give all the intermittent exponents and universal functions g(x) for general z.

4.15 INVARIANT DISTRIBUTIONS

We say that D(x) is an *invariant distribution* of the mapping T if:

$$D(x) = TD(x) . \tag{4.91}$$

Other names are invariant measure or probability distribution. We assume that D integrates to unity. In general there are many distributions invariant to a given mapping. However, a unique equilibrium distribution is generally singles out by repeated iteration of the map such that the time average is equal to the space average over the distribution for almost all initial conditions x_0. For a parameter value corresponding to a stable, period n cycle, P(x) is discrete, consisting of n δ-functions at the n stable fixed points of the map, each delta function having integrated value $\frac{1}{n}$. Except for a set of measure zero, every x_0 leads under repeated iteration of the map to this unique, steady-state distribution. Similarly for parameters yielding chaotic motion, all initial conditions, except for a set of measure zero, yield a unique, equilibrium distribution. This distribution may be discontinuous in x, but it is typically nonzero over a finite range of x values.

Numerically, D(x) can be constructed from (4.91). As illustrated in Figure 4.21, the number of trajectories D(x)dx within some small interval dx in x is equal to the number within the corresponding intervals at the inverse points of the mapping. Since there are two inverse points x_1 and x_2 for a unimodal map:

$$D(x)dx = D(x_1)dx_1 + D(x_2)dx_2 \tag{4.92}$$

writing $\frac{dx}{dx_1} = \left|\frac{dB}{dx}\right|_{x_1}$ etc., we have:

$$D(x) = \frac{(Dx_1)}{\left|\frac{dB}{dx}\right|_{x_1}} + \frac{D(x_2)}{\left|\frac{dB}{dx}\right|_{x_2}} . \tag{4.93}$$

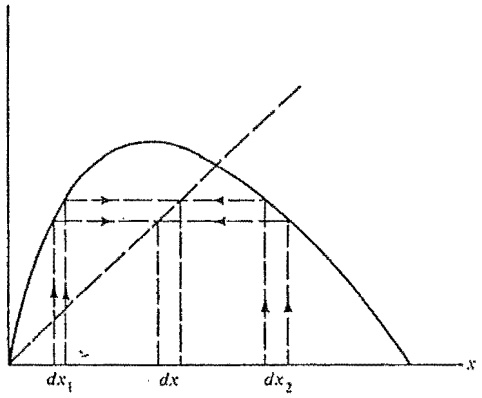

Figure 4.21 The construction of the invariant distribution D(x). The number of orbits within dx is equal to the number within the two pre-images dx_1 and dx_2. (after Lichtenberg and Lieberman, 1982)

This is a functional equation for D, that can rarely be solved analytically. However, a numerical solution is easily obtained by iterating (4.93) as follows:

(i) choose an initial guess $D_i = D_1(x)$

(ii) evaluate the right-hand side using D_i to obtain the next iterate D_{i+1}

(iii) repeat (ii) until convergence is achieved.

The procedure is illustrated in Figure 4.22, for the logistic mapping with $k = 4$. The first four iterations in Figure 4.22 are shown with the initial guess $D_i(x) = 1$. The procedure converges rapidly to the invariant distribution:

$$D(x) = \frac{1}{\pi}\left[x(1-x)\right]^{-\frac{1}{2}} \qquad (4.94)$$

which will be found analytically below.

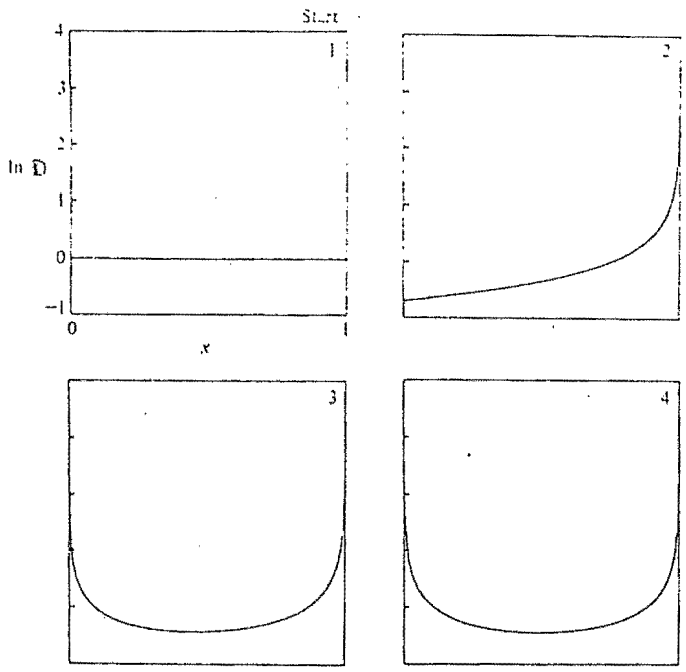

Figure 4.22 Numerical calculation of the invariant distribution D(x) for the logistic map with k = 4, showing the initial guess and the first three iterations. (after Shaw, 1981)

This method gives the invariant distributions for the logistic map with k = 3.8 and k = 3.825, as shown in Figure 4.23. In these cases, the motion appears chaotic and the distribution is nonzero over a finite range of x.

Use of the invariant distribution allows one to replace time averages by spatial averages over the invariant distribution. For example, the Lyapunov exponent may be found using:

$$\sigma = \int dx\ D(x)\ \ell n \left| \frac{dB}{dx} \right| . \qquad (4.95)$$

If an invertible transformation $\bar{x} = r(x)$ is introduced, then the invariant distribution transforms so as to conserve the number of trajectories within any small interval in x:

$$\bar{D}(\bar{x})d\bar{x} = D(x)dx . \qquad (4.96)$$

This equation yields the new invariant distribution in terms of the old.

4.15a THE TENT MAP

Some of the preceding ideas are illustrated using the symmetric

tent map shown in Figure 2.24. The map has a single maximum at $B(\frac{1}{2}) = a$ but it is not a quadratic map. The slope B' is 2a for the left half of the map and -2a for the right half. The motion is chaotic for $a > \frac{1}{2}$, since all trajectories diverge exponentially.

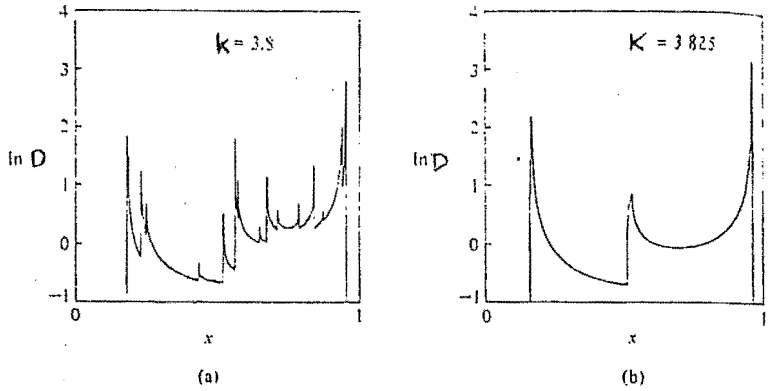

Figure 4.23 Two direct numerical calculations of the invariant distribution D(x) for the logistic map (a) k = 3.8; (b) k = 3.825. Note the discontinuous structure of D(x) and the evidence of a reverse bifurcation sequence as k increases. (after Shaw, 1981)

The invariant distribution is found from (4.93):

$$D(x) = \frac{1}{2a}\left[D\left(\frac{x}{2a}\right) + D\left(1 - \frac{x}{2a}\right)\right] . \qquad (4.97)$$

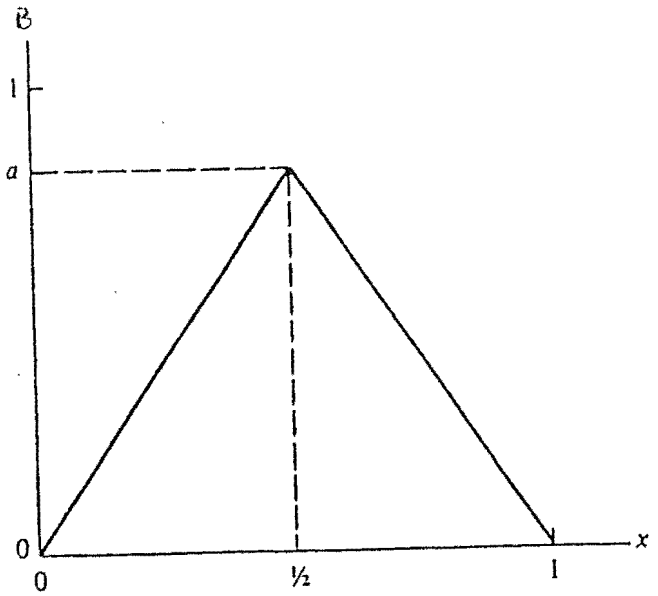

Figure 4.24 The symmetric tent map. (after Lichtenberg and Lieberman, 1982)

For a = 1, this has the obvious solution D(x) = 1. The Lyapunov exponent for this value of a is found from (4.95):

$$\sigma = \int_0^1 dx\ \ell n2 = \ell n\ 2\ . \tag{4.98}$$

Since $\sigma > 0$, the motion is chaotic.

Let us now consider the logistic map with k = 4:

$$B(x,k) = 4x(1-x)\ . \tag{4.99}$$

If we introduce the transformation:

$$\bar{x} = \left(\frac{2}{\pi}\right) \sin^{-1}\sqrt{x} \tag{4.100}$$

then (4.99) is transformed to the *symmetric tent map* with a = 1:

$$\bar{B}(\bar{x}) = \begin{cases} 2\bar{x} & 0 < \bar{x} < \frac{1}{2} \\ 2 - 2\bar{x} & \frac{1}{2} < \bar{x} < 1\ . \end{cases} \tag{4.101}$$

Using (4.96) with $\bar{D}(\bar{x}) = 1$, we obtain the invariant distribution for the logistic map (4.99):

$$D(x) = \frac{d\bar{x}}{dx} = \frac{1}{\pi}[x(1-x)]^{-\frac{1}{2}}\ . \tag{4.102}$$

This distribution was found numerically in Figure 4.22. If we evaluate the Lyapunov exponent from (4.95), for the logistic map (4.99), we obtain:

$$\sigma = \frac{1}{\pi}\int_0^1 \frac{\ell n\ |\ 4(1-2x)\ |}{[x(1-x)]^{\frac{1}{2}}}\, dx = \ell n\, 2\ . \tag{4.103}$$

It is no surprise that (4.99) and (4.101) have the same Lyapunov exponent since σ is invariant under coordinate transformations. The theory presented in this section is taken from Lichtenberg and Lieberman (1982).

CHAPTER 5

THE TRANSITION TO TURBULENCE

Observations of turbulence are as old as recorded history. Leonardo da Vinci was intrigued by turbulence, as one can see from his sketch, shown in Figure 5.1. The modern scientific study of turbulence dates from the late 1800's, with the work of O. Reynolds. In reviewing the subject from that date to the present, one is struck by the appearance of three distinct movements, each of which (despite some overlap), can be characterized by a definite point of view with a reasonable well-defined beginning. The earliest of these, which has a strong nondeterministic flavour, is referred to as the statistical movement; the next which is predominantly observational, is referred to as the structural movement, and the most recent (and that which concerns us) is the deterministic movement. For further details of the historical perspective, see Chapman and Tobak (1985).

Although in this chapter, turbulence is dealt with in respect to fluid dynamics, it is important to realize that the problem of turbulence pervades in many other fields. In fact, turbulence has become a general concept, related to many branches of the natural sciences. Hao (1984) points out that terms such as solid state turbulence, chemical turbulence, acoustic turbulence and optical turbulence are emerging into the literature.

The current viewpoint of many scientists is that the key to understanding turbulence may be hidden in the onset mechanism. In the following sections we shall discuss the various hypotheses for the mechanism by which a transition from regular to turbulent motion occurs in fluid systems. Each mechanism, except the earliest by Landau, can be described in finite-dimensional model systems that are investigated numerically. The evidence from real fluid turbulence experiments is not

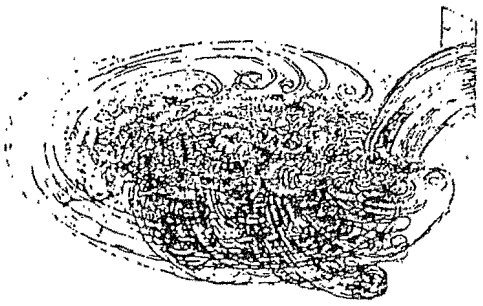

Figure 5.1 Very early observations of turbulence - sketch by Leonardo da Vinci, circa 1500. (Taken from Chapman and Tobak, 1985)

as clear, with some features predicted by each of the mechanisms appearing in different experiments. In some instances, evidence in support of two mechanisms can be found in the same experiment.

At this point it should be made clear, that at this time, chaotic phenomena in dissipative systems are relevant only to the onset mechanism of turbulence, i.e., to the stage of weak turbulence. It has nothing to do with fully developed turbulence. Chaos as we have treated it so far, concerns mainly erratic behaviour in time evolution, whereas turbulence necessarily involves stochasticity in the spatial distribution as well.

Detailed experimental measurements of the velocity flow, temperature distribution etc., near the transition to turbulence have only essentially been made during the last twenty years or so. The onset of turbulence typically occurs rather abruptly, preceded by the observation of one or a few *incommensurate* (not rationally related) frequencies, their harmonics and (sometimes) their subharmonics. Furthermore, real turbulence occurs in three-dimensional space. However, most mathematical models and experimental situations studied so far are confined to finite or low-dimensional geometry. The main experiments in which the above-mentioned observations have been made are Rayleigh-Bénard convection and Circular Couette flow. (see Appendix B)

Hao (1984) points out that fully developed turbulence must involve a great number of fluid motion modes, but the onset of turbulence may stem from the loss of stability of only a few modes. He suggests that finite geometry with dissipation provides the mechanism to suppress many irrelevant modes, and makes the experimental results closer to predictions based on simple theoretical models. We now examine the routes to turbulence.

5.1 THE LANDAU MODEL

The original picture of the transition to turbulence, suggested by Landau (1959), argued that turbulence may be viewed as a hierarchy of instabilities. As a control parameter such as the Reynolds number is increased from zero, a critical value is reached beyond which the first Hopf bifurcation occurs, i.e., a fixed point becomes unstable and an attracting limit cycle is generated. A second application of this argument suggests that at the next Hopf bifurcation the limit cycle becomes unstable (repelling) and an attracting 2-torus is generated around the limit cycle. Thus we have a sequence of Hopf bifurcations with successive flows on a one-torus, two-torus, three-torus etc. If two of the frequencies on a torus are incommensurable, then the motion is called *quasi-periodic*. Landau suggested that as the control parameter is increased from zero, a succession of unstable modes appear and saturate in nonlinear periodic states having frequencies $f_1, f_2, \ldots$, which are incommensurable. One should thus observe the successive appearance of singly periodic, doubly periodic, triply periodic, etc., motion as the parameter is increased. Landau allowed this process to continue infinitely and identified the final state with an infinite number of incommensurable frequencies as fully turbulent. By this reasoning, the motion will have a continuous spectrum only after an infinite number of frequencies have appeared and the motion is truly chaotic.

At present, no reasonable mathematical model which follows the

Landau route to turbulence is known. The most compelling objection against this model is as follows. This route to turbulence requires the successive appearance of new incommensurable frequencies in the power spectrum, which remains discrete all the time as the control parameter is increased. Observed power spectra do not show the necessary sequence of lines and always contain broadband components after either the appearance of two or three (or at most four) incommensurate frequencies or a period-doubling bifurcation cascade. Hence although a few independant modes have been observed in experiments, with as many as four independant modes observed in Couette flow (see Gorman et al (1980)), the generally abrupt transition to an aperiodic system is not consistent with the Landau scenario.

Secondly, there is no mechanism for sensitive dependence on initial conditions in the Landau model. The details of turbulent states however, do depend on initial conditions sensitively. Finally, the Landau model ignores the important physical phenomenon of phase locking (or frequency locking) discussed in section 2.9. In nonlinear systems, new incommensurate frequencies cannot appear infinitely without interacting with each other. Nearby frequencies tend to get locked, which will diminish the number of incommensurable frequencies. Furthermore, it has been shown by Eckman (1981) that a succession of Hopf bifurcations of the Landau type, and indeed multiply periodic motion is nongeneric. This model is now mainly of historical significance. The Landau model is shown schematically in Table 5.1 (a).

5.2 THE RUELLE-TAKENS MODEL

Ruelle and Takens (1971) showed that the Landau route to turbulence is unlikely to occur in nature. They proposed an alternate route in which they adopted the first three Hopf bifurcations of the Landau model, but conjectured that nonlinearities would destroy triply periodic motion leading to the appearance of a strange attractor. The original conjec-

ture required a four-dimensional flow.

i.e., fixed point → limit cycle → 2-torus → 3-torus → strange attractor

A few years later Newhouse et al., (1978) proved that triply periodic motion is generically unstable for a special class of attractor. Hence the scheme was reduced to:

fixed point → limit cycle → 2-torus → strange attractor.

i.e., quasi-periodic motion on a 2-torus may lose stability and give rise to turbulence.

The Ruelle-Takens route to turbulence appears to be fairly consistent with recent hydrodynamical experiments but it is still not very well understood in theoretical models. This model has been studied numerically using a simple two-dimensional map (Curry and Yorke (1978)), and the route listed in Table 5.1 (b) has been observed numerically. As pointed out in Lichtenberg and Lieberman (1982), it is significant that the 14-mode Gälerkin approximation to the Rayleigh-Bénard problem shows, contrary to the three-mode Lorenz system, that chaotic time dependence is proceeded by doubly periodic motion on a two-dimensional surface that is embedded in the 14-dimensional phase space (Curry (1978)).

This model, with some variation in the number of incommensurate frequencies that appear prior to chaos has been observed in both Rayleigh-Bénard convection (see for example, Ahlers and Behringer (1978)) and circular Couette flow (see for example Fenstermacher et al., (1978)).

Figure 5.2, taken from Gollub and Benson (1980), shows five different types of spectra for Rayleigh-Bénard convection, with the Prandtl number $\sigma = 5$. The different types of spectra are as follows:

(i) Top row $\left(\frac{R}{R_c} = 31.0\right)$: The flow is singly periodic. Only f_2 and its second harmonic appear above the instrumental noise.

(ii) Second row $\left(\frac{R}{R_c} = 35.0\right)$: The flow is doubly periodic. Two incommensurate frequencies; f_1 and f_2, their harmonics and various differences appear above instrumental noise.

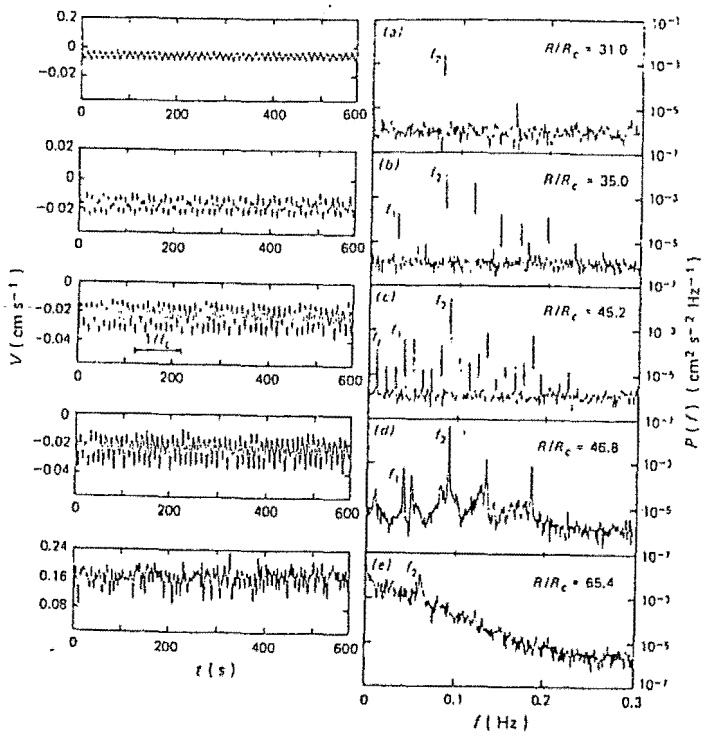

Figure 5.2 Velocity records and corresponding power spectra for Rayleigh-Bénard convection with Prandtl number $\sigma = 5$ and five different heat inputs. (after Gollub and Benson, 1980)

(iii) Third row $\left(\frac{R}{R_c} = 45.2\right)$: Phase locking with $\frac{f_1}{f_2} = \frac{9}{4}$ has occurred and the basic frequency $f_1 = \frac{f_2}{9} = \frac{f_1}{4}$ and its harmonics appear.

(iv) Fourth row $\left(\frac{R}{R_c} = 46.8\right)$: Broadband noise (well above instrumental noise) appears along with f_1 and f_2 and a few of their descendants.

(v) Fifth row $\left(\frac{R}{R_c} = 65.4\right)$: The flow is strongly chaotic.

In a Couette experiment (Gorman et al., (1980)), at least four incommensurate frequencies have been observed, thus indicating that the Ruelle-Takens transition does not always take place after two Hopf bifurcations.

Three-dimensional numerical integration has been carried out on the Boussinesq equations (which govern Rayleigh-Bénard convection) by McLaughlin and Orszag (1982). They used a 16 × 16 × 17 modal expansion with no-slip boundary conditions and $\sigma = 0.71$ (as for air). They obtained results that support the Ruelle-Takens scenario.

This model is probably the most significant in the development of a theory of turbulence. Many people now believe that the problem of turbulence onset can be settled within the framework of the Navier-Stokes equations. Lanford (1981) has compiled an excellent list of the presuppositions entailed by adoption of the Navier-Stokes equations as the framework for understanding turbulence. The Ruelle-Takens model is shown schematically in Table 5.1 (b).

5.3 THE PERIOD-DOUBLING MODEL

The third model of the transition to turbulence we consider is the period-doubling bifurcation sequence of Feigenbaum (1978). The first step is a Hopf bifurcation from a fixed point to a singly periodic orbit with frequency f_1, including its harmonics, as in the Landau and Ruelle-Takens scenarios. The bifurcations which follow are of the pitchfork variety. After the first pitchfork bifurcation, the period of the orbit doubles, and the frequency $\frac{1}{2}f_1$ and higher harmonics are obtained. Further pitchfork bifurcations yield repeated period-doublings that give rise to the frequencies $\frac{1}{4}f_1$, $\frac{1}{8}f_1$, ... etc. This sequence accumulates at a critical value of the parameter. Beyond this we have the onset of broadband noise and chaotic motion associated with a strange attractor. Period-doubling was discussed in section 4.5, where it was shown to have a universal nature. Also, near the accumulation point, the motion is essentially one-dimensional.

Period-doubling has been found in many low-dimensional systems, such as the Rössler system, Hénon map and the Duffing equation. Several experiments on Rayleigh-Bénard convection show period-doubling behaviour and other evidence of universal bifurcation sequences. High-resolution power spectra in Rayleigh-Bénard experiments on water (Gollub et al (1980, Giglio et al (1981)) exhibit a number of period-doublings. The Fourier amplitudes of the fully developed successive subharmonics have also been determined experimentally and compared with Feigenbaum's model.

Feigenbaum's model predicts that, after several bifurcations, the amplitudes of the subharmonics generated at each bifurcation should be 8.2 dB down from those of the preceding bifurcation. This prediction is tested in Figure 5.3 d, where the line drawn through the peaks at $\frac{1}{4}f_1$, $\frac{3}{4}f_1$, ... is found to be approximately 8.2 dB below the line drawn through the peaks at $\frac{1}{2}f_1$ and $\frac{3}{2}f_1$. The preceding patterns typically were reproduced on decreasing $\frac{R}{R_c}$, but the appearance of the incommensurate (with f_2) frequency f^* at $\frac{R}{R_c} = 27.0$ (in Figure 5.3 f) was a significant exception. In another Rayleigh-Bénard experiment in liquid helium (Libchaber and Maurer (1980)), the successive subharmonics f_1, $\frac{1}{2}f_1$, $\frac{1}{4}f_1$, $\frac{1}{8}f_1$ and $\frac{1}{16}f_1$ were observed in the power spectrum of the temperature. The ratio of successive subharmonics gives roughly the constant factor 8.2 dB, in agreement with Feigenbaum theory. Similar experiments have been carried out which do not show these features (Crutchfield and Huberman (1980)). In these instances, the presence of external noise would wash out the finer features of the subharmonic structure, and depending on the experiment, subharmonics may or may not be seen. The period-doubling model is shown schematically in Table 5.1 (c).

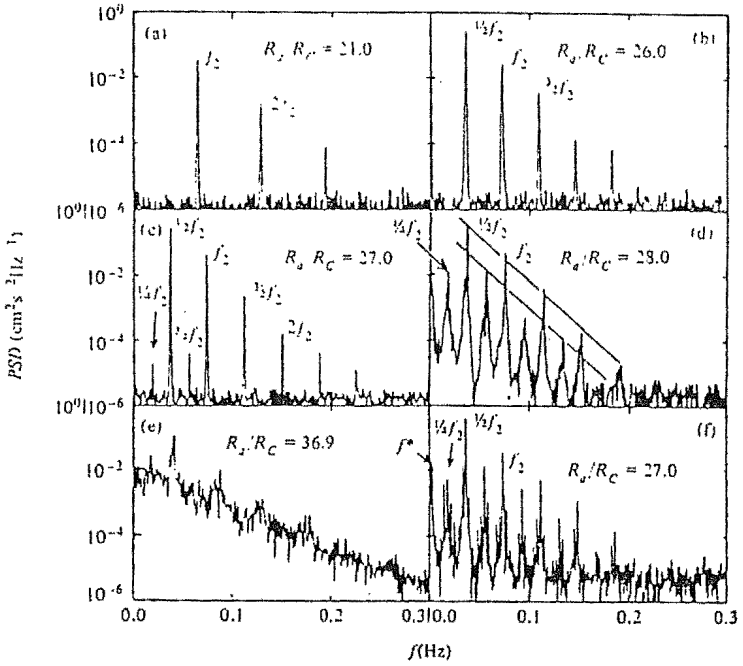

Figure 5.3 Period-doubling sequences in the velocity power spectral density of water in a Rayleigh-Bénard experiment. Note the creation of subharmonics at increasing Rayleigh numbers R_a, the creation of chaotic "bands" in (d) and a "continuous nonperiodic" spectrum in (e). Upon return to the R_a of (c) a second frequency f^* appears in (f). (after Gollub et al, 1980).

5.4 THE INTERMITTENT MODEL

The fourth model for the mechanism of the onset of turbulence, is the model of Pomeau and Manneville (1980). In this model, as the control parameter is increased, a singly periodic orbit becomes intermittently chaotic. The behaviour is associated with a reverse tangent bifurcation that destroys the stability of the periodic orbit. Intermittency has been discussed in section 4.14, where we pointed out that intermittency and period-doubling are in fact twin phenomena. See also Shimada and Nagashima (1979) and Eckmann (1981).

The Lorenz system displays this kind of behaviour in certain parameter ranges (see Pomeau and Manneville (1980)). Intermittent transitions to turbulence have been seen in many experimental systems, including the Rayleigh-Bénard system (Libchaber and Maurer (1980), Gollub

and Benson (1980)), and an experimental study on chemical turbulence (Roux et al (1980)). See Figure 5.4 for Rayleigh-Bénard flow. In both these cases there is an intermittent transition between two states of a bistable system, and it is not clear that this behaviour is described by the Pomeau-Manneville model. This model is shown schematically in Table 5.1 (d).

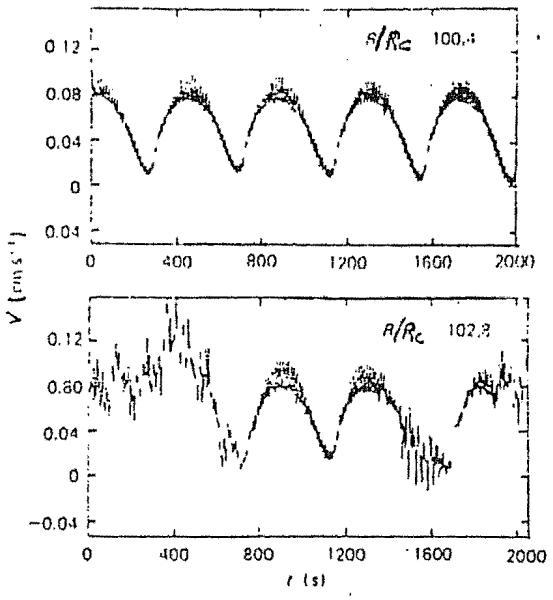

Figure 5.4 Velocity records in Rayleigh-Bénard flow with prandtl number = 5 (Gollub and Benson, 1980).
(a) doubly periodic flow at $\frac{R}{R_c}$ = 100.4;
(b) intermittent (doubly periodic/chaotic) flow at $\frac{R}{R_c}$ = 102.8.
The flow becomes completely chaotic for somewhat larger $\frac{R}{R_c}$.

In concluding this chapter, it is emphasized that no single mechanism for the transition to turbulence exists. We are now facing a situation of, all routes leading to turbulence. If, for example, a system does show period-doubling, then one can predict the rate of doubling as the parameter changes. At this time there is no way to tell in advance which systems will show period-doubling. The most well-studied models are those of Feigenbaum and Pomeau and Manneville.

Model	Mechanism								
(a) Landau	Stationary point	⟶ (Hopf)	Singly periodic orbit	⟶ (Hopf)	Doubly periodic orbit	⟶ (Hopf)	Triply periodic orbit	⇢ (Hopf)	Turbulent motion
(b) Ruelle–Takens–Newhouse	Stationary point	⟶ (Hopf)	Singly periodic orbit	⟶ (Hopf)	Doubly periodic orbit	⟶	Strange attractor		
(c) Feigenbaum	Stationary point	⟶ (Hopf)	Singly periodic orbit (period T)	⟶ (pitchfork)	Singly periodic orbit (period $2T$)	⟶ (pitchfork)	Singly periodic orbit (period $4T$)	⇢ (pitchfork)	Strange attractor
(d) Pomeau–Manneville	Stationary point	⟶ (Hopf)	Singly periodic orbit	⟶ Reverse tangent bifurcation	Intermittent chaotic motion				

Table 5.1 Models for the transition to fluid turbulence and their mechanisms. (after Lichtenberg and Lieberman, 1982)

CHAPTER 6

A FOURIER SERIES METHOD

In this section, we shall discuss a Fourier series method through which it is possible to obtain an analytical Fourier series expression, to any required degree of approximation, of the phase space trajectories for a particular value of the parameter. We shall illustrate this method by carrying out the required calculations for the spherical pendulum model of Miles (1984 b). Let us first establish the system with which we shall illustrate the procedure.

6.1 THE SPHERICAL PENDULUM

Miles (1984 b) studied the weakly nonlinear response of a damped spherical pendulum to the planar displacement $\varepsilon\ell \cos \omega t (\varepsilon << 1)$ of its point of suspension. The two control parameters in the problem are:

$$\alpha = 2\delta\varepsilon^{-\frac{2}{3}}\left(\frac{\omega_0}{\omega}\right) \tag{6.1}$$

and

$$\gamma = \varepsilon^{-\frac{2}{3}}(\omega^2 - \omega_0^2)/\omega^2 \tag{6.2}$$

where δ is the damping ratio (prescribed damping/critical damping for small oscillations), ε is the ratio of the maximum displacement of the point of suspension to the length of the pendulum, ω is the forcing frequency and ω_0 is the natural frequency. It is assumed that $0 < \varepsilon << 1$ (weak nonlinearity), $\alpha = 0(1)$ and $\gamma = 0(1)$. The control parameter α measures damping and the other control parameter γ, measures the proximity to resonance. Let the length of the pendulum be ℓ.

The projection of the pendulum-bob trajectory on a horizontal (x,y) plane is described by:

$$x = \varepsilon^{\frac{1}{3}}\ell\,(p_1(\tau)\cos\theta + q_1(\tau)\sin\theta) \tag{6.3a}$$

$$y = \varepsilon^{\frac{1}{3}}\ell\,(p_2(\tau)\cos\theta + q_2(\tau)\sin\theta) \tag{6.3b}$$

where

$$\theta = \omega t \tag{6.4}$$

and

$$\tau = (\tfrac{1}{2})\varepsilon^{\frac{2}{3}}\omega t\,. \tag{6.5}$$

The trajectory described by these equations is, in general, a slowly rotating ellipse with slowly varying axes. The quantities p_1, p_2, q_1, q_2 are slowly varying coordinates in a four-dimensional phase space. The $p_1 - p_2 - q_1 - q_2$ phase-space trajectories are Poincaré maps of the $x - \dot{x} - y - \dot{y} - \theta$ trajectories at $\theta = 0 \pmod{2\pi}$. The $p_1 - p_2$ projections (which are the projections of most interest, since they yield the most information about the system) are maps of the x - y pendulum trajectories at the periodically spaced instants: $\omega t = 0 \pmod{2\pi}$. By making various assumptions (see Miles (1984 b)), we are led to the following system of four nonlinear nonautonomous ODE's:

$$\dot{p}_1 = -\alpha p_1 - (\gamma + \tfrac{1}{8}E)q_1 - \tfrac{3}{4}Mp_2 \tag{6.6a}$$

$$\dot{p}_2 = -\alpha p_2 - (\gamma + \tfrac{1}{8}E)q_2 + \tfrac{3}{4}Mp_1 \tag{6.6b}$$

$$\dot{q}_1 = -\alpha q_1 + (\gamma + \tfrac{1}{8}E)p_1 - \tfrac{3}{4}Mq_2 + 1 \tag{6.6c}$$

$$\dot{q}_2 = -\alpha q_2 + (\gamma + \tfrac{1}{8}E)p_2 + \tfrac{3}{4}Mq_1 \tag{6.6d}$$

where the dots denote differentiation by τ. The quantities E and M are defined as:

$$E = p_1^2 + p_2^2 + q_1^2 + q_2^2 \tag{6.7}$$

$$M = p_1 q_2 - p_2 q_1 \tag{6.8}$$

where E is a measure of the energy of the pendulum and M is a measure of the angular momentum. The divergence of (6.6) is:

$$\Delta \equiv \frac{\partial \dot{p}_1}{\partial p_1} + \frac{\partial \dot{p}_2}{\partial p_2} + \frac{\partial \dot{q}_1}{\partial q_1} + \frac{\partial \dot{q}_2}{\partial q_2} = -4\alpha \tag{6.9}$$

From this we can see that an element of volume in the phase-space contracts like $\exp(-4\alpha\tau)$. Every trajectory must be confined to a limiting subspace of dimension less than four. Miles (1974b) shows that in fact every trajectory ultimately must lie in $R < \frac{1}{\alpha}$; where $R^2 = E$. Another problem which is of some importance on which is analogous to this is that of free-

surface motion of a liquid in a moving circular tank. See Hutton (1963) for details. We now have established the system with which we shall work.

6.2 THE METHOD

The basic idea behind the method under discussion is to approximate the quantities p_1, p_2, q_1, and q_2 by Fourier series expansions and then refine the coefficients by an iterative procedure. (Newton's method) Let us expand p_1, p_2, q_1 and q_2 in Fourier series:

$$p_1 = a_{10} + \sum_{k=1}^{K} (a_{1k} \cos kft + b_{1k} \sin kft) \tag{6.10a}$$

$$p_2 = a_{20} + \sum_{k=1}^{K} (a_{2k} \cos kft + b_{2k} \sin kft) \tag{6.10b}$$

$$q_1 = a_{30} + \sum_{k=1}^{K} (a_{3k} \cos kft + b_{3k} \sin kft) \tag{6.10c}$$

$$q_2 = a_{40} + \sum_{k=1}^{K} (a_{4k} \cos kft + b_{4k} \sin kft) \tag{6.10d}$$

where K is the number of the largest harmonic we wish to work with, $t = \tau$ in (6.5) and $f = \omega$. The quantity ft is fixed.

We can also rewrite equations (6.6) as follows:

$$F_1 = \dot{p}_1 + \alpha p_1 + (\gamma + \tfrac{1}{8} E) q_1 + \tfrac{3}{4} M p_2 \tag{6.11a}$$

$$F_2 = \dot{p}_2 + \alpha p_2 + (\gamma + \tfrac{1}{8} E) q_2 - \tfrac{3}{4} M p_1 \tag{6.11b}$$

$$F_3 = \dot{q}_1 + \alpha q_1 - (\gamma + \tfrac{1}{8} E) p_1 + \tfrac{3}{4} M q_2 - 1 \tag{6.11c}$$

$$F_4 = \dot{q}_2 + \alpha q_2 - (\gamma + \tfrac{1}{8} E) p_2 - \tfrac{3}{4} M q_1 \tag{6.11d}$$

where F_1, F_2, F_3 and F_4 are functions of a_{ij} $(i = 1,4;\ j = 0,K)$, $b_{mn} (m = 1,4;\ n = 1,K)$ and f. The quantities F_1, F_2, F_3 and F_4 have the following Fourier expansions:

$$F_1 = F_{10} + \sum_{k=1}^{K} (F_{1k} \cos kft + G_{1k} \sin kft) \tag{6.12a}$$

$$F_2 = F_{20} + \sum_{k=1}^{K} (F_{2k} \cos kft + G_{2k} \sin kft) \tag{6.12b}$$

$$F_3 = F_{30} + \sum_{k=1}^{K} (F_{3k} \cos kft + G_{3k} \sin kft) \tag{6.12c}$$

$$F_4 = F_{40} + \sum_{k=1}^{K} (F_{4k} \cos kft + G_{4k} \sin kft) . \tag{6.12d}$$

Now the unknowns we wish to find are the Fourier coefficients: $a_{10},\ldots, a_{1K}, a_{20},\ldots, a_{2K}, a_{30},\ldots, a_{3K}, a_{40},\ldots, a_{4K}, b_{11},\ldots, b_{1K}, b_{21},\ldots, b_{2K}, b_{31},\ldots, b_{3K}, b_{41},\ldots, b_{4K}$, and f, which amounts to $4(K+1) + 4K + 1 = 8K + 5$ unknowns. We have the following nonlinear equations to solve: $F_{10} = 0,\ldots, F_{1K} = 0, F_{20} = 0,\ldots, F_{2K} = 0, F_{30} = 0, \ldots, F_{3K} = 0, F_{40},\ldots, F_{4K} = 0, G_{11} = 0,\ldots, G_{1K} = 0, G_{21} = 0,\ldots, G_{2K} = 0, G_{31} = 0,\ldots, G_{3K} = 0, G_{41} = 0,\ldots, G_{4K} = 0$; which amounts to $4(K+1), 4K = 8K + 4$ equations. Thus we have an inconsistent system with more unknowns than equations. Without any loss of generality we can fix one coefficient, say $B = b_{11} = 0$, and then have a system of $8K + 5$ equations to solve in $8K + 5$ unknowns. The nonlinear system we then have to solve is:

$$
\begin{aligned}
&F_{10}(a_{10},\ldots, a_{1K},\ldots, a_{4K}, b_{11},\ldots, b_{1K},\ldots, b_{4K}, f, \alpha, \gamma) = 0 \\
&\vdots \qquad\qquad\qquad\qquad\qquad\qquad\qquad\qquad\qquad\qquad\qquad\qquad \vdots \\
&F_{4K}(a_{10},\ldots, a_{1K},\ldots, a_{4K}, b_{11},\ldots, b_{1K},\ldots, b_{4K}, f, \alpha, \gamma) = 0 \\
&G_{11}(a_{10},\ldots, a_{1K},\ldots, a_{4K}, b_{11},\ldots, b_{1K},\ldots, b_{4K}, f, \alpha, \gamma) = 0 \\
&\vdots \qquad\qquad\qquad\qquad\qquad\qquad\qquad\qquad\qquad\qquad\qquad\qquad \vdots \\
&G_{4K}(a_{10},\ldots, a_{1K},\ldots, a_{4K}, b_{11},\ldots, b_{1K},\ldots, b_{4K}, f, \alpha, \gamma) = 0 \\
&B = b_{11} = 0 \ . \qquad\qquad\qquad\qquad\qquad\qquad\qquad\qquad\qquad\qquad\qquad\qquad (6.13)
\end{aligned}
$$

For Newton's method, the Jacobian matrix of derivatives will have to be updated after each iteration. It will take the following form:

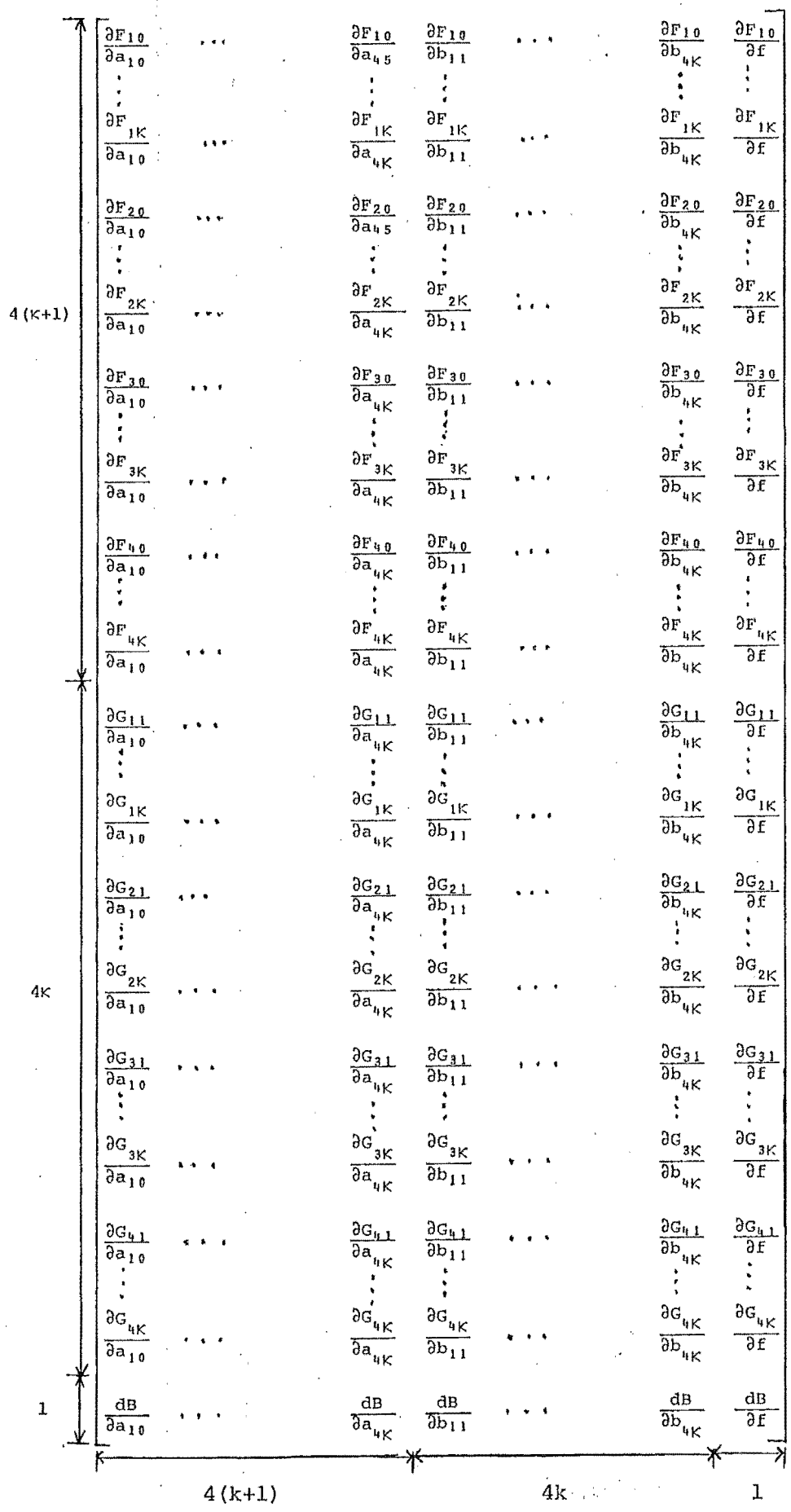

As one can see, there are three main types of quantity required to update the Jacobian. We shall look at how to calculate each type of expression.

(i) Expressions of the form $\frac{dB}{da_{ij}}$, $\frac{dB}{db_{ij}}$ and $\frac{dB}{df}$.

Now $\frac{dB}{da_{ij}} = 0$ $(i = 1,4 \quad j = 0,K)$, $\frac{dB}{db_{ij}} = 0$ $(i = 1,4 \quad j = 1,K \quad i \neq j =$

$\frac{dB}{db_{11}} = 1$ and $\frac{dB}{df} = 0$.

These entries fill the $(8K+5)$th row of the Jacobian. This row consists of all zeros except in the $(4K+5)$th position which contains a one.

(ii) We need to find expressions of the form $\frac{dF_{ij}}{df}$ and $\frac{dG_{ij}}{df}$, which fill the $(8K+5)$th column of the Jacobian.

example: $F_1 = \dot{p}_1 + \alpha p_1 + (\gamma + \frac{1}{8} E) q_1 + \frac{3}{4} M p_2$. (6.11a)

From this we can calculate the quantity:

$$\frac{dF_1}{df} = \frac{d\dot{p}_1}{df} + \alpha \frac{dp_1}{df} + \gamma \cdot \frac{dq_1}{df} + \frac{1}{8} \frac{d}{df} (E.q_1) + \frac{3}{4} \frac{d}{df} (M.p_2).$$

The quantity ft is fixed in our calculations and so the terms cos kft and sin kft are zero under differentiation by f. From the current value of the coefficients for the Fourier expansions for p_1, p_2, q_1 and q_2 we can evaluate:

$$\dot{p}_1 = \sum_{k=1}^{K} (- kfa_{1k} \sin kft + kfb_{1k} \cos kft) \quad (6.14a)$$

$$\dot{p}_2 = \sum_{k=1}^{K} (- kfa_{2k} \sin kft + kfb_{2k} \cos kft) \quad (6.14b)$$

$$\dot{q}_1 = \sum_{k=1}^{K} (- kfa_{3k} \sin kft + kfb_{3k} \cos kft) \quad (6.14c)$$

$$\dot{q}_2 = \sum_{k=1}^{K} (- kfa_{4k} \sin kft + kfb_{4k} \cos kft) \quad (6.14d)$$

and $$\frac{dF_1}{df} = \frac{d\dot{p}_1}{df} = \sum_{k=1}^{K} (- ka_{1k} \sin kft + kb_{1k} \cos kft) \quad (6.15)$$

It is easy to see that similar expressions exist for $\frac{dF_2}{df}$, $\frac{dF_3}{df}$ and $\frac{dF_4}{df}$.

We also know that

$$F_1 = F_{10} + \sum_{k=1}^{K} (F_{1k} \cos kft + G_{1k} \sin kft) \qquad (6.12a)$$

From this we calculate:

$$\frac{\partial F_1}{\partial f} = \frac{\partial F_{10}}{\partial f} + \sum_{k=1}^{K} \left(\frac{\partial F_{1k}}{\partial f} \cos kft + \frac{\partial G_{1k}}{\partial f} \sin kft \right) . \qquad (6.15)'$$

We now have two expressions: (6.15) and (6.15)', for $\frac{\partial F_1}{\partial f}$.

If we have the values of $\frac{\partial F_1}{\partial f}$ at various ft values, then we can use a fast Fourier transform subroutine (FFT) to calculate the coefficients of the Fourier expansion of $\frac{\partial F_1}{\partial f}$ through these points. If we have the current values of a_{1k} and b_{1k} $(k = 1,K)$, we can then calculate $\frac{\partial F_1}{\partial f}$ at various ft values using (6.15). These pairs of points yield the Fourier coefficients in (6.15)', after an application of the FFT routine. The Fourier coefficients from (6.15)' however, correspond to the values $\frac{\partial F_{10}}{\partial f}$, $\frac{\partial F_{1k}}{\partial f}$ $(k = 1,K)$ and $\frac{\partial G_{1k}}{\partial f}$ $(k = 1,K)$. The other terms of this form can be found in precisely the same manner. A FFT routine from Conte and de Boor (1980) is given in Appendix C.

(iii) We need to find the expressions $\frac{\partial F_{ij}}{\partial a_{mn}}$, $\frac{\partial F_{ij}}{\partial b_{mn}}$, $\frac{\partial G_{ij}}{\partial a_{mn}}$ and $\frac{\partial G_{ij}}{\partial b_{mn}}$.

These are relatively simple to calculate from (6.11 a-d)

example: $F_1 = \dot{p}_1 + \alpha p_1 + (\gamma + \frac{1}{8}\varepsilon) q_1 + \frac{3}{4} M p_2$

$$\frac{\partial F_1}{\partial a_{1k}} = \frac{\partial \dot{p}_1}{\partial a_{1k}} + \alpha \frac{\partial p_1}{\partial a_{1k}} + \gamma \frac{\partial q_1}{\partial a_{1k}} + \frac{1}{8} \frac{\partial}{\partial a_{1k}} (E.q_1) + \frac{3}{4} \frac{\partial}{\partial a_{1k}} (M.p_2)$$

$$= -kf \sin kft + \alpha \cos kft + \frac{1}{8} E . \frac{\partial q_1}{\partial a_{1k}} + \frac{1}{8} q_1 . \frac{\partial E}{\partial a_{1k}} + \frac{3}{4} M . \frac{\partial p}{\partial a_{1k}} + \frac{3}{4} . p_2 . \frac{\partial M}{\partial a_{1k}}$$

$$= -kf \sin kft + \alpha \cos kft + \frac{1}{8} q_1 . 2p_1 . \frac{\partial p_1}{\partial a_{1k}} + \frac{3}{4} p_2 q_2 \frac{\partial p_2}{\partial a_{1k}}$$

$$= -kf \sin kft + \alpha \cos kft + \frac{1}{4} q_1 p_1 \cos kft + \frac{3}{4} p_2 q_2 \cos kft$$

$$= -kf \sin kft + (\alpha + \frac{1}{4} q_1 p_1 + \frac{3}{4} p_2 q_2) \cos kft .$$

See Table 6.1 for the expressions for these derivative terms. With this information in hand, we can update the Jacobian matrix each iteration; once we have the current Fourier expansions for p_1, p_2, q_1 and q_2.

$k = 0, K$	$k = 1, K$
$\frac{\partial F_1}{\partial a_{1k}} = -kf \sin ft + (\alpha + \frac{1}{4}p_1q_1 + \frac{3}{4}p_2q_2)\cos kft$	$\frac{\partial F_1}{\partial b_{1k}} = kf \cos kft + (\alpha + \frac{1}{4}p_1q_1 + \frac{3}{4}p_2q_2)\sin kft$
$\frac{\partial F_1}{\partial a_{2k}} = (-\frac{1}{2}q_1p_2 + \frac{3}{4}M)\cos kft$	$\frac{\partial F_1}{\partial b_{2k}} = (-\frac{1}{2}q_1p_2 + \frac{3}{4}M)\sin kft$
$\frac{\partial F_1}{\partial a_{3k}} = (\frac{1}{8}E + \frac{1}{4}q_1^2 - \frac{3}{4}p_2^2 + \gamma)\cos kft$	$\frac{\partial F_1}{\partial b_{3k}} = (\frac{1}{4}q_1^2 + \frac{1}{8}E - \frac{3}{4}p_2^2 + \gamma)\sin kft$
$\frac{\partial F_1}{\partial a_{4k}} = (\frac{1}{4}q_1q_2 + \frac{3}{4}p_1p_2)\cos kft$	$\frac{\partial F_1}{\partial b_{4k}} = (\frac{1}{4}q_1q_2 + \frac{3}{4}p_1p_2)\sin kft$
$\frac{\partial F_2}{\partial a_{1k}} = (-\frac{1}{2}p_1q_2 - \frac{3}{4}M)\cos kft$	$\frac{\partial F_2}{\partial a_{1k}} = (-\frac{1}{2}p_1q_2 - \frac{3}{4}M)\sin kft$
$\frac{\partial F_2}{\partial a_{2k}} = -kf \sin kft + (\alpha + \frac{1}{4}q_2p_2 + \frac{3}{4}p_1q_1)\cos kft$	$\frac{\partial F_2}{\partial b_{2k}} = kf \cos kft + (\alpha + \frac{1}{4}p_2q_2 + \frac{3}{4}p_1q_1)\sin kft$
$\frac{\partial F_2}{\partial a_{3k}} = (+q_1q_2 + \frac{3}{4}p_1p_2)\cos kft$	$\frac{\partial F_2}{\partial b_{3k}} = (\frac{1}{4}q_1q_2 + \frac{3}{4}p_1p_2)\sin kft$
$\frac{\partial F_2}{\partial a_{4k}} = (\frac{1}{8}E + \frac{1}{4}q_2^2 - \frac{3}{4}p_1^2 + \gamma)\cos kft$	$\frac{\partial F_2}{\partial b_{4k}} = (\frac{1}{8}E + \frac{1}{4}q_2^2 - \frac{3}{4}p_1^2 + \gamma)\sin kft$
$\frac{\partial F_3}{\partial a_{1k}} = (-\frac{1}{4}p_1^2 - \frac{1}{8}E + \frac{3}{4}q_2^2 - \gamma)\cos kft$	$\frac{\partial F_3}{\partial b_{1k}} = (-\frac{1}{4}p_1^2 - \frac{1}{8}E + \frac{3}{4}q_2^2 - \gamma)\sin kft$
$\frac{\partial F_3}{\partial a_{2k}} = (-\frac{1}{4}p_1p_2 - \frac{3}{4}q_1q_2)\cos kft$	$\frac{\partial F_3}{\partial b_{2k}} = (-\frac{1}{4}p_1p_2 - \frac{3}{4}q_1q_2)\sin kft$
$\frac{\partial F_3}{\partial a_{3k}} = -k \sin kft + (\alpha - \frac{1}{4}p_1q_1 - \frac{3}{4}q_2p_2)\cos kft$	$\frac{\partial F_3}{\partial b_{3k}} = kf \cos kft + (\alpha - \frac{1}{4}p_1q_1 - \frac{3}{4}q_2p_2)\sin kft$
$\frac{\partial F_3}{\partial a_{4k}} = (\frac{1}{2}q_2p_1 + \frac{3}{4}M)\cos kft$	$\frac{\partial F_3}{\partial b_{4k}} = (\frac{1}{2}p_1q_2 + \frac{3}{4}M)\sin kft$
$\frac{\partial F_4}{\partial a_{1k}} = (-\frac{1}{4}p_1p_2 - \frac{3}{4}q_1q_2)\cos kft$	$\frac{\partial F_4}{\partial b_{1k}} = (-\frac{1}{4}p_1p_2 - \frac{3}{4}q_1q_2)\sin kft$
$\frac{\partial F_4}{\partial a_{2k}} = (-\frac{1}{4}p_2^2 - \frac{1}{8}E + \frac{3}{4}q_1^2 - \gamma)\cos kft$	$\frac{\partial F_4}{\partial b_{2k}} = (-\frac{1}{8}E - \frac{1}{4}p_2^2 + \frac{3}{4}q_1^2 - \gamma)\sin kft$
$\frac{\partial F_4}{\partial a_{3k}} = (\frac{1}{2}p_2q_1 - \frac{3}{4}M)\cos kft$	$\frac{\partial F_4}{\partial b_{3k}} = (\frac{1}{2}p_2q_1 - \frac{3}{4}M)\sin kft$
$\frac{\partial F_4}{\partial a_{4k}} = -kf \sin kft + (\alpha - \frac{1}{4}p_2q_2 - \frac{3}{4}q_1p_1)\cos kft$	$\frac{\partial F_4}{\partial b_{4k}} = kf \cos kft + (\alpha - \frac{1}{4}p_2q_2 - \frac{3}{4}p_2q_2)\sin kft$

Table 6.1 Expressions for elements of the Jacobian matrix used with Newton's method applied to (6.11 a-d).

For Newton's method to be applied to a system, we require one further piece of information. We need to find a functional update after each iteration, i.e., find $F_{10}, F_{11}, \ldots G_{11}, \ldots$ etc. using the most recent values of p_1, p_2, q_1 and q_2. The updates can be found by substituting the current values of p_1, p_2, q_1 and q_2 into (6.11 a-d) and finding F_1, F_2, F_3 and F_4 at the various ft values. By applying a FFT and equating coefficients with (6.12 a-d), we find the current values of $F_{10}, F_{11}, \ldots, G_{11}, \ldots$ etc.

After calculating initial expressions for p_1, p_2, q_1 and q_2, we can refine the Fourier coefficients by using Newton's method. In practice one takes m data points, i.e., $ft = j + (i-1) \cdot \frac{2\pi}{(m-1)}$ (6.16) where j is a starting point chosen sufficiently large to avoid transient behaviour, and i varies from $i = 1$ to $i = m$. One finds the initial values of the Fourier coefficients for series expansions of p_1, p_2, q_1 and q by applying a FFT routine to pairs of points obtained by time-stepping. The pairs of points just mentioned can be found effectively by using the system of equations [(6.6)a-d)], the collection of ft values (m equally spaced points) and by applying a Runge-kutta subroutine to these points. For example, one can use the subroutine Dverk, which is a Runge-kutta subroutine based on Verner's fifth and sixth order pair of formulas for finding approximations to the solution of a system of first order ODE's with initial conditions. At this point, we have values on the curve we are attempting to approximate by a Fourier series.

We can now translate the ft values by an appropriate shift to ensure the condition $b_{11} = 0$. Introduce the translation by ft_0 by considering p_1 as follows:

$$a_{1k} \cos k(ft - ft_0) + b_{1k} \sin k(ft - ft_0) = a'_{1k} \cos kft + b'_{1k} \sin kft \quad (k=1,K) \tag{6.17}$$

and $a'_{10} = a_{10}$. We want $b'_{11} = 0$ or:

$$a_{11} \cos(ft - ft_0) + b_{11} \sin(ft - ft_0) = a'_{11} \cos kft + b'_{11} \sin kft .$$

Now expanding the left hand side and equating coefficients with the right hand side we find:

$$b_{11}' = a_{11} \sin kft_0 - b_{11} \cos kft_0 = 0$$

$$\text{or} \quad ft_0 = \tan^{-1} \frac{b_{11}}{a_{11}} \tag{6.18}$$

Now relationships between the old and modified coefficients can be established by the method just shown. For example

$$a_{1k}' = a_{1k} \cos kft_0 + b_{1k} \sin kft_0$$

$$b_{1k}' = - a_{1k} \sin kft_0 + b_{1k} \cos kft_0 . \tag{6.19}$$

Similar relationships can be established for the remaining coefficients. At this point we have the system set up with initial values so that Newton's method can now be applied. A subroutine can be found which performs all the steps of this procedure and applies damping when necessary.

Once this procedure has been applied, we have analytical Fourier series expansions for p_1, p_2, q_1 and q_2. The parameters α and γ can be varied, and p_1 and p_2 calculated by this technique. This approach has an advantage over time-stepping in that one can observe an almost continuous transition from one phase-space diagram to another by slowly varying the parameter near the bifurcation point. The bifurcation structure can be seen in Miles (1984b). The bifurcation points can be obtained from (6.6). Figure 6.1 from Miles (1984b) shows the period-doubling bifurcations in the phase plane and the transition to chaos.

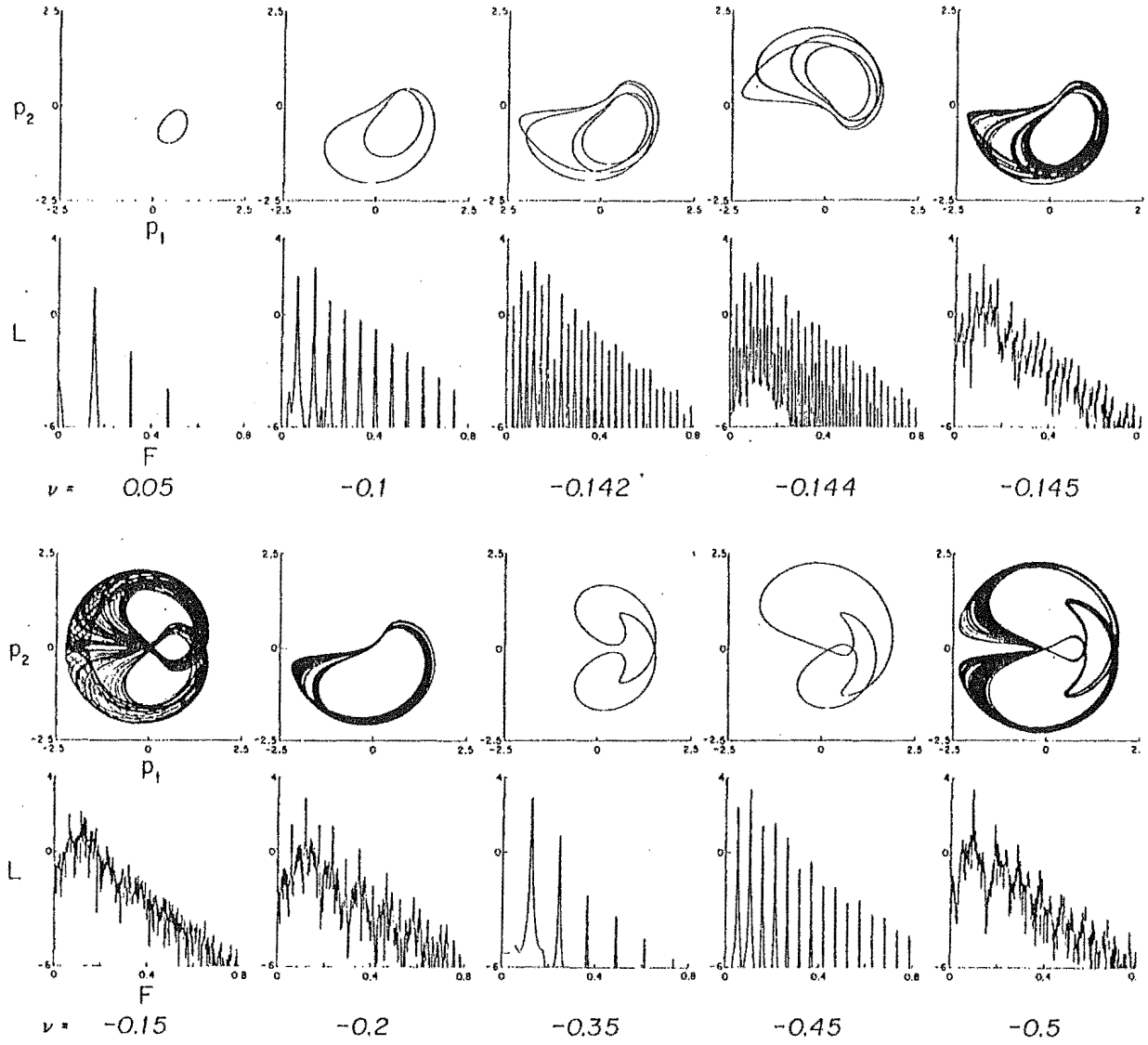

Figure 6.1 Phase plane ($p_1 - p_2$) trajectories and power spectra ($L \equiv \log_{10} p$ vs f) for $\alpha = 0.25$ and $\gamma = 0.05, -0.10, -0.142, -0.144, -0.145, -0.15, -0.20, -0.35, -0.45$, and -0.50. The initial conditions are $(p_1, q_1, p_2, q_2) = (0,0,0,1)$ except for $\gamma = 0.144$ where they were taken as $(0,0,1,0)$ in order to illustrate the reflection $(p_2, q_2) \rightarrow (p_2, q_2)$. After Miles, 1984b)

6.3 CONCLUDING REMARKS

The theory discussed in this dissertation, which has largely been developed during the last quarter century or so, forms a coherent theory which describes a great deal about the behaviour of solutions of a large class of differential equations (describing the evolution of dissipative dynamical systems). The correlations between the theoretical models and the experimental observations are excellent to date. One reservation which should be kept in mind is described in Miles (1984). He points out that these models lack predictive power. They do not provide apriori predic-

tions; which is a quality necessary of a good scientific model. There is a substantial amount of literature on chaos in dissipative dynamical systems, and research is still very active and proving fruitful, with articles on chaos still featuring frequently in the current literature.

APPENDIX A

CONTRACTION OF PHASE-SPACE VOLUME

The following derivation is taken from Lichtenberg and Lieberman (1982). We calculate the rate of change of a small rectangular volume $\Delta\tau$ about $\underset{\sim}{x}_0$. Write $\Delta\tau$ as a product

$$\Delta\tau(\underset{\sim}{x}_0, t) = \prod_i \Delta x_i \tag{1}$$

where:

$$\Delta x_i(\underset{\sim}{x}_0, t) = \frac{\partial x_i(\underset{\sim}{x}_0, t)}{\partial x_{i_0}} \Delta x_{i_0} . \tag{2}$$

The rate of change of $\Delta\tau$ is:

$$\Lambda(x) \equiv \frac{1}{\Delta\tau}\frac{\partial(\Delta\tau)}{\partial t} = \sum_i \frac{1}{\Delta x_i}\frac{\partial(\Delta x_i)}{\partial t} . \tag{3}$$

From (2) we have:

$$\frac{\partial(\Delta x_i)}{\partial t} = \frac{\partial}{\partial x_{0_i}}\frac{\partial x_i(\underset{\sim}{x}_0, t)}{\partial t}\Delta x_{i_0} . \tag{4}$$

Using $\frac{d\underset{\sim}{x}}{dt} = \underset{\sim}{V}(\underset{\sim}{x})$, with $\frac{dx_i}{dt} = \frac{\partial x_i(\underset{\sim}{x}_0, t)}{t}$ in (4) and evaluating near $t = 0$, we obtain from (3), the instantaneous rate of change of the volume as:

$$\Lambda = \sum_i \frac{dV}{dx_i} = \text{div } V . \tag{5}$$

The rate of change of volume is a local quantity, depending on $\underset{\sim}{x}(t)$ and may be positive (expanding) or negative (contracting). However, what we mean here by a dissipative system is that, averaged over an orbit, the volume must contract. Writing the average contraction rate as:

$$\Lambda_0(x_0) = \lim_{t\to\infty}\frac{1}{t}\ell n\left|\frac{\Delta\tau(\underset{\sim}{x}_0, t)}{\Delta\tau(\underset{\sim}{x}_0, 0)}\right| \tag{6}$$

we must have $\Lambda_0 = 0$ for all $\underset{\sim}{x}_0$.

For an N-dimensional map, the local volume $\Delta\tau$ contracts by a factor $|\det M(x)|$ for each iteration, where M is the Jacobian matrix of the map. This factor represents a rate of volume contraction of:

$$\Lambda(x) = \frac{1}{\Delta\tau}\frac{\partial(\Delta\tau)}{\partial n} = \ell n\,|\det M(x)| \tag{7}$$

where n is the iteration number. Averaging this contraction rate along an orbit as in (6), we obtain $\Lambda_0(\underset{\sim}{x}_0)$.

Not much is known about general dissipative systems, where the dependance of Λ on x is arbitrary. For many of the problems that have been studied,

$$\Lambda(\underset{\sim}{x}) = - c \tag{8}$$

where c is a positive constant, expressing the fact that in these systems the volume uniformly contracts everywhere in the phase-space. Obviously $\Lambda_0 = - c$ for such systems.

APPENDIX B

COUETTE FLOW

The following theory is taken from Marsden and McCracken (1976). A viscous, incompressible, homogeneous fluid fills the space between two long, coaxial cylinders which are rotating. For example they may rotate in opposite directions with frequency ω. see Figure (a).

For small values of ω, the flow is horizontal, laminar and stationary. If the frequency is increased beyond some value ω_0, the fluid breaks up into what are called Taylor cells. See Figure (b). Taylor cells are also a stationary solution of the Navier-Stokes equations. For larger values of ω, bifurcations to periodic, doubly periodic and more complicated solutions may take place. See Figure (c). For still larger values of ω, the structure of the Taylor cells becomes more complex and eventually breaks down completely and the flow becomes turbulent.

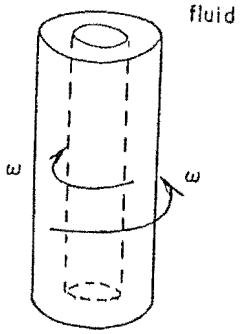

Figure (a)

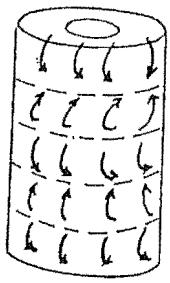

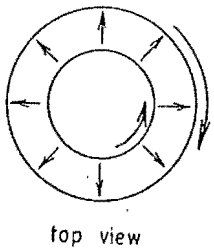

Figure (b) above, Figure (c) below

APPENDIX C: FAST FOURIER TRANSFORM SUBROUTINE

(from Conte and de Boor, 1980)

```
c       ------------------------------------------------------------------
        subroutine fft(z1,z2,inzee,pt)
constructs the discrete fourier transform of z1 (or z2) in the cooley-tukey
c       way,but with a twist.
        integer inzee,n,after,before,next,nextmx,now,prime(12),pt
        complex*16 z1(pt),z2(pt)
c******     i n p u t    ******
c  z1,z2 complex n-vectors
c  n=length of z1 and z2
   inzee integer indicating whether z1 or z2 is to be transformed
c      =1 , transform z1
c      =2 , transform z2
c****** work areas ******
c  z1 , z2 are both used as work arrays
c****** o u t p u t ******
c  z1 or z2 contains the desired transform (in the correct order)
c  inzee  integer indicating whether z1 or z2 contains the transform.
c      =1 , transform is in z1
c      =2 , transform is in z2
c****** m e t h o d ******
c       the integer n is divided into its prime factors (up to a point)
c       for each factor p , the p-transform of appropriate p-subvectors
c       of z1 (or z2) is calculated in fftstp and stored in a suitable way
c       in z1 (or z2).details in conte/deboor p282.
c
        data nextmx,prime / 12,2,3,5,7,11,13,17,19,23,29,31,37/
        n=pt
        after=1
        before=n
        next=1
c
 10     if ((before/prime(next))*prime(next) .lt. before) then
        next=next+1
        if(next.le.nextmx) then
                                goto 10
        else
            now=before
            before=1
        end if
        else
            now=prime(next)
           before= before/prime(next)
        end if
c
        if(inzee.eq.1) then
           call fftstp(z1,after,now,before,z2)
        else
           call fftstp(z2,after,nov,before,z1)
        end if
        inzee=3-inzee
        if(before.eq.1)                         return

        after=after*now
                                                goto 10
        end
c
c
        subroutine fftstp(zin,after,now,before,zout)
called in fft.
carries out one step of the fast fourier transform.
        integer after,before,nov,  ia,ib,in,k
        double precision angle,twopi
        complex*16 zin(after,before,now) , zout(after,now,before),
     +           arg,omega,value
        data twopi/6.2831 85307 17958 64769d0/
        angle=twopi/real(now*after)
        omega=cmplx(cos(angle),-sin(angle))
        arg=cmplx(1.,0.)
        do 100 k=1,now
           do 90 ia=1,after
              do 80 ib=1,before
                 value=zin(ia,ib,now)
                 do 70 in=now-1,1,-1
 70                 value=value*arg+zin(ia,ib,in)
 80              zout(ia,k,ib)=value
 90           arg=arg*omega
 100    continue
                                  return
        end
```

ACKNOWLEDGEMENTS

I should like to record my thanks and gratitude to my supervisor Dr. P.J. Bryant for his suggestion of this interesting topic and for his guidance during my work on this subject. I would also like to thank Mrs. Ann Tindall for her excellent typing.

REFERENCES

Ahlers, G. and Behringer, R.P. 1978: "Evolution of turbulence from the Rayleigh-Benard instability". Phys. Rev. Lett. 40 : 712-716.

Andronov, A.A., Vitt, E.A. and Khaiken, S.E, 1966: "Theory of oscillators" Pergamon Press: Oxford.

Bennetin, G., Galgani, L. and Strelcyn, J.M. 1976. Phys. Rev. A14 2338.

Birkhoff, G.D. 1927: "Dynamical systems". A.M.S. Publications: Providence

Chapman, G.T. and Tobak, M. 1985: "Observations, theoretical ideas, and modeling of turbulent flows - past, present, and future". In "Theoretical approaches to turbulence". A.M.S. Publications: Volume 58.

Collet, P. and Eckmann, J.P. 1980: "Iterated maps on the interval as dynamical systems". Comm. Math. Phys. 76 : 211.

Conte, S.D. and De Boor, C. 1980: "Elementary numerical analysis: an algorithmic approach. McGraw-Hill.

Coullet, P., Tresser, C. and Arnéodo, A. 1979: "Transition to stochasticity for a class of forced oscillators". Phys. Lett. A. 72: 268-270.

Crutchfield, J.P. and Huberman, B.A. 1980: "Fluctuations and the onset of chaos". Phys. Lett. 77A : 407.

Crutchfield, J.P., Farmer, J.D., Packard, N.H. and Shaw, R.S. 1980: "Geometry from a time series". Phys. Rev. Lett. 45 : 712.

Curry, J.H. 1978: "A generalized Lorenz system". Comm. Math. Phys. 60 : 193-204.

Curry, J.H., Herring, J.R., Lonearic, J. and Orszag, S.A. 1979: "Order and disorder in two- and three-dimensional Bénard convection". Comm. Math. Phys. 68 : 129.

Curry, J.H. and Yorke, J.A. 1978: "A transition from Hopf bifurcation to chaos: computer experiments with maps on R^2". In "The structure of attractors in dynamical systems". Lecture notes in Math 668. Springer-Verlag: 48.

Derrida, B., Gervois, A. and Pomeau, Y. 1978: "Iteration of endormorphisms

on the real axis and representation of numbers". Ann. de. 1' Inst. Henri Poincaré. Section A. 29 : 305.

Eckmann, J.P. 1981: "Roads to turbulence in dissipative dynamical systems". Rev. Mod. Phys. 53 : 643-654.

Fauve, S. and Libchaber, A. 1981: "Rayleigh-Bénard experiment in a low Prandtl number fluid, mercury". In "Chaos and order in nature" (H. Hacken ed). Springer-Verlag: 25-44.

Feigenbaum, M.J. 1978: "Quantitive universality for a class of nonlinear transformations". J. Stat. Phys. 19 : 25-52. Also see Feigenbaum (1979)

Feigenbaum, M.J. 1979: "The universal properties of nonlinear transformations". J. Stat. Phys. 21 : 186-223.

Fenstermacher, H.L., Gollub, J.P. and Swinney, H.L. 1978: "Dynamical Instabilities and the transition to chaotic Taylor vortex flow". J. Fluid. Mech. 94 : 103-128.

Foias, P. and Prodi, G. 1967: "Sur le comportement global des solutions non-stationaires des equations de Navier-Stokes en dimension 2". Rend. Sem. Mat. Univ. Padova. 39 : 1-34.

Foias, C. and Treve, Y.M. 1981: "Minimum number of modes for the approximation of the solutions of the Navier-Stokes equations in 2 and 3 dimensions". Phys. Lett. A85 , No.1 : 35-37.

Froehling, H., Crutchfield, J.P., Farmer, D., Packard, N.H. and Shaw, R. 1981: "On determining the dimension of chaotic flows". Physica 3D : 605

Gibbs, H.M., Hopf, F.A., Kaplan, D.L. and Shoemaker, R.L. 1981: "Observation of chaos in optical bistability". Phys. Rev. Lett. vol. 46, No.7 : 523-526.

Giglio, M., Muzatta, S., Perini, U. 1981: Phys. Rev. Lett. 47 : 243.

Gollub , J.P. and Benson, S.V. 1980: "Many routes to turbulent convection". J. Fluid. Mech. 100 : 449-470.

Gollub, J.P. and Swinney, H.L. 1978: Phys. Today. 31, No.8 : 41.

Gonzalez, D.L. and Piro, O. 1983: "Chaos in a nonlinear oscillator with exact solution". Phys. Rev. Lett. 50 : 870.

Gorman, M., Reith, L.A. and Swinney, H.L. 1980: "Modulation patterns, multiple frequencies, and other phenomena in circular Couette flow". Ann. N.Y. Acad. Sci. 357 : 10-27.

Grassberger, P. 1981: "On the Hausdorff dimension of fractal attractors". J. Stat. Phys. No.1, 26 : 173-179.

Grassberger, P. and Procaccia, I. 1983: "Characterization of strange attractors". Phys. Rev. Lett. 50 : 346.

Grossman, S. and Thomae, S. 1977: Z-Naturforsch. 32A , 1353.

Guckenheimer, J. 1979: "A brief introduction to dynamical systems". In "Lectures in Applied Mathematics". Vol.17. Amer. Math. Soc: Providence.

Guckenheimer, J. 1980: "Structural stability of the Lorenz attractor". Institut des Hautes Études Scientifiques. Publications Mathematiques. 50 : 73-100.

Guckenheimer, J. and Holmes, P. 1983: "Nonlinear oscillations, dynamical systems, and bifurcations of vector fields". Springer-Verlag.

Guckenheimer, J. and Williams, R.F. 1976: "The structure of Lorenz attractors". Appl. Math. Sci. 19 : 368-381.

Hao, Bai-Lin. 1984: "Chaos". Scientific Publications.

Hao, Bai-Lin. and Zhang, Shu-Yu. 1982: "Hierarchy of chaotic bands". J. Stat. Phys. 28. No.4.

Hassard, B.D., Kazarinoff, N.D. and Wan, Y.H. 1981: "Theory and applications of the Hopf bifurcation". Lon. Math. Soc. Lecture Notes. 41.

Helleman, R.H.G. 1980: "Nonlinear dynamics". Annals of New York Academy of Sciences: New York.

Hénon, M. 1976: "A two-dimensional mapping with a strange attractor". Comm. Math. Phys. 50 : 69-77.

Hille, E. 1976: "Ordinary differential equations in the complex domain". Chap. 10: Wiley.

Hirsch, J.E., Huberman, B.A. and Scalapino, D.J. 1982: "Theory of Intermittency". Phys. Rev. A25 : 519 .

Hirsch, M.W. and Smale, S. 1974: "Dofferential equations, dynamical systems and linear algebra". Academic Press: New York.

Hoppensteadt, F.C. and Hyman, J.M. 1975: Courant Institute, N.Y. Universit preprint, referred to in May (1976).

Huberman, B.A. and Rudnick, J. 1980: "Scaling behaviour of chaotic flows". Phys. Rev. Lett. 45. No.3: 154-156.

Hutton, R.E. 1963: "An investigation of resonant, nonlinear, nonplanar, free surface oscillations of a fluid. NASA Tech. Note D-1870. (Washington).

Kaplan, J.L. and Yorke, J.A. 1979: "Preturbulence, a regime observed in a fluid flow model of Lorenz". Comm. Math. Phys. 67 : 93-108.

Landau, L. and Lifschitz, L. 1959: "Fluid mechanics". Pergamon Press: Oxford.

Lanford, O.E. 1977: "Computer pictures of the Lorenz attractor". In "Turbulence Seminar Berkely 1976/77". P. Bernard and T. Ratiu (eds.) Springer-Verlag.

Lanford, O.E. 1981: "Strange attractors and turbulence". In "Hydrodynamic instabilities and the transition to turbulence". Topics in Applied Physics. 45.

H.L. Swinney and J.P. Gollub (eds.). Springer-Verlag: 7-26.

Levinson, N. 1949: "A second-order differential equation with singular solutions". Ann. Math. 50 : 127-153.

Li, T.Y. and Yorke, J.A. 1975: "Period three implies chaos". Amer. Math. Monthly. 82 : 985-992.

Libchaber, A. and Maurer, J. 1982: "A Rayleigh-Bénard experiment: helium in a small box". In "Nonlinear phenomena at phase transitions and instabilities". T. Riste (ed.) Plenum Publication Corp: New York: 259-286.

Lichtenberg, A.J. and Lieberman, M.A. 1982: "Regular and stochastic motion". Springer-Verlag.

Lorenz, E.N. 1963: "Deterministic non-periodic flow". J. Atmos. Sci. **20** : 130-141.

Lorenz, E.N. 1979: "On the prevalence of aperiodicity in simple systems". Edited by M. Grmela and J.E. Marsden. Lect. Notes in Math. **755**. Springer-Verlag: 53-75.

Lozi, R. 1978: "Un attracteur étrange? du type attracteur de Hénon". J. Phys. (Paris). **39** (5) : 9-10.

Malkus, W.V.R. 1972: "Non-periodic convection at high and low Prandtl number:. Liége Series, **6**, Vol.lV: 125-128.

Mandelbrot, B. 1977: "Fractals form chance and dimension". San Francisco: Freeman.

Mandelbrot, B. 1982: "The fractal geometry of nature". Freeman: San Fransisco: 195.

Marcus, P.S. 1981: "Effects of truncation in modal representations of thermal convection". J. Fluid. Mech. **103** : 241-255.

Marsden, J. and McCracken, M. 1976: "The Hopf-bifurcation and its applications". App. Math. Sci. **19**. Springer-Verlag.

May, R.M. 1976: "Simple mathematical models with very complicated dynamics". Nature. Vol. **261**.

May, R.M. and Oster, G.F. 1976: Amer. Nat. **110** : 1573.

McLaughlin, J.B. and Martin, P.C. 1975: "Transitions to turbulence in a statically stressed fluid system". Phys. Rev. **A 12** : 186-203.

McLaughlin, J.B. and Orszag, S.A. 1982: "Transition from periodic to chaotic thermal convection". J. Fluid. Mech. **122** : 123-142.

Metropolis, N. Stein, M.L. and Stein, P.R. 1973: "On finite limit sets for transformations on the unit interval". J. Combin. Theor. **A 15** : 25-44.

Miles, J. 1984a: "Strange attractors in fluid dynamics". In "Advances in Applied Mechanics". Vol. **24**.

Miles, J. 1984b: "Resonant Motion of a spherical pendulum". Physica **110** : 309-323.

Misiurewicz, M. 1980: "The Loz: mapping has a strange attractor". In "Nonlinear Dynamics". R.H.G. Helleman (ed.): 348-358.

Moon, F.C. and Holmes, P.J. 1979: "A magnetoelastic strange attractor". J. Sound. Vib. 65(2): 285-296.

Moore, D.R. and Weiss, N.O. 1973: "Two-dimensional Rayleigh-Bénard convection". J. Fluid. Mech. 58 : 289-312.

Moore, D.R., Toomre, J., Knobloch, E. and Weiss, N.D. 1983: "Period doubling and chaos in partial differential equations for thermosolutal convection". Nature. Vol. 303.

Mori, H. 1980: "Fractal dimensions of chaotic flows of autonomous dissipative systems". Proq. Theor. Phys. 63 : 1044.

Newhouse, S.E., Ruelle, D. and Takens, F. 1978: "Occurrence of strange axiom A attractors near quasiperiodic flows on T^m, $m \geqslant 3$". Comm. Math. Phys. 64 : 35-40.

Pomeau, Y. 1976: Refer to Hénon (1976).

Pomeau, Y. and Manneville, P. 1980: "Intermittent transition to turbulence in dissipative dynamical systems". Comm. Math. Phys. 74 : 189-197.

Rayleigh, Lord. 1916: "On convection currents in a horizontal layer of fluid when the higher temperature is on the underside". Philos. Mag. 32 : 529-546. Scientific papers 6 : 432-446.

Robbins, K. 1979: "Periodic solutions and bifurcation structure at high r in the Lorenz system". SIAM J. Appl. Math. 36 : 457-472.

Rössler, O.E. 1979: "Chaotic oscillations: an example of hyperchaos". Lectures in Applied Mathematics. Vol. 17.

Roux, J.C., Rossi, A., Bachelart, S. and Vidal, C. 1989: "Representation of a strange attractor from an experimental study of chemical turbulence". Phys. Lett. 77A. No.6 : 391.

Roux, J.C., Simoyi, R.H. and Swinney, J.L. 1983: "Observation of a strange attractor". Physica 8D : 257-266.

Ruelle, D. and Takens, F. 1971: "On the nature of turbulence". Commun. Math. Physica. 20 : 167-192.

Russel, D.A., Hanson, J.D. and Ott, E. 1980: "Dimension of strange attractors". Phys. Rev. Lett. 45 : 1175.

Saltzman, B. 1962: "Finite amplitude free convection as an initial value problem". J. Atmos. Sci. 19 : 329-341.

Šarkovskii, A.N. 1964: "Coexistence of cycles of a continuous map of a line into itself". Ukr. Mat. Z. 16 : 61-71.

Shaw, R., Farmer, D., Packard, N., Crutchfield, J., Jones, G. and Donnelly, R.J. 1980: "Power spectral analysis of a dynamical system". Phys. Lett. Vol. 76A. No.1 : 1-4.

Shimada, I. and Nagashima, T. 1979: "A numerical approach to ergodic problem of dissipative dynamical systems". Proq. Theor. Phys. 61 : 1605-1616.

Singer, D. 1978: "Stable orbits and bifurcations of maps of the interval". SIAM J. Appl. Math. 35 : 260-267.

Stefan, D. 1977: "A theorem of Šarkovskii on the existence of periodic orbits of continuous endomorphisms of the real line". Comm. Math. Phys. 54 : 237-248.

Takens, F. 1981: "Detecting strange attractors in turbulence". Lecture notes in Mathematics, ed. by D.A. Rand and L.S. Young. Springer-Verlag.

Treve, Y.M. 1981: J. Comput. Phys. 41 : 217.

Wang, Y.Q. and Chen, S.G. 1984: Acta Physica Sinica. 33 : 351.

Yorke, E.D. and Yorke, S.A. 1979: "Metastable chaos: transition to sustained chaotic behaviour in the Lorenz model". J. Stat. Phys. 21 (3) : 263-277.

Welander, P. 1967: "On the oscillatory instability of a differentially heated fluid loop". J. Fluid. Mech. 29 : 17-30.